

School of Civil and Mechanical Engineering

**Development of efficient methods for prediction of BLEVE pressure in
open space and loading on structures**

Yang Wang

(ORCID: 0000-0002-4881-9627)

**The thesis is presented for the degree of
Doctor of Philosophy
of
Curtin University**

February 2024

Declaration

To the best of my knowledge and belief, this thesis contains no material previously published by any other person except where due acknowledgment has been made.

This thesis contains no material which has been accepted for the award of any other degree or diploma in any university.

Signature: Yang Wang

Date: 21/12/2023

Abstract

Petroleum products, such as liquid petroleum gas (LPG), are widely used in residential, commercial and industrial sectors. As the demands on LPG continue to grow, gas explosion incidents are expected to occur more frequently. Boiling Liquid Expanding Vapour Explosions (BLEVE) is one of the most severe gas explosions that occur worldwide every year. It can result in a significant loss of lives and economy, as well as cause serious structural damage. Various civilian structures (e.g., buildings, bridges, tunnels and highways) and onshore/offshore facilities might be subjected to BLEVE loads, which could occur during transportation, processing and storage and cause damage to structures. Currently, the commonly used methods for predicting BLEVE loads on structures are based mainly on energy equivalence methods and numerical simulations based on Computational Fluid Dynamics (CFD) modelling. Energy equivalence methods use theoretical-based empirical models derived from various thermodynamics assumptions and energy laws, based on the TNT equivalence curve. However, using equivalent high explosives to predict BLEVE loads could result in an inaccurate prediction of the loading profile. This is due to the fact that compared to high explosive detonations of the same released energy, gas explosions usually generate lower peak overpressure, slower pressure rising, longer duration and higher impulse. Inaccurate prediction of BLEVE load would lead to inaccurate or even incorrect structural response analysis. Although CFD numerical simulations can more accurately predict BLEVE load, it is time-consuming and requires profound understanding and experience in CFD modelling, which may not be viable for practical applications in design and consulting offices. Therefore, it is necessary to develop reliable models for efficient and accurate predictions of BLEVE load that can be used for design and analysis to minimize the threats of BLEVE to structures.

This thesis primarily focuses on developing numerical-based empirical models. These models are derived to provide engineers with reliable empirical formulae and charts to easily and accurately predict BLEVE pressure-time profile for structural analysis and design, and hence provide effective and economic protective designs of structures against BLEVE loads. Firstly, empirical models for predicting BLEVE pressure wave propagation in open space are developed. Empirical formulae and charts for the critical parameters required to fully define the BLEVE pressure-time history in open space, including side-on peak pressure, peak pressure rise time, duration, arrival time and

impulse are established using the non-linear regression method. Subsequently, to predict BLEVE loads acting on structures, the interaction of BLEVE pressure wave with a rigid structure is analysed. The reflection coefficient chart is derived from the numerical simulations as a function of peak pressure and incident angle. The diffraction and clearing effects are also analysed by considering the structure dimensions and the corresponding clearing coefficients are determined from the numerical data. Using the derived free-field BLEVE pressure time history, reflection coefficient and clearing parameter, the BLEVE load acting on structures can be straightforwardly estimated. Additionally, since the duration of BLEVE pressure is relatively long, in an order comparable to the vibration periods of structural components, i.e., columns and walls, structural deformation during the action of BLEVE pressure could significantly affect the BLEVE pressure-structure interaction, which in turn affects the BLEVE loads acting on the structure. To assess the influence of structural deformation on BLEVE wave-structure interaction, interactions of BLEVE pressure wave with structures of different stiffnesses are modelled and analysed. The BLEVE loads acting on structures are derived as a function of positive BLEVE pressure duration and fundamental period of structure, leading to more accurate predictions of BLEVE loads on structures.

This thesis consists of six chapters. **Chapter 1** presents the thesis introduction, followed by the literature review in **Chapter 2**, which summarizes the experimental studies, and systematically discusses and compares BLEVE prediction methods, including empirical, numerical and ANN models. **Chapter 3** develops accurate empirical models to predict BLEVE pressure-time profile in open space. Since numerical simulation can provide more accurate prediction of BLEVE overpressure but is time-consuming, the corresponding simulation results and the results predicted by the ANN model trained with the CFD results are used to develop reliable empirical models for fast prediction of BLEVE pressure-time profile. Eight critical parameters are derived to determine the pressure-time profile of BLEVE, including the positive and negative side-on peak pressure, positive and negative peak pressure rise time, positive and negative duration, arrival time and impulse.

To design structures against BLEVE, BLEVE loads acting on a structure, instead of BLEVE occurring in open space, should be applied in the structural response analysis. **Chapter 4** focused on the prediction of the BLEVE load on a rigid structure. The

reflection coefficient chart is developed to predict the reflected BLEVE overpressure on a rigid structure by considering the angle of incidence of BLEVE pressure wave. In addition, the diffraction and clearing effects of BLEVE waves are analysed as a function of structural dimensions. Combined with the empirical models of open space BLEVE pressure prediction in Chapter 3, the BLEVE loads acting on a rigid structure can be predicted.

The structures in the real world are flexible. Due to the relatively long duration of BLEVE, the structural deformation during the action of BLEVE wave could significantly affect the interaction between the blast wave and the structure, and further influence the blast loads acting on the structure. **Chapter 5** considers the structural deformation in the numerical models of BLEVE pressure wave interaction with structures, and analyses how wave-structure interaction affects the BLEVE loads on the structure. Empirical models for more accurately predicting the reflected BLEVE pressure-time profile are proposed as a function of the BLEVE wave duration and structural fundamental vibration period to improve the accuracy of BLEVE load predictions for better design of structures against BLEVE.

Chapter 6 summarises the key findings of this research and offers suggestions for further studies. BLEVE experiments could be conducted to refine and validate the proposed empirical models. In addition, the continuous explosions can also be further investigated since the BLEVE and VCE can trigger each other. In the future, a practical safety manual for engineers related to BLEVE can be developed and used for structural design.

Overall, this study develops empirical formulae and charts for BLEVE load predictions, including the prediction of BLEVE pressure wave propagation in open space as well as BLEVE loads acting on structures. The outcomes obtained from this research offer valuable means for engineers to predict BLEVE loads for structural analysis and design against BLEVE.

Acknowledgement

First and foremost, I would like to express my deepest gratitude to my supervisors, John Curtin Distinguished Professor Hong Hao, Associate Professor Wensu Chen, and Dr. Jingde Li, for their unwavering support, encouragement, patience and guidance throughout my PhD journey. Their invaluable insights and constructive feedback are instrumental in shaping the direction and quality of this thesis.

I would also like to extend my gratitude to the members of our group at the Centre for Infrastructural Monitoring and Protection (CIMP) at Curtin University, who shared their knowledge and experiences, contributing to the success of this research project. Additionally, I wish to express my gratitude to all the participants and individuals who generously contributed their time and insights to this study. Without their cooperation, this research would not have been possible.

I sincerely thank my family for their constant encouragement, love, and understanding during this journey. Their unwavering belief in me is a constant source of motivation for me to keep moving forward.

Lastly, this work was made possible through the support of Australian Research Council (ARC) via Australian Laureate Fellowship (FL180100196), and I am sincerely thankful for the financial assistance.

Thank you to everyone who contributed to the completion of this thesis and supported me throughout my PhD journey. I will embark on the next chapter of my life with a heart full of gratitude. Thanks!

List of published work and work prepared for publication

The published papers and work prepared for publication, with the full bibliographic citations in the thesis, are listed below.

Wang, Y., Chen, W., Hao, H., 2024. Prediction of BLEVE loading on structures. *Journal of Loss Prevention in the Process Industries*, 105325.

Wang, Y., Hao, H., Chen, W., Li, J. & Wang, Z., 2023. Prediction of BLEVE loading on a rigid structure. *Process Safety and Environmental Protection*, 175, 1-16.

Wang, Y., Li, J., Hao, H., 2022. A state-of-the-art review of experimental and numerical studies on BLEVE overpressure prediction. *Journal of Loss Prevention in the Process Industries*, 104920.

Wang, Y., Li, J., Hao, H., 2022. Development of efficient methods for prediction of medium to large scale BLEVE pressure in open space. *Process Safety and Environmental Protection* 161, 421-435.

List of relevant additional publications

The additional publications relevant to the thesis but not forming part of it with the bibliographical details are listed below.

Li, Q., **Wang, Y.**, Chen, W., Li, L. & Hao, H. 2024. Machine learning prediction of BLEVE loading with graph neural networks. *Reliability Engineering & System Safety*, 241, 109639.

Li, Q., **Wang, Y.**, Li, L., Hao, H., Wang, R. & Li, J. 2023. Prediction of BLEVE loads on structures using machine learning and CFD. *Process Safety and Environmental Protection*, 171, 914-925.

Li, Q., **Wang, Y.**, Shao, Y., Li, L., Hao, H., 2023. A comparative study on the most effective machine learning model for blast loading prediction: From GBDT to Transformer. *Engineering Structures* 276, 115310.

Statement of contribution

The work presented in this thesis is primarily conducted by the Ph.D. candidate, Yang Wang, which includes carrying out the numerical simulations, analysing the results, deriving empirical formulae and charts, and preparing the manuscripts. Contributions by others are described as follows. The signed contribution forms are attached in the Appendix I.

Chapter 2

Prof. Hong Hao and Dr. Jingde Li defined the research topic and scope, revised the manuscript and provided intellectual input toward data analysis and discussion of the results.

Chapter 3

Prof. Hong Hao and Dr. Jingde Li defined the research topic and scope, revised the manuscript and provided intellectual input toward data analysis and discussion of the results.

Chapter 4

Prof. Hong Hao and A/Prof. Wensu Chen defined the research topic and scope, revised the manuscript and provided intellectual input toward data analysis and discussion of the results. Dr. Jingde Li and Mr. Zitong Wang provided intellectual input toward data analysis.

Chapter 5

Prof. Hong Hao and A/Prof. Wensu Chen defined the research topic and scope, revised the manuscript and provided intellectual input toward data analysis and discussion of the results.

Table of Contents

Declaration	I
Abstract	II
Acknowledgement	V
List of published work and work prepared for publication	VI
List of relevant additional publications	VII
Statement of contribution	VIII
Table of Contents	IX
List of Figures	XII
List of Tables	XVII
Chapter 1 Introduction	1
1.1 Background	1
1.2 Research objective	3
1.3 Research outline	4
Chapter 2 Literature review	6
2.1 Introduction	6
2.2 Experimental study of BLEVE overpressure prediction	7
2.2.1 Near-field overpressure prediction	7
2.2.2 Far-field overpressure prediction	12
2.2.3 Theoretical-based empirical models and comparison	14
2.3 Numerical study of BLEVE overpressure prediction	21
2.3.1 FLACS	21
2.3.2 ANSYS Fluent	24
2.3.3 Artificial Neural Network method	24
2.3.4 Numerical-based empirical models	29
2.3.5 Comparison of numerical simulation models	31
2.4 Summary	37

Chapter 3 Prediction of medium to large scale BLEVE pressure in open space	39
3.1 Introduction	39
3.2 BLEVE energy calculation	39
3.3 BLEVE pressure prediction equations	41
3.3.1 Side-on peak pressure	43
3.3.2 Duration of the blast wave	45
3.3.3 Arrival time	46
3.3.4 Peak pressure rise time.....	47
3.3.5 Impulse.....	48
3.3.6 Pressure prediction equations' fitting test.....	49
3.4 BLEVE pressure prediction charts	51
3.5 Evaluation of the pressure prediction equations and charts	55
3.5.1 Comparison of predicted data with experimental data	55
3.5.2 Comparison of the new prediction methods with the empirical methods..	62
3.6 Summary.....	68
Chapter 4 Prediction of BLEVE loading on rigid structures	69
4.1 Introduction	69
4.2 Numerical modelling	69
4.2.1 Validation of CFD models	70
4.2.2 CFD simulation.....	75
4.3 Blast wave-structure interaction	77
4.4 Reflected overpressure of BLEVE pressure wave	79
4.4.1 Reflected overpressure profile	79
4.4.2 Reflection coefficient (C_r) for positive overpressure (P_r^+).....	82
4.4.3 Reflected negative overpressure (P_r^-)	84
4.4.4 Peak pressure rise time (t_p)	85
4.5 BLEVE pressure relief.....	86

4.5.1 BLEVE wave diffraction	86
4.5.2 Clearing time (t_c).....	89
4.5.3 Reflected impulse (I_r)	92
4.6 Case study.....	94
4.7 Summary	97
Chapter 5 Prediction of BLEVE loading on flexible structures.....	98
5.1 Introduction	98
5.2 Numerical validation and modelling	98
5.2.1 BLEVE simulation by using FLACS	98
5.2.2 BLEVE wave–structure interaction by using ANSYS Workbench	99
5.3 Reflected BLEVE positive pressure	103
5.3.1 Effect of the structural stiffness	104
5.3.2 Effect of the incident BLEVE wave duration	107
5.4 Reflected negative peak pressure, duration and peak pressure rise time	108
5.4.1 Reflected negative peak overpressure.....	109
5.4.2 Reflected overpressure duration	110
5.4.3 Reflected peak pressure rise time and pressure rise rate	110
5.5 Case study.....	112
5.6 Summary	115
Chapter 6 Conclusions and future works	117
6.1 Main findings	117
6.2 Recommendations for future works	118
References	120
Appendix I Statement of contribution of co-authors.....	132
Appendix II Copyright Clearance	134

List of Figures

Figure 1-1. Research roadmap	5
Figure 2-1. BLEVE incidents and prediction methods.	6
Figure 2-2. Pressure evolution: (a) stationary shock; (b) moving shock [29].	8
Figure 2-3. Comparison of the theoretical-based empirical models with the experimental data.	18
Figure 2-4. ANN structure [84, 85]	25
Figure 2-5. Feedforward neuron network [84]	26
Figure 2-6. Comparison of the numerical-based empirical models with the experimental data.	33
Figure 2-7. Comparison of the empirical model, numerical-based empirical model, CFD model and ANN model with the experimental data.	36
Figure 3-1. Pseudo-source space modelling in FLACS simulation [23].	42
Figure 3-2. BLEVE tank.	42
Figure 3-3. Comparison between CFD simulation data and equation predicted scaled positive side-on peak pressure.	43
Figure 3-4. Comparison between CFD simulation data and equation predicted scaled negative side-on peak pressure.	44
Figure 3-5. Comparison between CFD simulation data and equation predicted scaled duration: (a) positive pressure duration; (b) negative pressure duration.	45
Figure 3-6. Comparison between CFD simulation data and equation predicted scaled arrival time.	46
Figure 3-7. Comparison between CFD simulation data and equation predicted scaled peak pressure rise time: (a) positive; (b) negative.	47
Figure 3-8. Comparison between CFD simulation data and equation predicted scaled impulse.	48
Figure 3-9. Histogram of pressure prediction model fitting test: (a) positive scaled side-on peak pressure; (b) negative scaled side-on peak pressure; (c) positive scaled	

duration; (d) negative scaled duration; (e) positive scaled impulse; (f) scaled arrival time; (g) positive scaled peak pressure rise time; (h) negative scaled peak pressure rise time.	51
Figure 3-10. Scaled side-on peak pressure: (a) positive pressure; (b) negative pressure.	52
Figure 3-11. Scaled duration: (a) positive pressure duration; (b) negative pressure duration.	52
Figure 3-12. (a) Scaled impulse; (b) Scaled arrival time.	52
Figure 3-13. Scaled peak pressure rise time: (a) positive; (b) negative.	53
Figure 3-14. $\gamma < 5$: (a) scaled peak pressure, duration & impulse; (b) scaled arrival time & peak pressure rise time.	53
Figure 3-15. $5 \leq \gamma \leq 10$: (a) scaled peak pressure, duration & impulse; (b) scaled arrival time & peak pressure rise time.	54
Figure 3-16. $\gamma > 10$: (a) scaled peak pressure, duration & impulse; (b) scaled arrival time & peak pressure rise time.	54
Figure 3-17. Comparison between experimental data and predicted positive side-on peak pressure (by pressure prediction equation & chart).	58
Figure 3-18. Comparison between experimental data and predicted negative side-on peak pressure (by pressure prediction equation & chart).	59
Figure 3-19. Comparison between experimental data and predicted arrival time (by pressure prediction equation & chart).	59
Figure 3-20. Comparison between experimental data and predicted positive peak pressure rise time (by pressure prediction equation & chart).	60
Figure 3-21. Comparison between experimental data and predicted negative peak pressure rise time (by pressure prediction equation & chart).	60
Figure 3-22. Comparison between experimental data and predicted positive duration (by pressure prediction equation & chart).	61
Figure 3-23. Comparison between experimental data and predicted negative duration (by pressure prediction equation & chart).	61

Figure 3-24. Comparison between experimental data and predicted impulse (by pressure prediction equation & chart).	62
Figure 3-25. Comparison of experimental data with those predicted by the Prugh's TNT equivalence method, Hemmatian's empirical method and the proposed equations and charts in this study.....	65
Figure 4-1. Pseudo-source simulation: (a) Modelling in FLACS; (b) Pressure time history of monitor point inside the pseudo-source.	71
Figure 4-2. Large-scale BLEVE experiments: (a) BAM's test [50]; (b) 3D model in FLACS.	71
Figure 4-3. Pressure time history (numerical results vs experimental data): (a) BAM's experiment [50]; (b) Johnson's experiment [49].	73
Figure 4-4. Comparison of numerical results and experimental data in (a) scatter plot and (b) parabola plot.	74
Figure 4-5. Grid sensitivity study of BLEVE loads on a rigid structure.....	75
Figure 4-6. Schematic diagram of numerical model.	76
Figure 4-7. Schematic top view and side view of BLEVE wave interaction with a rigid structure [111, 112]: (a) Incident waves at the front surface; (b) Reflected and diffracted waves at the front surface; (c) Diffracted waves at the rear surface; (d) Diffraction complete at the rear surface.	79
Figure 4-8. Typical overpressure-time profiles: (a) TNT explosion; (b) BLEVE.	80
Figure 4-9. BLEVE pressure-time profile (P_s : incident peak overpressure & P_r : reflected peak overpressure).....	81
Figure 4-10. BLEVE pressure wave propagation: (a) in open space; (b) interaction with a rigid structure.....	81
Figure 4-11. BLEVE reflection coefficient for positive overpressure (C_r) charts: (a) $0 \text{ bar} < P_{s+} \leq 0.15 \text{ bar}$; (b) $0.15 \text{ bar} < P_{s+} \leq 0.25 \text{ bar}$; (c) $0.25 \text{ bar} < P_{s+} \leq 0.4 \text{ bar}$; (d) $0.4 \text{ bar} < P_{s+} \leq 0.5 \text{ bar}$; (e) $0.5 \text{ bar} < P_{s+} \leq 1 \text{ bar}$.	84
Figure 4-12. Comparison of reflection coefficient for positive overpressure (C_r) charts: (a) BLEVEs (incident overpressure $\leq 1 \text{ bar}$); (b) TNT explosions [18].	84

Figure 4-13. Correlation between reflected negative peak pressure ($Pr -$) and reflected positive peak pressure ($Pr +$).	85
Figure 4-14. Correlation between reflected peak pressure rise time (tp, r) and incident peak pressure rise time (tp, i): (a) Positive; (b) Negative.	86
Figure 4-15. BLEVE wave pressure relief from a rigid structure: (a) CFD model; (b) Schematic diagram.	88
Figure 4-16. Rigid structures with different widths.	88
Figure 4-17. Monitoring points at the centre points of different surfaces on a rigid structure.	88
Figure 4-18. Reflected pressure-time histories on a rigid structure surface at monitoring points (MP1-5).	89
Figure 4-19. Pressure relief in FLACS simulation.	90
Figure 4-20. Sound speed in the BLEVE reflected region.	91
Figure 4-21. Comparison of sound velocity in the reflection regions of TNT explosion (UFC, 2008) and BLEVE.	92
Figure 4-22. Reflected impulse (I_r) [18].	93
Figure 4-23. Correlation between the reflected impulse (I_r) and incident impulse (I_i) at the centre of the front surface.	93
Figure 4-24. Schematic diagram of two cases: (a) open space; (b) at the front centre of rigid structure.	94
Figure 4-25. Reflected and incident pressure-time histories.	96
Figure 5-1. FLACS model: (a) BLEVE in open space; (b) BLEVE acts on a structure.	99
Figure 5-2. Schematic diagram of the whole simulation process and finite element model in ANSYS.	102
Figure 5-3. Mesh convergence study in ANSYS.	103
Figure 5-4. Comparing ANSYS and FLACS prediction of BLEVE reflected pressure-time profile.	103

Figure 5-5. Reflected pressure-time profile from structures of different stiffness.	105
Figure 5-6. The ratio of the positive reflected peak overpressure ($P_r, flex +$) to incident peak overpressure ($P_s +$) versus td/T	107
Figure 5-7. The ratio of the positive reflected peak overpressure ($P_r, flex +$) to incident peak overpressure ($P_s +$) versus td/T for various incident duration ranges.	108
Figure 5-8. Typical BLEVE overpressure-time profile.	109
Figure 5-9. The ratio of the negative reflected peak overpressure on flexible structure ($P_r, flex -$) to rigid structure ($P_r, rigid -$) versus td/T	109
Figure 5-10. The ratio of the reflected duration ($td, flex$) to incident duration (td, i) versus td/T : (a) Positive ($td, flex +$); (b) Negative ($td, flex -$).	110
Figure 5-11. The ratio of the reflected peak pressure rise time ($tp, flex$) to incident peak pressure rise time (tp, i) versus the ratio of td/T : (a) Positive ($tp, flex +$); (b) Negative ($tp, flex -$).	111
Figure 5-12. The ratio of the reflected pressure rise rate ($R_p, flex +$) to incident pressure rise rate ($R_p, i +$) versus the ratio of td/T	111
Figure 5-13. Schematic diagram of BLEVE cases: (a) open space; (b) a structure in the area	112
Figure 5-14. Reflected pressure-time profiles (on the rigid and flexible structure) and incident pressure-time profiles (experimental data [28] and predicted results [92]).	115

List of Tables

Table 2-1. Comparison between the experimental data and theoretical-based empirical models with RAIE assumption.	19
Table 2-2. Advantages & limitations of ANN [86].....	26
Table 2-3. Training variable constraints in ANN model [24].....	28
Table 2-4. Comparison between the experimental data and numerical-based empirical models.	31
Table 2-5. Comparison among the CFD models, ANN models and numerical-based empirical models.	34
Table 3-1. Training variable ranges for BLEVE data.	42
Table 3-2. Fitting distribution, mean and standard deviation for critical parameters.	49
Table 3-3. Experimental data.	57
Table 3-4. Equation predicted data and the corresponding errors with experimental results.	57
Table 3-5. Chart predicted data and the corresponding errors with experimental results.	57
Table 3-6. Pressure-time parameters at 20m of both the experimental and FLACS data [23].	58
Table 3-7. Pressure parameters predicted by Prugh’s TNT equivalence method and the corresponding errors with respect to the available experimental data.	66
Table 3-8. Error between the experimental results and those predicted by Prugh’s TNT equivalence method, BLEVE equations & charts.....	66
Table 3-9. Pressure parameters predicted by Hemmatian’s empirical model and the corresponding errors with respect to the available experimental data.	67
Table 3-10. Error between the experimental results and those predicted by Hemmatian’s empirical model, BLEVE equations & charts.	67
Table 4-1. Details of large-scale BLEVE experiments [49, 50, 53].	71

Table 4-2. Performance metrics of numerical results for large-scale BLEVE experiments.	74
Table 4-3. Variables of BLEVE simulation [24].	77
Table 4-4. Predictions by using the equations in Wang et al. [92].	95
Table 5-1. Reflected peak overpressure and pressure rise rate for each case.	105
Table 5-2. Predicted BLEVE overpressure in open space [92].....	113

Chapter 1 Introduction

1.1 Background

Currently, with the increasing popularity of clean alternative fuels, petroleum products like liquid petroleum gas (LPG) have become important energy sources in various fields, such as residential, commercial and industrial fields [1-3]. The consumption of these petroleum products has witnessed significant growth since 1980, contributing to more than half of the total energy consumption around the world [4, 5]. However, as the demands of LPG continue to grow, Boiling Liquid Expanding Vapour Explosion (BLEVE) incidents are expected to occur more frequently than before during transportation, processing and storage. Various civilian structures (e.g., buildings, bridges, tunnels and highways) and onshore/offshore facilities might be subjected to BLEVE loads induced by LPG, which may result in structural damages [6, 7]. One of the devastating BLEVE events was the 2018 accident in Bologna, Italy, where a traffic accident involving an LPG truck on a highway bridge led to a BLEVE, which caused at least 3 deaths, 67 injuries, and the partial collapse of the bridge [8]. In 2005, multiple BLEVEs occurred at the Texas City Refinery (i.e., onshore/offshore facility) due to the overfilling of an isobutene sphere tank, which led to explosions in a tank farm. The main cause of the accident was the failure of a pressure control valve and a high-level alarm defector, resulting in severe damage to the refinery and surrounding areas. This accident resulted in 15 fatalities, over 180 injuries, and millions of dollars in losses, with the entire isomerization process unit being out of operation for more than two years [9]. Such explosions can also generate debris, which can pose a significant risk to individuals and properties in the vicinity. Hence, it is essential to accurately predict the blast loads generated by BLEVE for effective structural designs to resist such loads.

A BLEVE occurs when the pressurized tank ruptures suddenly and the internal liquid temperature exceeds its boiling point [10, 11]. Two BLEVE types can be classified based on the failure temperature, i.e., non-superheated BLEVE and superheated BLEVE. To explain the difference between the two types, a definition of ‘superheat limit temperature (SLT)’ is introduced for the temperature limit, referring to the highest temperature at which superheat liquid (i.e., liquid excess of its boiling point) remains in the liquid phase without undergoing a phase transition at constant pressure

[12-14]. Non-superheated BLEVEs occur when the failure temperature is between the ambient boiling point and SLT. Only vapour expansion is taken into account in the energy calculation. While superheated BLEVEs occur when the failure temperature is higher than SLT. At the initial stage, the bubble nuclei are very small, and thus more superheat is required to grow the bubble nuclei. When the liquid temperature is significantly higher than SLT under ambient pressure, homogeneous nucleation and evaporation can occur rapidly [11, 12]. The gradual vaporization of the liquid within the pressurized vessel leads to an increase in the internal pressure, eventually resulting in ruptures when the stress of the vessel exceeds its ultimate tensile strength [15, 16]. Heat resulting from the liquid is used for nucleation and vaporization. During this process, a very violent phase transition occurs (i.e., the liquid phase instantly changes to the vapour phase). Eventually, the energy from liquid flashing also contributes to the formation of the blast waves along with the vapour expansion energy [11, 17].

To predict BLEVE loads, two methods are commonly used, i.e., energy equivalence method and numerical simulation. Energy equivalence methods use theoretical-based empirical models derived from various thermodynamics assumptions and energy laws, relying on TNT equivalence curves from the design manuals, such as the Unified Facilities Criteria UFC-3-340-02 [18]. However, the pressure-time history of TNT explosion rises instantaneously with an extremely short duration. With the same released energy, BLEVE usually generates lower peak overpressure, slower pressure rising, longer duration and higher impulse [19]. Therefore, the design against BLEVE differs from that against TNT explosions. Using equivalent high explosives to predict BLEVE, could result in an inaccurate prediction of loading profile [20]. For example, the loading duration predicted by using the TNT-equivalence method is very short and much smaller than the vibration period of the structure and structural components, while the actual BLEVE loading duration is in an order of tens of milliseconds, which could be comparable to the vibration period of structural components such as columns, hence using blast load predicted by TNT-equivalence method may lead to inaccurate predictions of structural responses induced by BLEVE loads.

Unlike the empirical models, Computational Fluid Dynamics (CFD) models can yield more accurate predictions and are widely accepted by both engineers and researchers since the actual scenarios and complex geometries can be modelled. With the development of BLEVE models in recent years [21-23], CFD simulations, such as

FLACS, become a reliable method for predicting BLEVE pressure wave. However, each simulation of a BLEVE case required hours of computational time, and a profound understanding and experience in CFD modelling and simulations [24]. Therefore, it may not be viable for practical applications in many design and consulting offices. To improve the efficiency in predicting the BLEVE pressures, based on the extensive database of simulation results, machine learning approaches such as Artificial Neural Network (ANN) and Graph Neural Network (GNN) were employed to predict BLEVE pressure [24-27]. However, it is worth mentioning that these functions are still not straightforward to use since the complex machine learning function setups need to be initialized before running the calculation, which is not straightforward to use. Thus, developing a straightforward method for efficient and accurate BLEVE pressure prediction is important. As a result, a series of empirical formulae and charts are developed in this thesis to provide an efficient and reliable approach for engineers. These empirical models facilitate the proper design of protective measures for structures, minimizing the threats of BLEVE to structures.

1.2 Research objective

The main objective of this thesis is to develop the empirical formulae and charts for BLEVE pressure-time profile prediction, which can be convenient for engineers to design the structure against the BLEVE. Both BLEVE occurring in open space and BLEVE load on the structure (i.e., rigid and flexible) are studied. The objective is achieved by implementing the following research tasks:

- (1) Explore the causes and mechanisms of BLEVE.
- (2) Review and compare existing BLEVE prediction methods.
- (3) Setup numerical models of BLEVE by conducting CFD model validation, grid sensitivity study and parametric study, etc.
- (4) Develop easy-to-use empirical models based on numerical and CFD-based ANN models to predict BLEVE pressure-time profiles in open space.
- (5) Depict a reflection coefficient chart to predict reflected BLEVE overpressure on rigid structures.
- (6) Investigate pressure relief phenomena affected by structural dimensions, such

as diffraction and clearing effects on BLEVE loads.

- (7) Consider the effect of structural deformation on BLEVE wave-structure interaction during the action of BLEVE wave, examining how structural stiffness and incident BLEVE wave duration affect BLEVE loads.

1.3 Research outline

This thesis consists of six chapters. An overview of the research roadmap is presented in Figure 1-1, and the contents of each chapter are introduced below.

Chapter 1 provides an overview of the research background, objective and outline.

Chapter 2 conducts a comprehensive literature review, summarizes existing BLEVE experiments, and compares commonly used BLEVE prediction methods.

Chapter 3 develops empirical models to predict the BLEVE pressure-time profile in open space. Although numerical simulations can provide precise BLEVE overpressure predictions, they are time-consuming. To address this, simulation results, along with an Artificial Neural Network (ANN) model trained using these results, are utilized to create reliable empirical models for rapidly estimating BLEVE pressure-time profiles.

Chapter 4 focuses on designing structures to withstand BLEVE loads, rather than examining BLEVE events in open space. This chapter depicted a reflection coefficient chart to predict reflected BLEVE overpressure on the rigid structure. This prediction takes into account the angle of incidence from the BLEVE centre to the structure centre. Additionally, the study investigates pressure relief phenomena influenced by structural dimensions, such as diffraction and clearing effects on BLEVE waves, and proposes corresponding empirical models for prediction.

Chapter 5 conducts a more in-depth study of structural deformation effects during the action of BLEVE wave, since structures in real-world scenarios are flexible. This analysis is crucial because the deformation of structure during the action of BLEVE wave has a significant effect on wave-structure interaction due to the long duration of BLEVE pressure, consequently affecting the blast loads on the structure. Structural stiffness and incident BLEVE wave duration are discussed as two critical factors. The corresponding empirical models to predict the BLEVE loads on the structure are derived.

Chapter 6 summarises the main findings of this thesis and offers suggestions for future studies, aiming to further refine and validate the proposed BLEVE empirical models by conducting additional experiments and exploring real accident scenarios, which can be better applied in BLEVE-resistant structural design.

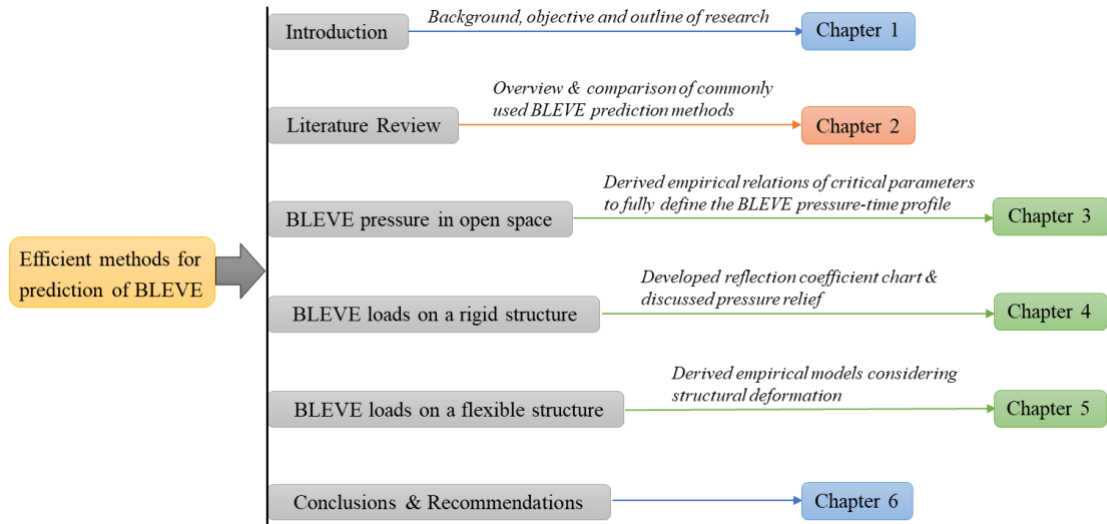


Figure 1-1. Research roadmap.

Chapter 2 Literature review

2.1 Introduction

As discussed in Chapter 1, accidents of BLEVEs, which have been often reported worldwide, can bring about significant economic and environmental damages as well as injuries and loss of lives. Studies of BLEVE overpressure prediction and its effect on surrounding structures are, however, relatively limited. Current practice in BLEVE loads predictions for analysis and design of structures against BLEVE effects is based primarily on theoretical-based TNT equivalence empirical methods, which do not necessarily give accurate explosion load predictions. Some experimental tests and numerical simulations have also been carried out to predict BLEVE loads. This chapter presents a systematic review of the experimental and numerical studies on BLEVE overpressure prediction, as shown in Figure 2-1. First, the experimental studies on critical parameters of tank rupture pressure, rupture temperature, liquid fill ratio, and tank's volume that affect the BLEVE overpressure generation are reviewed and discussed. The theoretical-based empirical models are also compared. Subsequently, the commonly-used CFD models, the recently developed ANN models and numerical-based empirical methods for BLEVE overpressure predictions are reviewed and discussed. It is concluded that the BLEVE overpressure prediction using CFD models is more accurate than theoretical-based TNT equivalence empirical methods since complex BLEVE conditions such as tank geometries and surrounding environments can be considered in the CFD model, but it is time consuming and requires relatively large computer power. A properly trained ANN model and numerical-based empirical models could also reliably predict BLEVE overpressures with significantly improved efficiency than CFD simulation. The advantages and disadvantages of the different prediction methods are summarized and discussed in detail.

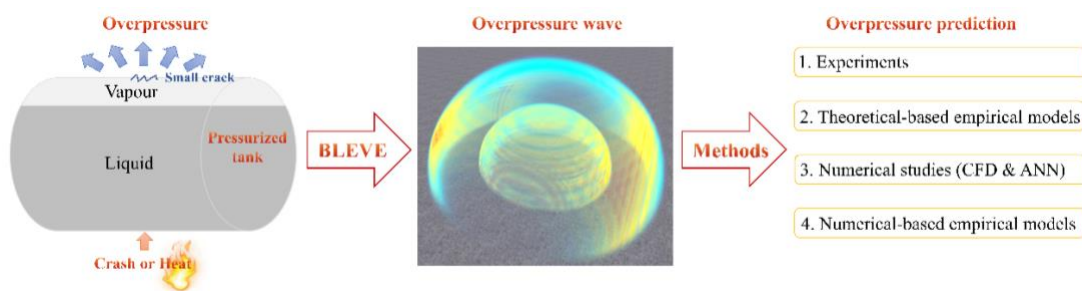


Figure 2-1. BLEVE incidents and prediction methods.

The related work in this chapter has been published in Journal of Loss Prevention in the Process Industries.

Wang, Y., Li, J., Hao, H., 2022. A state-of-the-art review of experimental and numerical studies on BLEVE overpressure prediction. Journal of Loss Prevention in the Process Industries, 104920.

2.2 Experimental study of BLEVE overpressure prediction

The immense overpressures resulting from a BLEVE can cause severe structural damage, loss of life, and substantial economic consequences. Therefore, accurate prediction of gas explosion overpressure is imperative for designing effective measures to resist explosion loads. Current practice in predicting BLEVE overpressure is based primarily on theoretical-based TNT equivalence empirical methods. As will be discussed later in this paper, these methods do not necessarily give accurate BLEVE load predictions, resulting in ineffective analysis and design of structures to resist BLEVE loads. Most of these empirical methods are based on simplified fluid thermodynamics and gas behaviour assumptions, which are validated using experimental data. This section reviews the experimental studies of BLEVE for predicting near-field and far-field overpressures, as well as the theoretical-based empirical models and comparisons with experiments.

2.2.1 Near-field overpressure prediction

Near-field distance is defined as the distance from the BLEVE centre to the target, measured in the range within ten times of the diameter of the BLEVE vessel [28, 29]. The vapour expansion and liquid flashing lead to a shock wave and a high-velocity flow near the vessel [28]. The near-field pressures can be divided into two categories based on the damage level of the vessel. Namely, if the vessel partially ruptures, the stationary shock phenomenon is observed in the near field. While in the complete vessel rupture scenario, the near-field shock wave generates the moving shock

phenomenon, as shown in Figure 2-2. For the stationary shock, it is seen that the pressurized liquid begins to expand to the sonic condition (i.e. the fluid velocity equals the sound speed, at P_1). Subsequently, the expansion continues until the liquid velocity reaches the shock wave generation condition (i.e. P_2). After the shock, the pressure returns to the ambient pressure (P_3). While for the moving shock, the pressurized liquid expands and pushes the surrounding air after escaping from the vessel at the initial stage (i.e. P_1). Since the expanding velocity is high enough, the ambient air is compressed to P_2 due to the piston effect. Like the stationary shock case, the final pressure will eventually fall back to the ambient pressure (P_3) [29, 30]. When the vessel fully opens, the ground loading and drag loading will also be generated by the blast wind [31].

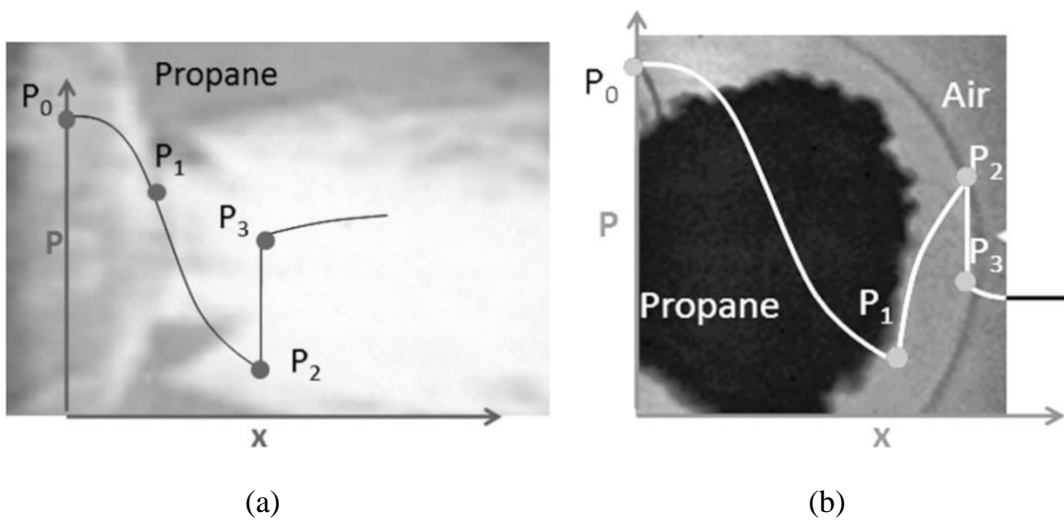


Figure 2-2. Pressure evolution: (a) stationary shock; (b) moving shock [29].

By far, many researchers have conducted experimental studies on the near-field pressures of BLEVE. For instance, Laboureur et al. [32] performed several propane BLEVE experiments in a BABELs facility to study the groove length effect on overpressure generation. The liquefied propane was contained in a $9.5 \times 10^{-5} \text{ m}^3$ cylindrical reservoir filled at 86%, and the internal fluid stayed in the supercritical condition (i.e. liquid and vapour no distinction) when BLEVE occurs. Tests with different groove lengths were conducted. The results showed that when BLEVE occurred, the smaller groove length corresponded to the higher rupture pressure, the larger opening width and the higher blast wave intensity. Additionally, Birk et al. [31] and Birk et al. [33] conducted a series of propane BLEVEs in a 0.0006 m^3 aluminium tube with a rather thin wall. The tube was heated until BLEVE occurred. Overpressures

in different directions were measured by sensors (i.e. in vertical, 45°, and horizontal directions) corresponding to the different tank rupture pressures (i.e. ranging from 800 to 4000 kPa), different liquid fill ratios (i.e. between 50% and 66%) and different crack lengths (i.e. from 50 to 200 mm). Based on the previous experimental studies, Birk et al. [30] and Birk et al. [34] further investigated the tube failure procedure at the early moment and the near-field hazard using the overpressure data obtained from the same apparatus of propane BLEVE experiments. In addition, Eyssette et al. [35] conducted an experimental study on the ground force effect of BLEVEs, since the ground forces had a significant impact when the BLEVEs occurred on bridges or other critical infrastructures. The authors used the same experimental apparatus (i.e. 0.0006 m³ aluminium tube) designed by Birk et al.. It was found that the liquid fill ratio and weakened length of the vessel determined the magnitude of the ground force, and the maximum ground force and impulse were linearly related to the rupture pressure and liquid fill ratio. The experiment apparatus in the above studies used a thin aluminium wall different in thickness from the actual wall. However, the effect of the wall thickness on the near-field overpressure was not further investigated.

Additionally, for more practical applications, the experiments of commercial Liquefied Petroleum Gas (LPG) cylinders subjected to BLEVE were carried out by Tschirschwitz et al. [36]. They exposed propane cylinders to three different fire sources (i.e. wood fire, petrol pool fire and propane gas fire) in a horizontal position. The burst pressures and near-field overpressures were measured. It was found that the type of fire source has no significant effect on BLEVE. Following the previous investigation of commercial LPG, Tschirschwitz et al. [37] conducted experiments on toroidal LPG vehicles with different propane fill ratios. It was found that the 20% fill ratio generates higher near-field overpressure and more fragments. This experiment also demonstrated that near-field overpressure could lead to serious injuries regardless of the liquid fill ratio. However, the effect of crack length on commercial LPG cylinders and its difference with aluminium tubes requires further study.

For non-flammable BLEVEs occurring in the near field, carbon dioxide (CO₂) is one of the most commonly investigated fluids in experiments [38], but most studies of CO₂ BLEVE were focused on investigating vessels' internal pressures instead of external pressures. For example, Bjerketvedt et al. [39] conducted a small-scale CO₂ experiment to measure the tank rupture pressures and the internal overpressures.

Subsequently, Van der Voort et al. [40] investigated the near-field overpressure difference from BLEVEs of a 0.04 m³ CO₂ cylinder at the symmetrical defect positions. It was concluded that the overpressure decreases with the distance of the monitor point away from the defect, and the asymmetry of gas dynamics becomes more pronounced as the distance of the monitor point is closer. Van Der Voort et al. [41] further investigated the temperature (i.e., from 247.6 K to 294.3 K) effect on the BLEVE overpressure. The authors found that the CO₂ BLEVE is dangerous, and it is possible to generate large overpressure even at low temperatures. Hence, the authors put forward a suggestion that hazard assessments and risk management still need to be considered when liquefied CO₂ is at low temperatures during transportation and storage. In addition, the effects of the groove defects of a vessel on the tank rupture pressure of BLEVE were investigated. Zhou et al. [42] studied the tank rupture pressure of CO₂ BLEVE with different depths of longitudinal groove defects. It was concluded that the smaller depth had larger rupture pressure. However, the effect of the length and width of longitudinal defects on the rupture pressure still needs to be further studied.

Similarly, Li et al. [43] further investigated the vessel groove shape effect on the tank rupture pressure of CO₂ BLEVE. It was stated that the V-shaped groove led to a larger tank rupture pressure than that of the X-shaped one. However, this study only focused on the shape of the groove defects and did not consider the dimension (i.e., width, length & depth) of the groove. The experimental study on longitudinal groove defects was also lacking. Furthermore, Li et al. [44] studied BLEVE overpressures in a high-pressure gas cylinder with different burst vent sizes when the tank rupture pressure was at 3000 kPa and 5000 kPa. The heterogeneous nucleation process was analysed by observing the liquid to vapour changing phase of CO₂ after a sudden rupture. The effect of burst vent size on overpressure was also discussed. It was concluded that the pressure amplitude depended on the burst vent size, in that particular case, the burst vent size of 8 mm generated the highest peak pressure for both scenarios. Zhou et al. [38] conducted more tests based on similar experimental setups used by Li et al. [44]. Since the CO₂ would result in a complex phase transition (i.e., transition from liquid to supercritical state) under the higher internal pressure, the authors carried out BLEVE tests with rupture pressures up to 10000 kPa. Two critical burst vent sizes were determined, one is the size corresponding to the highest intensity of BLEVE, and

another is the size that prevents the BLEVE occurrence. Meanwhile, the ideal BLEVE rupture pressure corresponding to the critical vent size was also investigated. However, in their experimental study, the authors did not consider the rupture temperature, which is an essential parameter affecting the CO₂ BLEVE initiation.

In addition, tanks containing water at a relatively high temperature and internal pressure may undergo a BLEVE if the tank collapses and fails under certain conditions. Steam boiler explosion is a good example of water BLEVEs. In order to study water BLEVE in the near field, Chen et al. [45] heated a vertical cylindrical vessel containing water until BLEVE occurred to analyse the effect of liquid water fill ratio, orifice area size and initial temperature on the overpressure generation. It was found that when the fill ratio was increased from 60% to 80%, BLEVE generated stronger overpressures. The smaller orifice areas would delay and reduce the first peak pressure. In contrast, the higher liquid superheating degree led to a stronger peak overpressure. Furthermore, Chen et al. [46] conducted a similar BLEVE experiment using a vertical rectangular vessel to observe the boiling process and the process of two-phase flow. The 60% fill ratio, 19.6% orifice area, 230 kPa of initial pressure and 398 K initial temperature were selected to study the BLEVE internal pressure-time profile of two-phase flow at the top and bottom of the vessel. Chen et al. [45, 2008] used a heating source installed inside the vessel. However, in reality, external fires often initiate the BLEVE accidents. The authors did not investigate the difference between the internal and external heating generated BLEVE consequences. Furthermore, Eyssette [47] studied near field overpressure from water BLEVE with 60% liquid ratio, using the same experiment apparatus as Birk et al. (i.e. 0.0006 m³ aluminium tube). Both partial failure and complete failure conditions were tested. The authors found that the vessel fully opened when the ratio of crack length to vessel diameter was larger than 1.

It is worth mentioning that the weakened groove size significantly affects the rupture pressure and further affects the near-field overpressure. The effect of groove length and depth has been studied in the experiments. However, the effects of groove width and the width to vessel volume ratio have not been discussed yet. Moreover, although the ground loading effect on near-field overpressure was studied, no researchers have ever investigated the drag loading effects. Additionally, the testing tube with only one thickness was considered in the experiments. Therefore, the wall thickness's influence on the rupture and external overpressure was not clear. Furthermore, only small-scale

experiments to predict the near-field overpressure were conducted. It is therefore necessary to perform large-scale experiments to explore more realistic cases.

2.2.2 Far-field overpressure prediction

In terms of the far-field overpressure, it was concluded that the overpressure recorded in the far field is due to the shock wave propagation [28]. Namely, the shock wave carries the energy by changing the surrounding pressure as it propagates, resulting in the far-field overpressure. In other words, the prediction of far-field overpressure heavily depends on the initial external pressure and energy source in the near field.

The main components of LPG, propane and butane are often studied in far-field overpressure investigations. For instance, Melhem et al. [48] from the National Fire Protection Association (NFPA) conducted several small-scale 1.893 m³ propane BLEVE experiments under different heating sources to study the BLEVE overpressures. Johnson and Pritchard [49] performed a series of medium-large-scale BLEVE experiments containing butane and propane in a 5.689 m³ or 10.796 m³ tank with different liquid fill ratios and rupture pressures to record the generated overpressures in the far field. In addition, Balke et al. [50] conducted even larger scale BLEVE experiments in a 45 m³ full-scale tank filled with 22% propane. The authors observed the heating behaviour and failure strength limits of the tank. In order to study the LPG for residential usage purposes, Stawczyk [51] conducted a BLEVE experiment using 5 kg or 11 kg standard cooking gas cylinder filled with the propane or mixture of propane and butane. The experiments were carried out using different liquid fill ratios and confinement conditions in the study. It was concluded that the liquid fill ratio determined the maximum rupture pressure of tank, and BLEVE in confined space should generate higher overpressure than that in open space. Birk and VanderSteen [15] performed a 1.8 m³ propane BLEVE test with 10% to 50% liquid ratio. The authors found that the partially opened vessels did not necessarily cause a BLEVE, whereas the BLEVE would occur when the vessel was fully opened. BLEVE occurred when the critical crack length was larger than one vessel diameter hence the critical crack length was determined for judging whether BLEVEs could be initiated or not. However, the relationship between the critical crack length and the vessel diameter needs to be further investigated, especially when the liquid fill ratio is larger

than 50%. Later, to investigate the non-superheated and superheated BLEVEs' consequences in the far field, Birk et al. [28] conducted another medium-scale propane BLEVE experiment. 0.4 m³ and 2 m³ cylindrical tank were selected as experiment vessels. Under different fill ratios, tank rupture pressures and temperature conditions, the non-superheated and superheated BLEVEs were graphically recorded. According to the data, it was concluded that the superheated BLEVE generated stronger overpressure than that of the non-superheated BLEVE.

Other flammable materials, such as propylene and Liquefied Natural Gas (LNG) were also the research focuses in the far-field BLEVE overpressure studies. For instance, Giesbrecht et al. [52] carried out various propylene BLEVE experiments to analyse the peak pressures of BLEVEs in different cylindrical vessels and investigate the relationship between the peak pressure and distance. The experimental vessels with different diameters and wall thicknesses were used while the heating condition and initial internal pressures were constant. Betteridge and Phillips [53] carried out a series of medium-large-scale BLEVE experiments containing LNG in 0.935 m³ and 5.055 m³ tanks with different liquid fill ratios and initial conditions. The experimental equipment was the same as those used by Johnson and Pritchard [49]. However, the investigation object was changed from LPG to LNG. The overpressure-time history profiles were obtained to study the LNG explosion mechanism. Compared to the LPG explosion, it was found that the LNG BLEVE generated blast wave with longer duration and lower peak overpressure than that of LPG BLEVE.

Additionally, the BLEVE triggered by non-flammable materials was investigated. Heymes et al. [54] performed a series of water BLEVE experiments using a 0.014 m³ vertical tube to study the far-field overpressures. The overpressure in the vertical, 45° and horizontal directions was measured and analysed under 398 K temperature and 7500 kPa internal pressure. Compared to the smaller influence of the liquid fill ratio on the overpressure generation, it was found that the vent size of the outlet has a much stronger effect on the BLEVE consequence. By using the high-speed camera and conducting the data analysis, it was observed that the second peak overpressure occurred during the liquid boiling process. In other words, the liquid flashing provided more energy to the second peak. For safety considerations, the vessel tube was designed to withstand the intense pressure change (i.e., depressurization and re-pressurization) without damaging the structure itself. However, in reality, the vessel

walls could be completely busted. Such scenarios in experiments should also be considered.

To sum up, the essential factors (i.e., liquid fill ratio, tank volume and failure conditions) that influence the far-field overpressures have been investigated by different researchers. However, the number of experiments and the experimental conditions to investigate these factors are limited. For instance, there is a lack of the experiment with high liquid fill ratios (i.e., the liquid fill ratio larger than 50%) to investigate the effect of the groove length to vessel diameter ratio on BLEVE's far-field pressure. Furthermore, the overpressure propagation in the far-field is directional. In other words, the far-field overpressure along the tank's longitudinal axis is different from that recorded in the perpendicular direction, but in most of the tests reported in the literature usually only measurements in the perpendicular direction were conducted. Therefore, more studies on the far-field overpressure in different directions should be carried out in the future. Moreover, the confinement and obstacle effects on far-field overpressures have not been explored yet as most reported tests were conducted in open space. Therefore, experiments that study the effects of confinement and obstacle ratio on BLEVE pressures need to be conducted.

2.2.3 Theoretical-based empirical models and comparison

In the above section, the experimental studies on the critical parameters of tank rupture pressure, rupture temperature, liquid fill ratio, tank's volume, etc., have been reviewed. Some of these experimental data were used to verify the theoretical-based empirical models that are commonly used in practice to predict BLEVE overpressures. It should be noted that since the available experimental data are limited, most of these theoretical-based empirical models were proposed based on simplified fluid thermodynamics and gas behaviour assumptions. As a result, some prediction errors are expected. This section reviews these theoretical-based empirical models and evaluates their prediction accuracy against the testing data available in the literature.

2.2.3.1 Theoretical-based empirical models

The theoretical-based empirical models, such as TNT equivalence method, TNO Multi-Energy method (MEM) and Barker-Strehlow-Tang (BST) method, are most commonly used in industry for gas explosion overpressure prediction. These methods

have their respective pros and cons. Taking the TNT equivalence method as an example, TNT is a high explosive which generates blast waves with rather different characteristics from gas explosions in terms of amplitude, duration and rise time. Pressure waves from gas explosions usually have lower amplitude, longer duration and slower rise time compared to those from TNT explosions with the same energy [19]. However, the TNT equivalence method gained popularity in predicting gas explosion overpressures in practice probably because it is straightforward to use. Nonetheless, it should be noted that the TNT equivalence method is only suitable for predicting far-field overpressures generated from the symmetrical gas explosion geometry scenarios [11, 28]. When using this method to study gas explosions, the energy in a vapour cloud is converted into an equivalent TNT charge weight. Additionally, the yield factor used for the TNT charge weight conversion is difficult to determine since the fuel released for blast wave generation is uncertain. Some researchers consider that the yield factor depends on the total amount of fuel, while others believe only vapour cloud within the flammable range plays a significant role. The amount of fuel indeed can affect the yield factor, which in turn affects the determination of the equivalent TNT charge weight. Meanwhile, the specific combustion mode (i.e., deflagration or detonation mode) also significantly influences the prediction results. However, the deflagration and detonation status of combustion is not considered in the TNT equivalent method [55]. Compared to the TNT equivalence method with a strong dependency on the yield factor determination, the TNO Multi-Energy method and Barker-Strehlow-Tang method heavily rely on the selection of blast curves to predict gas explosion overpressures. Unlike the TNT equivalence method, the confinement level, obstacle ratio and reactivity of the fuel-air mixture that affect the initial blast strength (i.e., Mach number) are considered in the TNO Multi-Energy method and Barker-Strehlow-Tang method [11]. However, the prediction of a blast resulting from the asymmetric vapour cloud shape is out of the capability of these two methods [11, 55].

It is worth mentioning the above theoretical-based empirical methods are more commonly used for the estimation of vapour cloud explosion (VCE), which has a more prolonged blast wave duration. In contrast, a BLEVE generates a sharper blast wave with a shorter duration, as shown in Figure 2-3. Therefore, using the same theoretical-based empirical models to predict BLEVE overpressures may result in larger errors. Considering the different overpressure-time profiles and mechanisms of BLEVE,

different thermodynamics and energy laws were used by researchers to develop more BLEVE-suitable theoretical-based empirical models. For instance, based on a larger number of previous comparative and analytical studies [10, 56-59], Hemmatian et al. [60] conducted a comprehensive comparison of the BLEVE overpressure predictions. The authors compared the theoretical-based empirically calculated data and experimental data, and concluded that because of the isentropic expansion, isothermal expansion, ideal gas behaviour and constant volume energy assumptions, the predicted overpressures using the theoretical-based empirical models were conservative [61-66]. In contrast, the predicted overpressures were much closer to the experimental data if the real gas behaviour and adiabatic irreversible expansion (RAIE) were assumed [67, 68].

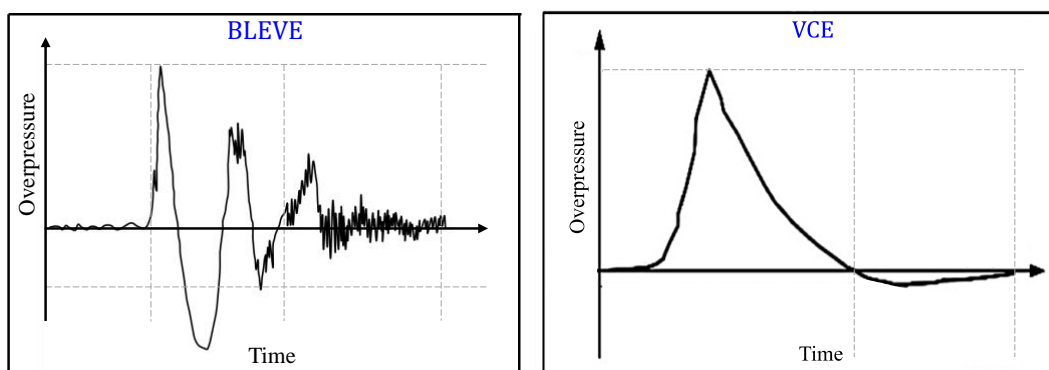


Figure 2-3. Typically BLEVE [28] and VCE [11] overpressure-time profiles.

Based on the RAIE assumption and TNT curves, Planas-Cuchi et al. [68] proposed a BLEVE prediction model by considering the three states during the BLEVE (i.e. initial state, explosion state and final state). Mechanical energy using this method is the difference between the total internal energy in the final state and the explosion state. Since the amount of mechanical energy that contributes to breaking the containment vessel and ejecting the fragments is uncertain, the energy used to generate overpressure is difficult to obtain. In this model, the authors assumed that the energy conversion rate to generate overpressure is 40% for ductile failure and 80% for fragile failure. Subsequently, the equivalent TNT mass and scaled distance can be obtained. However, vapour volume and liquid volume in the explosion state are difficult to determine because the phase transition of the internal vessel is complex before the BLEVE occurs. Additionally, Casal and Salla [67] presented a simple BLEVE pressure prediction method. This method introduced the superheating energy (SE) into the TNT equivalence method to obtain the BLEVE energy and determine the equivalent TNT

mass. The superheating energy is the liquid enthalpy difference between the ambient boiling temperature and superheat limit temperature during energy balance. Through multiplying the SE by the mass of liquefied fuel in the vessel, mechanical energy can be obtained. Since different thermodynamic processes are assumed, the amount of mechanical energy converted to overpressure is different. The conversion rate in the isentropic process is 7% to 14% SE, while the conversion rate in the irreversible process is between 3.5% and 5% SE. The authors also provided the conversion rate of commonly used BLEVE fuels for both processes. However, this method only considered the liquefied fuel and ignored the vessel's previously existing vapour. The error will be generated when the liquid fill ratio is low since the previously existing vapour will also contribute to the blast wave during the BLEVE. To simplify the overpressure prediction model, Hemmatian et al. [69] further proposed a new theoretical-based empirical method considering the liquid fill ratio and failure temperature. The updated method was developed to reflect the real gas behaviour and adiabatic irreversible expansion and provided the yield factor. Therefore, the equivalent TNT mass and scaled distance could be more accurately calculated. However, the shape effect of the BLEVE vessel still could not be considered in the new theoretical-based empirical method. Furthermore, Laboureur et al. [29] proposed two theoretical-based empirical models for the near-field (i.e., within 10 times the tank diameter) BLEVE overpressure prediction. The theoretical-based empirical models were calibrated using the experimental data obtained from BLEVEs of partially ruptured and completely failed tanks. The authors assumed that the fluid in the BLEVE was an ideal gas, while the expansion process was adiabatic.

Since the BLEVE pressure prediction is essential for designing effective and appropriate structural protection measures to minimize the BLEVE effects, prediction methods require high accuracy. Hence, the performance of BLEVE theoretical-based empirical models need be further evaluated. The comparison of the experimental results and theoretical-based empirical models with RAIE assumption (i.e., Casal and Salla's model, Planas-Cuchi's model and Hemmatian' model) are shown in Section 2.2.3.2. Since other theoretical-based empirical models without RAIE assumptions have been relatively conservative, as proved by Hemmatian et al. [60] mentioned above, this paper does not evaluate and discuss the accuracies of the other methods.

2.2.3.2 Comparison of theoretical-based empirical models with experimental data

To validate the accuracy of the theoretical-based empirical models with RAIE assumptions, the predicted results are compared with experimental data in the literature [15, 28, 49]. The detail experimental parameters and results are given in Table 2-1, including the fluid types, liquid fill ratio (*LFR*), tank failure pressure (*P_i*), tank volume (*V*), distance from the BLEVE tank to the measurement point (*r*) and the experimental results (*P_{exp}*). The comparison of pressure prediction results from theoretical-based empirical models (i.e., Hemmatian’ model (*P_{Hem}*), Casal and Salla’s model (*P_{CS}*) and Planas-Cuchi’s model (*P_{PC}*) and experimental data are also given in Figure 2-4, and the corresponding average errors are presented in Table 2-1. The performance ranking of theoretical-based empirical models is also evaluated. When the predicted data is within 25% deviation from the experimental data, the predicted performance is ranked as ‘Excellent’. When the prediction error is between 25% and 50%, the predicted results are ‘Acceptable’. If the prediction error is larger than 50%, the model is considered not performing well [70].

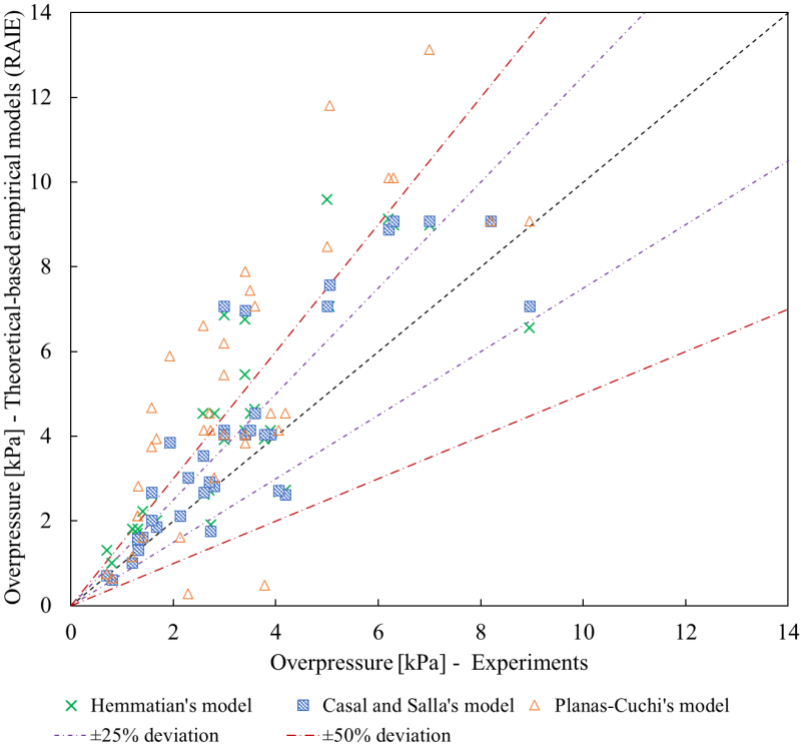


Figure 2-4. Comparison of the theoretical-based empirical models with the experimental data.

The theoretical-based empirical models' performance with RAIE assumptions is shown in Figure 2-4. More than half of the data predicted by the Casal and Salla's model are within the 25% deviation range, while less than a third of the prediction results are within the 25% deviation range for both Hemmatian's model and Planas-Cuchi's model. Additionally, the majority of predicted data using Casal and Salla's model are in the 50% deviation range compared to the experimental data. Whereas around two thirds of the predicted data using the Hemmatian's model fall in the 50% deviation range, and less than half of the data obtained from the Planas-Cuchi's model are within the 50% deviation range. Furthermore, the average errors of the Hemmatian's model, Casal and Salla's model and Planas-Cuchi's model are 44.38%, 30.78% and 69.11%, respectively. The comparison above reveals that Casal and Salla's model has the best prediction performance. However, the average error is still larger than 25% (i.e., the excellent performance rank).

These theoretical-based empirical models were proposed based on reasonable assumptions and experimental data. One limitation is that they cannot model the complex geometry effect on overpressure development. Therefore, these models are exclusively suitable for investigating BLEVEs occurring in simplified and symmetrical explosion scenarios. Additionally, since only a portion of BLEVE energy could be converted into overpressure generation, the reliable determination of the conversion rate in the theoretical-based empirical formula remains a challenge. Therefore, the accuracy of the final prediction results cannot be guaranteed. To obtain more accurate BLEVE overpressure prediction results, numerical simulations become more and more popular, which are discussed in Section 2.3 in more details.

Table 2-1. Comparison between the experimental data and theoretical-based empirical models with RAIE assumption.

Fluid	P_i [kPa]	LFR	V [m^3]	r [m]	P_{exp} [kPa]	P_{Hem} [kPa]	P_{CS} [kPa]	P_{PC} [kPa]
butane	1460	0.75	5.659	25	6.20	9.14	8.89	10.10
				100	1.30	1.72	1.52	2.12
	1510	0.76	5.659	25	6.30	8.99	9.09	10.10
				50	3.90	4.14	4.04	4.55

Table 2-1 (Continued)

Fluid	P_i [kPa]	LFR	V [m ³]	r [m]	P_{exp} [kPa]	P_{Hem} [kPa]	P_{CS} [kPa]	P_{PC} [kPa]
butane	1520	0.38	5.659	25	5.00	9.60	7.07	8.48
				50	2.80	4.55	2.83	3.03
				100	1.20	1.82	1.01	1.16
				150	0.80	1.01	0.62	0.66
	1510	0.4	10.796	25	8.20	14.14	9.09	9.09
				50	3.40	5.45	4.04	3.84
				100	1.40	2.22	1.62	1.62
				150	0.70	1.31	0.71	0.76
	1520	0.76	5.659	25	7.00	8.99	9.09	13.13
				50	3.40	4.14	4.04	4.04
				100	1.30	1.62	1.58	2.12
	propane	1863	0.17	2	20	3.50	4.55	4.14
30					4.19	2.73	2.63	4.55
40					2.73	1.92	1.77	4.14
1846		0.35	2	20	3.78	3.94	4.04	0.48
				30	2.29	3.03	3.03	0.28
				40	2.13	2.12	2.12	1.62
1894		0.21	2	40	1.68	2.02	1.87	3.94
1573		0.12	2	20	2.58	4.55	3.54	6.61
				30	1.58	2.63	2.02	4.68
				40	1.31	1.82	1.31	2.83
1803		0.51	2	20	8.95	6.57	7.07	9.09
				30	2.99	3.92	4.14	4.04
	40			4.06	2.69	2.73	4.14	
1563	0.52	2	20	3.40	6.77	6.97	7.90	
			30	1.93	3.84	3.86	5.90	

Table 2-1 (Continued)

Fluid	P_i [kPa]	LFR	V [m ³]	r [m]	P_{exp} [kPa]	P_{Hem} [kPa]	P_{CS} [kPa]	P_{PC} [kPa]
propane	1563	0.52	2	40	1.58	2.68	2.68	3.76
	1813	0.53	2	20	2.99	6.87	7.07	6.20
				30	2.99	4.04	4.04	5.45
	1813	0.53	2	40	2.60	2.63	2.69	4.14
				20	5.05	7.07	7.58	11.82
	1858	0.61	2	30	3.59	4.65	4.55	7.07
				40	2.70	2.73	2.93	4.55
	Average Error (between theoretical-based empirical models and experimental data)						44.38%	30.78%

2.3 Numerical study of BLEVE overpressure prediction

Compared to the experimental study, the numerical study has gained more popularity in both industry and academia since conducting numerical simulation is less expensive than performing an experimental test. Moreover, compared to the aforementioned theoretical-based empirical models, the complex geometries/scenarios of BLEVE can be numerically modelled for more accurate pressure predictions in both the near field and the far field. This section reviews the most widely-used Computational Fluid Dynamics (CFD) models and the artificial intelligence (AI) algorithm for the BLEVE overpressure estimation, as well as numerical-based empirical models and comparisons with experiments.

2.3.1 FLACS

There are a few CFD models for explosion overpressure prediction. Most of these models were designed for VCEs, and only very few models have been validated and applied for modelling BLEVEs. Among these models, the Flame Accelerator Simulator (FLACS), validated against a complete experimental database and widely accepted by industries worldwide, is a user-friendly CFD software used to simulate

different types of gas explosions, including BLEVEs [70]. The FLACS code solves three-dimensional transient gas dynamic partial differential equations using Reynolds-averaged Navier–Stokes (RANS) equations. A finite volume method and a defined number of control volumes are used in FLACS simulation [71]. The geometrical details of simulation can be imported from Auto-CAD or defined in the pre-processor of CASD in FLACS. The $k - \varepsilon$ turbulence model is applied in FLACS to calculate the turbulent burning velocity [72, 73]. Compared to other CFD models, the geometry modelling in FLACS is straightforward, the simulation procedures are more accessible, and the good quality of meshing grids can be readily guaranteed. Therefore, FLACS has become one of the most popular CFD software in the industry [74].

FLACS has been more commonly used in the studies of VCEs. For instance, Rui et al. [75] investigated the overpressure of the vented gas explosion in a 1 m³ rectangular stainless vessel with low vent burst pressure. Wang et al. [76] studied the effect of the vessel size, length of connection pipe and ignition location on VCE overpressure in a linked vessel. Li and Hao [77] predicted the overpressures of vented gas explosions in medium-scale cylindrical tanks with different vent areas and gas concentrations. For these VCEs, the explosion sources, congestion environment and ignition conditions are ready to be modelled using FLACS. Whereas for BLEVEs, it is not straightforward to use FLACS to set up the explosion scenarios. The main reason is that there are two different pressure regions (i.e., vapour region and liquid region) in BLEVE which cannot be modelled by following the standard FLACS simulation procedure [22]. Therefore, Hansen and Kjellander [21] proposed a method that the liquid flashing of BLEVE is modelled using a pseudo-source in FLACS. The pseudo-source is used to determine the rupture pressure attributed to the liquid phase. It was assumed that around 20% of the initial rupture pressure was equal to the pressure in the pseudo-source. A back-forward calculation method was used to determine BLEVE pressure in the numerical study. Hutama [22] further investigated BLEVE overpressures by using the FLACS simulation method proposed by Hansen and Kjellander [21]. However, unlike the open space scenarios investigated earlier, a series of BLEVEs were modelled both in the uncongested and congested tunnels. One simulation case was a 2 m³ propane BLEVE with a 21% liquid fill ratio and 1900 kPa initial pressure, while the other was a 37.85 m³ LPG BLEVE with a 60% liquid fill ratio and 1700 kPa initial pressure.

Furthermore, Li and Hao [23] proposed two CFD methods (i.e., the liquid correction method and shock tube method) to predict BLEVE overpressures by using FLACS based on the concept mentioned above. Since only one high-pressure region can be used in FLACS, the pseudo-source was introduced in the simulation to obtain the overpressure effect from the liquid flashing process. The liquid correction method can simulate the vapour expansion and liquid flashing simultaneously. However, the predicted pressures may be slightly overestimated. In comparison, the shock tube method was proposed to model vapour expansion and liquid flashing separately. It was stated that the predicted overpressures were marginally more accurate by the shock tube method than the liquid correction method. However, the shock tube method required more preliminary assumptions, which was not straightforward to use if it lacked critical experimental data for validation. Li and Hao [7] also studied BLEVE overpressure in a congested environment using the liquid correction method. The influences of obstacles on blast wave propagation, reflection and diffraction were investigated. The overpressure in front and behind an obstacle wall was analysed by comparing the pressure-time profile between the BLEVE occurred in an open space and a congested area. A realistic case, i.e., the Bologna highway accident, was investigated by modelling the complex geometries in three dimensions. However, due to many uncertain factors, only a simplified prediction was made for this accident. Regarding the confinement effect on BLEVE overpressure generation, Li et al. [78] used FLACS to study a more complex BLEVE scenario occurring in tunnels. The large scale BLEVEs in the circular and rectangular tunnels were investigated. The reflected pressure was obtained by using FLACS with the liquid correction method. The authors considered the incident angles in different planes (i.e., the x-y, y-z and x-z planes) in obtaining the reflected pressure and the velocity of the reflected blast wave in the tunnel. It was seen that the incident pressures with different incident angles would result in different reflected pressures. It is worth mentioning that the liquid flashing in FLACS was still modelled simultaneously with the vapour expansion. The real-time difference between the instant vapour expansion and delayed liquid flashing could not be considered in the authors' CFD method. Further investigations of the delayed liquid flashing need be conducted.

2.3.2 ANSYS Fluent

ANSYS Fluent is another CFD software using Reynolds Averaged Navier-Stokes equations and finite volume method to model complex turbulent flows in a gas explosion. The complex geometries and different mesh cells (e.g., coarse, medium and fine mesh cells) can be generated in ANSYS Fluent's 3D model. However, unlike FLACS, which uses $k - \varepsilon$ model exclusively, different turbulence models, such as $k - \varepsilon$, $k - \omega$ and Reynolds Stress model, are available in ANSYS Fluent for different numerical simulations [79].

Similar to FLACS, ANSYS Fluent is also a popular CFD tool for VCE overpressure prediction, but its application for BLEVE simulation is very limited. For instance, Scarponi et al. [80] observed the pressure build-up of LPG tanks exposed to fire until BLEVE occurred using a 2D model in ANSYS Fluent. In another study, Scarponi et al. [81] extended the work and developed a 3D model in Fluent to analyse the internal pressure before BLEVE occurrence to more accurately predict the internal fluid behaviour after the failure of a pressure relief valve. In addition, Zhao et al. [82] used ANSYS Fluent to investigate the CO₂ BLEVE in a symmetrical cylinder. A 2D rectangular model was developed as the simplified model to study the changing process of pressure during BLEVE development. The internal pressure dropped rapidly when the vessel opened, causing the superheated liquid to boil violently and rapidly and form a two-phase expanding flow. The CO₂ gas was generated during the phase change; the subsequent two-phase flow pushed the vapour outwards, increasing the external pressures. As the density of the two-phase flow decreased, the push ability was reduced. Therefore, the pressure dropped over time. It is worth pointing out that the above investigated numerical model was only in two dimensions (2D). Although the 2D simulation can capture the essential BLEVE characteristics, more realistic cases should be modelled in three dimensions (3D). By far, no existing literature with the realistic 3D model by using ANSYS Fluent has been reported yet.

2.3.3 Artificial Neural Network method

Compared to expensive physical experiments, the CFD methods indeed have the advantages of reducing the investigation cost and enabling engineers to simulate different physical BLEVE conditions numerically. However, individual CFD

simulations should be conducted for each study case, and it is still computationally costly. Therefore, Artificial Intelligence (AI) methods have been proposed to balance the pressure prediction accuracy and efficiency [83]. As a part of the numerical study tools, AI has been rapidly developed and applied to various fields. It can reduce human errors and achieve accuracy with high speed. By applying AI algorithms, a series of initial data obtained from experiments or numerical simulations can be used to derive the AI-based equations, which can then be used to predict the overpressure of gas explosions more efficiently.

The Artificial Neural Network (ANN), which is one of the most popular methods using the AI algorithm for the BLEVE overpressure prediction, is reviewed in this paper. The analysis procedure of ANN was developed based on the biological neural network (BNN) of the human brain. In the human brain, neurons are the essential BNN elements. A neuron receives data from neighbouring neural cells by dendrites, synapses then transfer the data between two neurons in electrochemical signals. In comparison, the ANN has the same pattern as the BNN that can solve a complex problem by parallel and distributed processes, as shown in Figure 2-5.

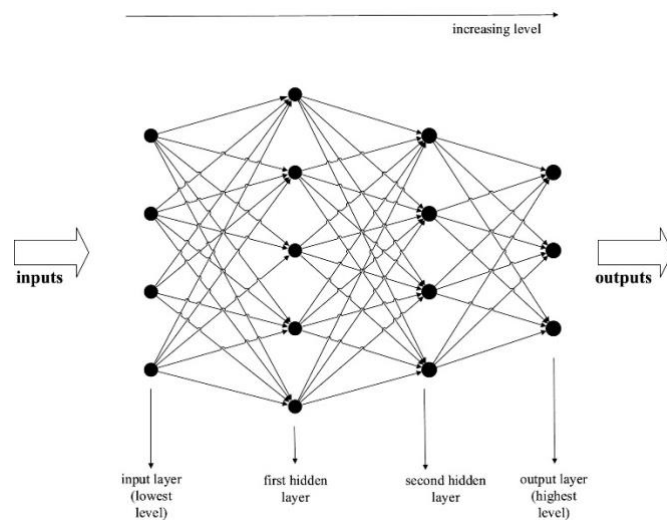


Figure 2-5. ANN structure [84, 85].

Each neuron model contains a segment that functions like a synapse to import signals (i.e., input data). Initially, each input (x_i) is multiplied by the synaptic connection weight (w_i), and a bias value (b) is introduced to obtain relatively accurate results. Then, all results are entered into a transfer function (f) to get the output value (y). Equations (2-1) and (2-2) are listed below. Figure 2-6 illustrates the content of the feedforward neuron network [84]. A network including more than one layer can be

divided into two types, namely feedforward neural networks and feedback neural networks [84]. When predicting explosion overpressure, the feedforward neuron network is chosen.

$$net = \left(\sum_{i=1}^n w_i x_i \right) + b \tag{2-1}$$

$$y = f(net) \tag{2-2}$$

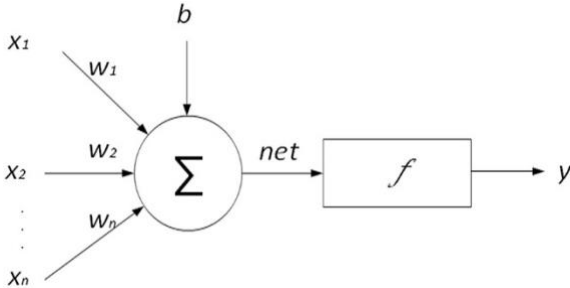


Figure 2-6. Feedforward neuron network [84]

The advantages and limitations of ANN are summarized in Table 2-2. In using ANN, the main task is to define the weights and biases with minimum errors. Then, a training algorithm is introduced to modify the weights and biases. The backpropagation (BP) algorithms, such as the Levenberg - Marquardt, Bayesian Regularization (BR) algorithm, and Scaled Conjugate Gradient, are commonly used to tune ANN.

Table 2-2. Advantages & limitations of ANN [86].

Advantages	1. Work with incomplete data
	2. Fault tolerance
	3. Machine learning capability by learning similar events
	4. Parallel processing capability
Limitations	1. Difficult to explain the behaviour of the network
	2. Proper network structure only determined by experience and trial and error
	3. Unable to show the problem on ANN, the problem must be translated to numerical values by the user

Numerous unbiased data are required to train a reliable ANN model. Due to the high cost of experiments, it is generally impossible to obtain a large amount of training data by conducting experimental tests only. Therefore, numerical simulations are usually carried out to supplement the data needed for training ANN models. Since the experimental test results and numerical simulation results of BLEVE are limited, only a few studies on BLEVE pressure wave predictions are conducted using the ANN method. Hemmatian et al. [84] estimated the mechanical energy of propane and butane BLEVEs. The datasets used for training the ANN model were calculated using the real gas behaviour and adiabatic irreversible expansion method. Temperature, liquid fill ratio and tank volume as the input data were used to predict the mechanical energy of BLEVE. However, the corresponding peak pressures were predicted using the TNT equivalence method. Since the yield factor is difficult to determine, as discussed above, this ANN model is used for predicting the equivalent BLEVE energy. To predict more accurate peak pressure, Li et al. [24] utilized the CFD model to generate a large dataset of BLEVE-induced pressure time histories in open space for training an ANN model to predict the peak pressure of BLEVE. A thousand propane and butane BLEVE cases with different variable constraints were simulated using FLACS, as shown in Table 2-3. The initial rupture pressure ranged from the experimental lowest rupture value (i.e., 500 kPa) to liquid critical pressure (i.e., 3700 kPa for butane and 4200 kPa for propane). The LPG tank shape was simplified as cuboid, and the volume was selected from 10 m³ to 90 m³, which covers the actual size of most standard LPG tanks. In terms of BLEVE simulation, the aforementioned liquid correction method was applied in FLACS for superheated BLEVE simulation. Only the vapour expansion was modelled for non-superheated BLEVE simulation. The generated training data were used to train the ANN model to predict BLEVE peak pressures at different distances from the explosion. However, the authors only predicted the overpressure perpendicular to the tank axis. The overpressure in other directions needs to be further investigated since the blast wave propagation in the near field, i.e., in the range close to the explosion centre is direction dependent. It is also worth pointing out that the training data were collected from CFD simulation data. Therefore, the CFD-based ANN model will inherit the weaknesses of CFD models as mentioned above.

Recently, some new integrated and hybrid AI models have been developed. These advanced approaches may provide some new methods for training models to predict

BLEVE overpressure. For example, Shi et al. [87] applied the Bayesian Regularization Artificial Neuron Network (BRANN) to the Bauwens models to predict the peak overpressure of the vented gas explosions, which can effectively avoid the overfitting problem. Subsequently, Shi et al. [88] further proposed an NFPA-68-BRANN model to design appropriate vent size to mitigate hydrogen-air mixture explosion within obstructed cubic enclosures. Additionally, more advanced hybrid machine learning models are proposed to predict gas explosion clouds. By considering physical constraints on the basis of machine learning, the interpretable and physically consistent prediction results are obtained [89, 90]. The integrated and physics-guided machine learning algorithms can also be studied in the future for BLEVE overpressure predictions.

Table 2-3. Training variable constraints in ANN model [24]

Variable	Variable options
Tank failure pressure, P_i (kPa)	500 – 3700 (butane), 500 – 4200 (propane)
Liquid fill ratio, LFR (%)	10 – 90
Tank width, W_{tank} (m)	0.2 – 3
Tank length, L_{tank} (m)	0.2 – 10
Tank height, H_{tank} (m)	0.2 – 3
Height of BLEVE, H_{BLEVE} (m)	0 – 2.2
Liquid failure temperature, T_l (°C)	1 – 152 (butane), 1 – 96 (propane)
Vapour failure temperature, T_v (°C)	1 – 304 (butane), 1 – 192 (propane)
Liquid status at failure	superheated or saturated
Vapour height in a tank, H_{vapour} (m)	$H \times (1 - LFR)$
Pressure monitor distance to BLEVE (m)	5 – 50

2.3.4 Numerical-based empirical models

In the above sub-sections, it is concluded that numerical simulations can accurately predict BLEVE overpressures. However, conducting the numerical simulation is time-consuming. For instance, to obtain the overpressure at a distance of 20 m resulting from a 2m³ BLEVE tank, one individual simulation could take hours [24]. In contrast, the ANN method to predict the overpressure generated from the same BLEVE in the same range takes only a few seconds. However, ANN methods require the user to understand programming and to be able to handle a large amount of training data. In other words, ANN methods are not user-friendly. Therefore, numerical-based empirical models have been proposed to simplify and improve the speed of overpressure prediction.

Van Den Berg [91] empirically derived a series of blast charts to predict the BLEVE overpressure from numerical data obtained using the numerical simulation module of BLAST. Different gas properties, including ammonia, butane, carbon dioxide, propane and LNG, are considered in developing the charts. However, it is worth mentioning that the author considered only the vapour expansion energy and neglected the liquid flashing energy in the numerical simulations. Therefore, the developed charts may not lead to accurate predictions of blast wave generation and propagation from BLEVEs. Subsequently, these empirical prediction models were further developed by Laboureur et al. [29] through introducing a series of new decay coefficients. Additionally, Wang et al. [92] developed BLEVE pressure prediction equations and charts using the training data from FLACS and a CFD-based ANN model, which reasonably considered vapour expansion and liquid flashing energy. When the failure temperature is above the boiling point but below the SLT of internal pressurized liquid, only vapour expansion provides BLEVE energy. Whereas, when failure temperature is higher than the SLT, liquid flashing replenishes the vapour expansion energy, resulting in the BLEVE waves. However, the newly-proposed empirical methods are only suitable for estimating BLEVE overpressures in open space.

When the BLEVE occurs in a congested environment, the reflection and diffraction of pressure wave need to be considered. Li and Hao [7] derived a series of empirical overpressure prediction equations based on the numerical simulation data. The authors considered the interactions between the BLEVE overpressure wave with surrounding environments. The isentropic expansion theory was used to calculate the overpressure

generation energy. It was concluded that when an obstacle exists in the BLEVE wave propagation path, a portion of blast waves would be reflected and diffracted. In front of an obstacle, the reflected pressure could superimpose the incident pressure, thereby strengthening the final overpressure magnitude. Pressures might weaken at locations behind the obstacle due to the blast shadowing effect. However, the diffracted pressure and the reflected pressure from the ground could enhance the pressure in the far field. The authors provided empirical equations to estimate overpressures in front of and behind the obstacle wall by considering these effects. Furthermore, Li et al. [78] derived another empirical method to obtain the BLEVE overpressures inside a tunnel. The main improvement of this empirical method, which was developed using FLACS simulation data, was that the confinement effects on blast reflection and diffraction in a complex environment were considered. Moreover, this proposed empirical method was proved to be effective for the overpressure prediction in two types of tunnels (i.e., circular and rectangular tunnels). However, this empirical model was only validated using CFD simulation data since no BLEVE experiments have ever been carried out inside a tunnel. In other words, it is worth conducting confined BLEVE experiments in the future to further evaluate this empirical model. The performance of BLEVE numerical-based empirical models occurring in open space are evaluated below.

In general, compared to the theoretical-based empirical models, the rise time and duration of BLEVE in numerical-based empirical models can be predicted more accurately since the theoretical-based empirical models are based on various thermodynamics assumptions and TNT-equivalence approach. The numerical-based empirical models take three-dimensional geometrical effects into account. Therefore, the overpressures resulting from complex and asymmetrical explosions with different BLEVE shapes can be estimated. However, the delayed liquid flashing still could not be accurately calculated. Furthermore, the numerical-based empirical models are only compared to the BLEVE occurring in open space, since BLEVE experiments have not been performed in congested areas. Additional experiments that consider the congestion and confinement effects should be carried out to calibrate these empirical models.

2.3.5 Comparison of numerical simulation models

2.3.5.1 Comparison of numerical-based empirical models with experimental data

Based on the high precision of CFD models, numerical-based empirical models are developed to efficiently and accurately predict BLEVE overpressure. To verify the accuracy of the numerical-based empirical models, the prediction results are compared with experimental data (i.e., the available experimental data presented in Section 2.3.2). Table 2-4 presents the comparisons of the results from experimental tests and numerical-based empirical models, including the Van Den Berg's model (P_{VDB}), Laboureur's model (P_L), and Wang's models (P_{W-E} & P_{W-C}). The performance of the numerical-based empirical models is clearly shown in Figure 2-7. Most predictions from the Van Den Berg's model highly overestimate the BLEVE pressure with an average error larger than 50% (i.e., 57.34%). The Laboureur's model improved the Van Den Berg's model (i.e., adding decay coefficients), which greatly enhanced the accuracy of the predictions. Although its average error has reduced to an 'Acceptable' level of 35.99%, more than a quarter of predictions significantly underestimate the BLEVE pressures (i.e., 50% smaller than experimental data). It is worth mentioning that the Van Den Berg's model (P_{VDB}) and Laboureur's model ignore the liquid flashing energy and only consider the vapour expansion energy. Recently, Wang's equations and charts comprehensively considered the contribution of liquid flashing energy to BLEVE overpressure, which improved the prediction accuracy, with average errors of 28.38% and 32.90%, respectively from the empirical equations and charts. Among them, Wang's equations yield the most accurate predictions, with more than half of the results within the 25% deviation range and the majority of them falling in the 50% deviation range.

Table 2-4. Comparison between the experimental data and numerical-based empirical models.

Fluid	P_i [kPa]	LFR	V [m ³]	r [m]	P_{exp} [kPa]	P_{VDB} [kPa]	P_L [kPa]	P_{W-E} [kPa]	P_{W-C} [kPa]
butane	1460	0.75	5.659	25	6.20	10.06	3.09	6.40	7.00
				100	1.30	2.12	0.69	1.14	1.94
	1510	0.76	5.659	25	6.30	10.11	3.09	7.03	7.09

Table 2-4 (Continued)

Fluid	P_i [kPa]	LFR	V [m ³]	r [m]	P_{exp} [kPa]	P_{VDB} [kPa]	P_L [kPa]	P_{W-E} [kPa]	P_{W-C} [kPa]
butane	1510	0.76	5.659	50	3.90	4.64	1.46	3.28	5.43
				25	5.00	7.80	3.09	7.97	7.11
				50	2.80	3.58	1.46	3.04	3.15
	1520	0.38	5.659	100	1.20	1.64	0.69	1.16	1.33
				150	0.80	1.04	0.45	0.66	0.80
				25	8.20	10.13	3.09	11.47	9.53
	1510	0.4	10.796	50	3.40	4.65	1.46	4.38	4.09
				100	1.40	2.14	0.69	1.67	1.73
				150	0.70	1.35	0.45	0.95	1.05
	1520	0.76	5.659	25	7.00	10.11	3.09	5.85	11.07
				50	3.40	4.64	1.46	2.24	5.43
				100	1.30	2.13	0.69	0.85	2.06
propane	1863	0.17	2	20	3.50	5.02	3.49	5.86	5.27
				30	4.19	3.17	2.22	3.34	3.87
				40	2.73	2.29	1.61	2.24	2.70
	1846	0.35	2	20	3.78	6.60	3.49	5.11	6.15
				30	2.29	4.16	2.22	2.91	2.86
				40	2.13	3.01	1.61	1.95	2.69
	1894	0.21	2	40	1.68	2.48	1.61	2.20	2.72
				20	2.58	4.40	3.49	5.41	4.12
				30	1.58	2.78	2.22	3.08	2.45
	1573	0.12	2	40	1.31	2.01	1.61	2.06	2.04
				20	8.95	7.60	3.49	7.78	9.73
				30	2.99	4.80	2.22	3.79	3.83
1803	0.51	2	40	4.06	3.46	1.61	2.97	4.17	
			20	3.40	7.66	3.49	3.89	5.31	

Table 2-4 (Continued)

Fluid	P_i [kPa]	LFR	V [m ³]	r [m]	P_{exp} [kPa]	P_{VDB} [kPa]	P_L [kPa]	P_{W-E} [kPa]	P_{W-C} [kPa]
1563	0.52	2	30	1.93	4.84	2.22	2.22	3.04	
			40	1.58	3.49	1.61	1.48	2.53	
1813	0.53	2	20	2.99	7.72	3.49	4.25	5.12	
			30	2.99	4.87	2.22	2.42	3.83	
1813	0.53	2	40	2.60	3.52	1.61	1.62	2.68	
			20	5.05	8.14	3.49	6.01	6.16	
1858	0.61	2	30	3.59	5.14	2.22	3.42	3.86	
			40	2.70	3.71	1.61	2.29	2.70	
Average Error (between numerical-based empirical models and experimental data)					57.34%	35.99%	28.38%	32.90%	

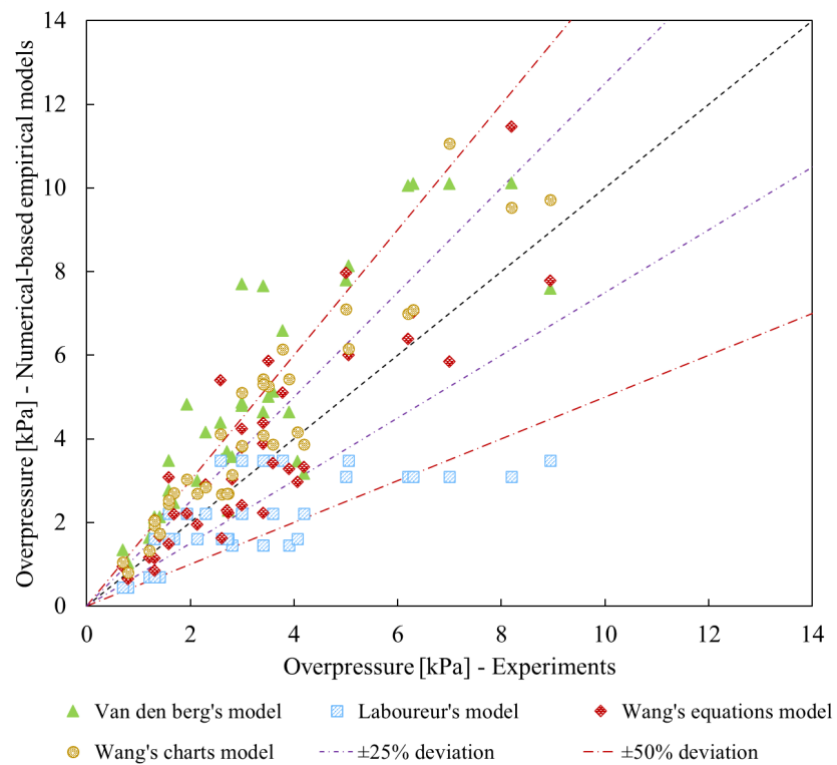


Figure 2-7. Comparison of the numerical-based empirical models with the experimental data.

2.3.5.2 Comparison of numerical models and empirical models with experimental data

To clearly compare the BLEVE prediction models, the average error and computation time for each model are given in Figure 2-8 and Table 2-5, including theoretical-based empirical models, numerical-based empirical models, CFD models and ANN models. Since the developed ANN model is valid only for the BLEVE distance from 5 to 50 m, the same validation cases of Section 2.2.3.2 within 50 m are used. Among them, the theoretical-based and numerical-based empirical models used for comparison are the models with the best prediction performance obtained in the previous section, i.e., the Casal and Salla's model and Wang's equations. It is worth pointing out that the overpressure prediction accuracy of these four models is relatively high, the majority of the prediction results are within 50% errors and more than half of the results have errors less than 25%. Compared with experimental data, the CFD model has the lowest error (i.e., 22.06%), which is within the excellent prediction rank. While the Casal and Salla's model (i.e., 33.73%), Wang's equations (i.e., 29.91%) and ANN model (i.e., 28.64%) have relatively large errors, falling in the acceptable prediction range. Although CFD model can obtain more accurate results than others, it requires a long simulation time. For example, the validation cases used in this paper, a desktop with 10-core and 3.3 GHz CPU took approximately 6 - 8 hours per case. Whereas, empirical models (i.e., theoretical-based and numerical-based empirical model) only need to use their corresponding equations and charts to obtain the prediction results in less than an hour. The fastest prediction methods are using the ANN models, which can make predictions in seconds. However, ANN models need to be developed in advance with a deeper understanding of programming, and also require a large number of reliable training data.

Table 2-5. Comparison among the CFD models, ANN models and numerical-based empirical models.

Fluid	P_i [kPa]	LFR	$V [m^3]$	r [m]	P_{exp} [kPa]	P_{CS} [kPa]	P_{W-E} [kPa]	P_{CFD} [kPa]	P_{ANN} [kPa]
butane	1460	0.75	5.659	25	6.20	8.89	6.40	7.37	8.41
	1510	0.76	5.659	25	6.30	9.09	7.03	7.43	5.98

Table 2-5 (Continued)

Fluid	P_i [kPa]	LFR	V [m ³]	r [m]	P_{exp} [kPa]	P_{CS} [kPa]	P_{W-E} [kPa]	P_{CFD} [kPa]	P_{ANN} [kPa]
				50	3.90	4.04	3.28	3.88	2.57
	1520	0.38	5.659	25	5.00	7.07	7.97	5.04	9.23
				50	2.80	2.83	3.04	2.44	4.01
butane	1510	0.4	10.796	25	8.20	9.09	11.47	9.28	10.27
				50	3.40	4.04	4.38	4.55	4.43
	1520	0.76	5.659	25	7.00	9.09	5.85	7.44	7.11
				50	3.40	4.04	2.24	3.88	3.09
				20	3.50	4.14	5.86	3.15	4.57
	1863	0.17	2	30	4.19	2.63	3.34	1.68	2.82
				40	2.73	1.77	2.24	1.19	2.03
propane				20	3.78	4.04	5.11	3.32	4.39
	1846	0.35	2	30	2.29	3.03	2.91	1.86	2.70
				40	2.13	2.12	1.95	1.25	1.87
	1894	0.21	2	40	1.68	1.87	2.20	1.41	1.99
				20	2.58	3.54	5.41	2.60	4.61
	1573	0.12	2	30	1.58	2.02	3.08	1.47	2.81
				40	1.31	1.31	2.06	1.13	1.91
				20	8.95	7.07	7.78	3.89	7.05
	1803	0.51	2	30	2.99	4.14	3.79	2.08	4.22
				40	4.06	2.73	2.97	1.47	2.88
propane				20	3.40	6.97	3.89	3.52	3.82
	1563	0.52	2	30	1.93	3.86	2.22	1.97	2.37
				40	1.58	2.68	1.48	1.54	1.63
				20	2.99	7.07	4.25	3.92	3.05
	1813	0.53	2	30	2.99	4.04	2.42	2.17	1.83
				40	2.60	2.69	1.62	1.71	1.27

Table 2-5 (Continued)

				20	5.05	7.58	6.01	4.36	6.58
propane	1858	0.61	2	30	3.59	4.55	3.42	2.36	3.92
				40	2.70	2.93	2.29	1.88	2.66
Average Error (between empirical models and experimental data)						33.73%	29.91%	22.06%	28.64%
Calculation/Simulation time (per case)						Around 30 min	6 -8 hours	16 seconds	
							(10-core, 3.3 GHz CPU)		

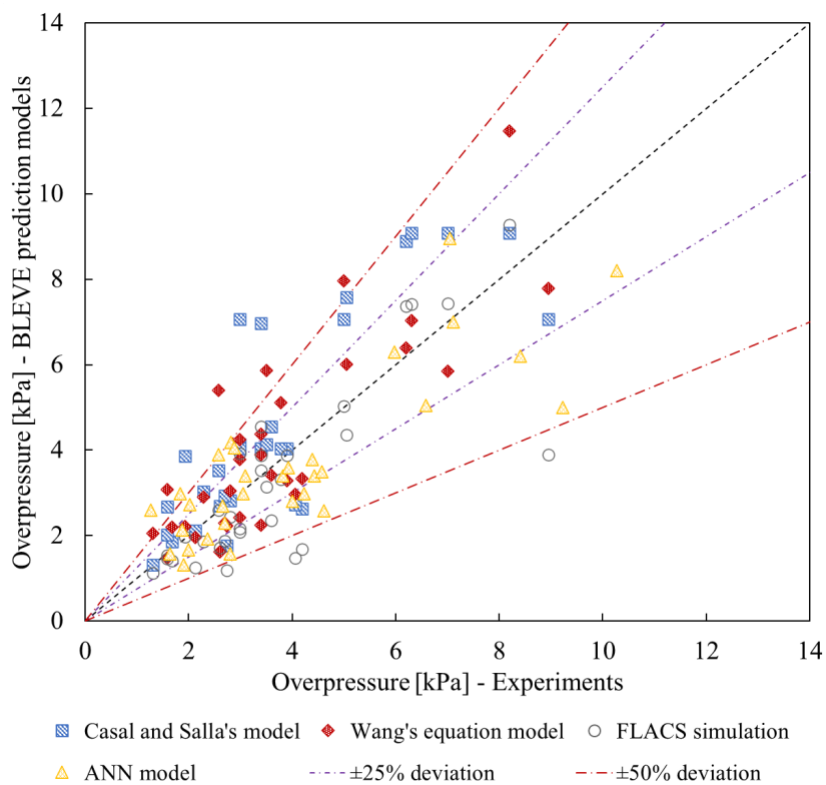


Figure 2-8. Comparison of the empirical model, numerical-based empirical model, CFD model and ANN model with the experimental data.

2.4 Summary

The primary objective of this section is to systematically review the studies of BLEVE overpressure predictions. BLEVE experiments for overpressure prediction both in near-field and far-field are reviewed. Meanwhile, the accuracy and efficiency of empirical methods (i.e., theoretical and numerical-based), numerical simulations and ANN models are discussed. The main conclusions are deduced as follows:

Predicting near-field overpressure is complex due to the nozzle effect on the crack development and the ground loading effect on pressure overlapping. To investigate near-field overpressure, the liquid ratio and weakened grooves as two essential parameters have been analysed by conducting a series of experiments. These two parameters have a great influence on the rupture pressure, which affects the BLEVE overpressure. It is worth mentioning that researchers only used the weakened groove in the experiments. The possible crack shape and crack depth to wall thickness ratio were not studied. The relationships among the wall thickness, crack conditions, and BLEVE overpressure should be further investigated. Additionally, the ground loading effect was studied with different liquid fill ratios and lengths of weakened grooves, however, the drag loading effect on near-field overpressures is still not clear. Lastly, most near-field overpressure experiments were conducted at a small scale, large-scale experiments need to be conducted in the future.

Compared to near-field BLEVE studies, fewer number of far-field BLEVE experiments have been conducted. Most existing experiments were carried out in the open space, and it was concluded that far-field overpressure generation mainly relies on the initial blast energy. However, experiments with different congestion and confinement levels need to be further conducted to investigate the BLEVE-induced pressure wave propagation and interaction with surrounding environments for predictions of BLEVE loads on structures. Additionally, the effect of different pressurized liquid types on BLEVE overpressure was not studied. Meanwhile, more experiments with liquid fill ratios exceeding 60% need also be conducted to ensure that the BLEVE can occur under the same conditions (i.e. when the ratio of groove length to vessel diameter is larger than one). Furthermore, the directional effect of blast propagation should be further analysed.

Based on the different assumptions and experiment validation, the theoretical-based empirical models for predicting BLEVE overpressures have been developed and commonly used in industry. However, these empirical models neglect the effect of complex geometry on pressure development. Additionally, the decisions of the conversion rate for energy calculation were deemed to be arbitrary in these empirical models, thereby affecting the accuracy of BLEVE overpressure prediction. Furthermore, the prediction of these models is based on TNT-equivalence approach, which may not give good predictions of the rise time and duration of BLEVE pressure waves.

In comparison, the CFD model can simulate more complex geometries and obtain more accurate pressure-time profiles. However, CFD simulations are time-consuming. Currently, FLACS is deemed to be the most popular commercial CFD tool in predicting BLEVE overpressures. By far, it is still a technical issue about how to accurately adjust the timing between the vapour expansion and the delayed liquid flashing in CFD simulation.

Compared to the numerical simulation, the recently developed ANN model is efficient in predicting BLEVE overpressures. ANN model can well balance the prediction accuracy and efficiency. However, a large number of training data are required to train a reliable ANN model. Additionally, integrated and physics-guided machine learning algorithms can be adopted to predict BLEVE overpressures.

Based on numerical simulation data, the numerical-based empirical models are proposed. Compared to the theoretical-based empirical models, numerical-based empirical models yield more accurate predictions of pressure wave time history of BLEVE both in open space and congested areas. However, these models inherit the weaknesses of CFD models.

Chapter 3 Prediction of medium to large scale BLEVE pressure in open space

3.1 Introduction

As reviewed in Chapter 2, the current practice in predicting the BLEVE pressure for structural response analysis and design is based mainly on some semi-empirical energy equivalency methods. These methods are relatively easy to use but may not give accurate BLEVE pressure predictions. Using numerical simulations can yield better BLEVE pressure predictions, but it requires profound modelling knowledge and is time-consuming, which may not be viable to many design and consulting offices. This chapter generates empirical formulae and charts for easy and accurate predictions of BLEVE pressure for the analysis and design of structures against BLEVE loads. The empirical relations of critical parameters, namely the side-on peak pressure, peak pressure rise time, duration, arrival time and impulse that are needed to fully define the pressure-time history, as functions of BLEVE parameters are established. The performances of the proposed empirical formulae and charts are evaluated by comparing the prediction results with experimental data. It is proven that the developed BLEVE pressure prediction equations and charts are easy to use and yield more accurate BLEVE pressure predictions than other commonly used empirical methods.

The related work in this chapter has been published in Process Safety and Environmental Protection.

Wang, Y., Li, J., Hao, H., 2022. Development of efficient methods for prediction of medium to large scale BLEVE pressure in open space. Process Safety and Environmental Protection 161, 421-435.

3.2 BLEVE energy calculation

A BLEVE occurs when the internal pressurized liquid is superheated (i.e., failure temperature larger than its boiling point) and the vessel ruptures suddenly with a rapid pressure drop. If the failure temperature of the BLEVE is above its boiling point but below its SLT, the vapour volume of BLEVE is only equal to the vapour space inside

the tank. Whereas if the failure temperature of the BLEVE is larger than the SLT, the liquid flashing energy and the vapour evaporation energy are considered together for the pressure generation calculation. Because when the BLEVE fluid reaches the SLT, a violent phase transition can occur, that is, the phase of the internal liquefied fluid changes instantaneously [11]. Hence, both the vapour expansion and the liquid flashing contribute to an enlarged volume of the BLEVE.

Therefore, the BLEVE energy is determined using the equation proposed by Strehlow et al. [93], as shown in Equation (3-1).

$$E = \left(\frac{P_i}{\gamma - 1} \right) V_{vap}^* \left[1 - \left(\frac{P_o}{P_i} \right)^{\frac{\gamma-1}{\gamma}} \right] \quad (3-1)$$

where P_i = the vessel failure pressure

$P_o = 10^5 Pa$ is the ambient pressure

γ = specific heat ratio

V_{vap}^* = vapour volumes including vaporization volume

Vapour volume (V_{vap}^*) includes both the vapour inside the vessel before the BLEVE and the evaporation volume generated by instantaneous liquid flashing during the BLEVE [68]. Equation (3-2) and Equation (3-3) represent the vapour volumes of BLEVE.

A BLEVE occurs when $T_i < SLT$:

$$V_{vap}^* = V_{vap} (f = 0) \quad (3-2)$$

where f = vaporization fraction

$V_{vap} [m^3]$ = vapour inside of the vessel

A BLEVE occurs when $T_i > SLT$:

$$V_{vap}^* = V_{vap} + f V_{liq} \left(\frac{\rho_{liq}}{\rho_{vap}} \right) \quad (3-3)$$

where $V_{liq} [m^3]$ = liquid inside of the vessel

$\rho_{liq} [kg m^{-3}]$ = liquid density at explosion state

$\rho_{vap} [kg\ m^{-3}]$ = vapour density at explosion state

The vaporization fraction (f) can be calculated by Equation (3-4), in which f represents the vaporized liquid in the depressurization during the BLEVE [68, 94].

$$f = 1 - e^{-2.63(C_p/H_v)(T_c-T_b)(1-((T_c-T_i)/(T_c-T_b))^{0.38})} \quad (3-4)$$

where $T_c [K]$ = critical temperature of the substance

$T_b [K]$ = boiling temperature of the substance at atmospheric pressure

$T_i [K]$ = failure temperature

$H_v [kJ\ kg^{-1}]$ = enthalpy of vapourization of the substance

$C_p [kJ\ kg^{-1}\ K^{-1}]$ = specific heat capacity of the liquid at boiling temperature
(at constant pressure)

Subsequently, the total energy of the BLEVE can be calculated by substituting the vapour volume equation into Equation (3-1).

3.3 BLEVE pressure prediction equations

A large amount of training data is required to derive the unbiased BLEVE pressure prediction equations. The training data used are obtained from 45000 sets of FLACS simulations in a previous study and another 45000 new sets of overpressure data predicted using the ANN method (i.e., the method developed by Li et al. [24]). The previous study [23] used the liquid correction method, which considers the vapour evaporation and liquid flashing energies, to predict the BLEVE pressure. This method simulates the vapour expansion and liquid flashing simultaneously. Since only one high-pressure region can be used in FLACS, the pseudo-source was introduced to obtain the liquid flashing energies, as shown in Figure 3-1 [23].

In total, there were 1000 sets of propane and butane BLEVE simulations [24]. The pressure monitor points were arranged from 5 m to 50 m from the BLEVE source in the direction normal to the tank length. For each simulation, 45 monitor points were allocated in the blast wave propagation direction. Therefore, 45000 pressure data sets were extracted from the 1000 numerical simulations. Furthermore, another 45000 new sets of data (i.e., the overpressure data predicted from 1000 BLEVE cases) derived

using the CFD-based ANN method [24] are also used to develop the BLEVE pressure prediction equations.

Table 3-1 lists the ranges of BLEVE parameters considered in the numerical simulations (i.e., CFD & ANN). The tank length (L), tank width (W), tank height (H), liquid ratio (lr), failure pressure (P_i), failure temperature (T_i) and distance from BLEVE to the target location (r) are the most critical factors that affect the severity of BLEVE. The length, width and height of the BLEVE tank are defined in Figure 3-2. Therefore, these parameters are considered as the BLEVE parameters in the derivation of the prediction equations. The non-linear regression method is used for the equation derivation. The corresponding distribution types of BLEVE pressure variables are also derived from the numerical data.

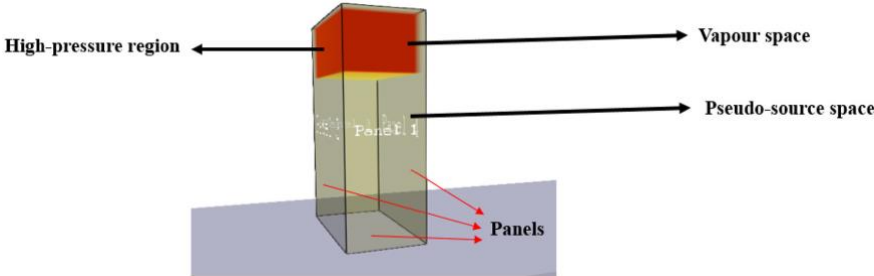


Figure 3-1. Pseudo-source space modelling in FLACS simulation [23].

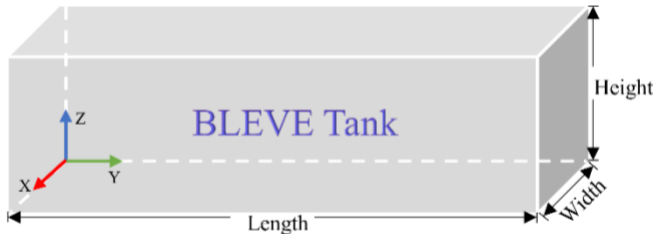


Figure 3-2. BLEVE tank.

Table 3-1. Training variable ranges for BLEVE data.

Variable	Variable options
Tank failure pressure, P_i (kPa)	500 – 3700 (butane), 500 – 4200 (propane)
Tank failure temperature, T_i (K)	274 – 425 (butane), 274 – 369 (propane)
Liquid ratio, lr (%)	10 – 90

Table 3-1 (Continued)

Variable	Variable options
Tank width, W (m)	0.2 – 3
Tank length, L (m)	0.2 – 10
Tank height, H (m)	0.2 – 3
Pressure monitor distance to BLEVE (m)	5 – 50

3.3.1 Side-on peak pressure

3.3.1.1 Positive side-on peak pressure

Overpressures resulting from a BLEVE can cause catastrophic structural damage, life loss and loss of economy. Hence, the accurate prediction of the BLEVE pressure is imperative for designing effective measures to resist blast loads. Positive side-on peak pressure is derived by using 90000 sets of BLEVE data, shown in Equation (3-5). The coefficients of the critical influencing parameters in the equations are determined by using a non-linear regression method. In comparing the pressure prediction results and numerical simulation data (i.e., CFD and CFD-based ANN simulation data), it can be seen in Figure 3-3 that the fitted equations represent the peak positive pressures well.

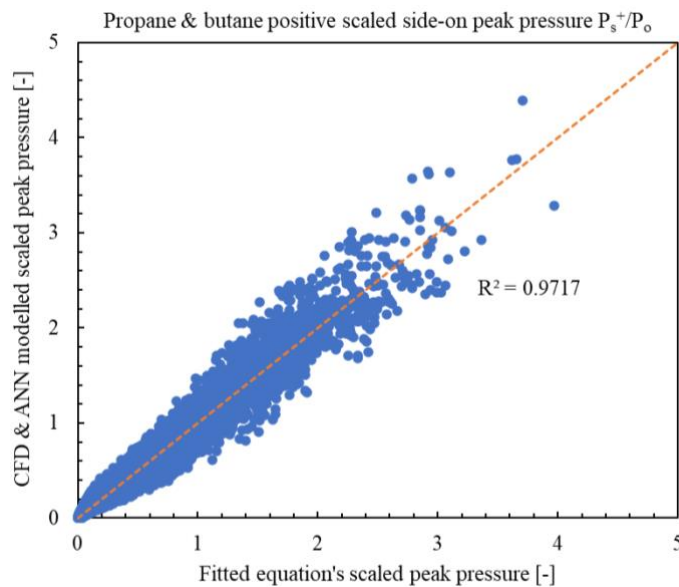


Figure 3-3. Comparison between CFD simulation data and equation predicted scaled positive side-on peak pressure.

$$\frac{P_s^+}{P_o} = 0.58(R + 0.10)^{-0.44} \times (1 - lr)^{0.53} \times \left(\frac{W}{L}\right)^{-0.30} \times \left(\frac{H}{L}\right)^{0.16} \times \left(\frac{P_i}{P_o}\right)^{0.53} \times \left(\frac{r}{\sqrt[3]{V}}\right)^{-0.95} \quad (3-5)$$

$$R = r(P_o/E)^{1/3} \quad (3-6)$$

where lr = liquid ratio; W [m] = tank width; H [m] = tank height; L [m] = tank length; V [m³] = tank volume; P_i [Pa] = failure pressure; $P_o = 10^5$ Pa ambient pressure; R = the dimensionless scaled distance; r [m] = distance from BLEVE to target location; E [J] = BLEVE energy

3.3.1.2 Negative side-on peak pressure

After the positive pressure, the blast transforms to a period where the pressure becomes negative [95]. Although the negative pressures are generally much smaller than the positive pressures, the secondary structures, such as windows, could be shattered due to the suction force [4, 96]. Therefore, it is also critical to investigate the negative side-on pressures generated from gas explosions. The negative peak pressure prediction equation is expressed as Equation (3-7). By using Equation (3-7), ninety thousand negative pressures (i.e., dimensionless) were predicted and compared with the corresponding CFD and CFD-based ANN simulation data. In Figure 3-4, it is seen that the proposed equation can well predict the negative peak pressures as compared with the CFD modelling data.

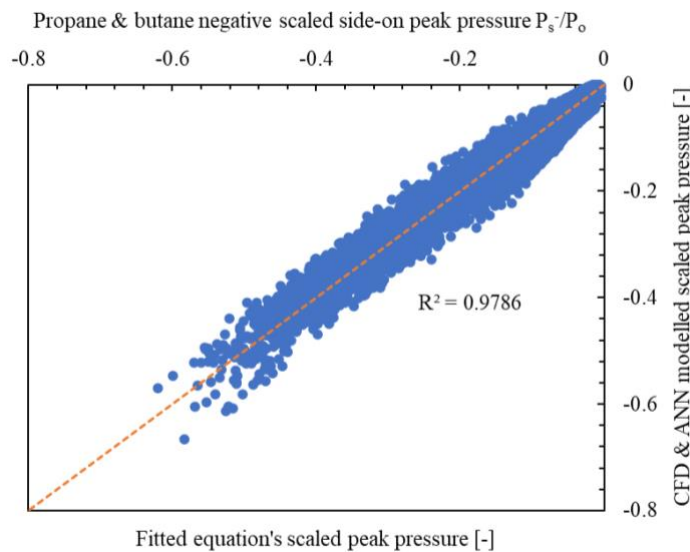


Figure 3-4. Comparison between CFD simulation data and equation predicted scaled negative side-on peak pressure.

$$\frac{P_s^-}{P_o} = -0.50(R + 2.58)^{-0.54} \times (1 - lr)^{0.22} \times \left(\frac{W}{L}\right)^{-0.14} \times \left(\frac{H}{L}\right)^{0.01} \times \left(\frac{P_t}{P_o}\right)^{0.25} \times \left(\frac{r}{\sqrt[3]{V}}\right)^{-0.65} \quad (3-7)$$

3.3.2 Duration of the blast wave

The duration of the blast wave is defined as the time between the pressure changing point (i.e., the moment when pressure increases or decreases from zero) and the point where the pressure returns to the atmospheric pressure [11]. Since the impulse is the integration of the pressure-duration history, the longer duration would result in a greater impulse [97]. Therefore, it is imperative to predict the duration accurately. A dimensionless scaled duration is here presented as:

$$\tau_d = \frac{t_d c_o}{r} \quad (3-8)$$

Equation (3-9) and Equation (3-10) are derived to predict the positive and negative duration. As shown in Figure 3-5, the proposed empirical relations can reliably predict both the positive and negative duration as compared with those obtained from the CFD simulations.

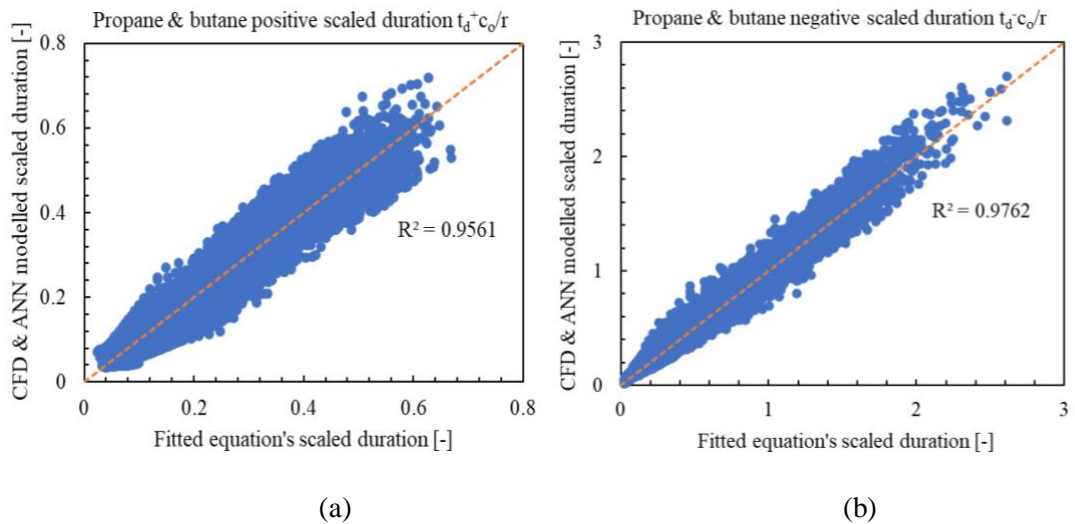


Figure 3-5. Comparison between CFD simulation data and equation predicted scaled duration: (a) positive pressure duration; (b) negative pressure duration.

$$\frac{t_a^+ c_o}{r} = 1.09(R + 6.23)^{-0.40} \times (1 - lr)^{0.07} \times \left(\frac{W}{L}\right)^{0.11} \times \left(\frac{H}{L}\right)^{-0.05} \times \left(\frac{P_i}{P_o}\right)^{0.13} \times \left(\frac{r}{\sqrt[3]{V}}\right)^{-0.49} \quad (3-9)$$

$$\frac{t_a^- c_o}{r} = 1.01R^{-0.20} \times (1 - lr)^{0.21} \times \left(\frac{W}{L}\right)^{0.09} \times \left(\frac{H}{L}\right)^{-0.01} \times \left(\frac{P_i}{P_o}\right)^{0.32} \times \left(\frac{r}{\sqrt[3]{V}}\right)^{-0.75} \quad (3-10)$$

3.3.3 Arrival time

The arrival time is measured as when the blast wave arrives at the target location, which infers the blast wave velocity and the corresponding blast peak pressure [98]. Additionally, the arrival time of the blast wave is an important metric for understanding the blast wave behaviour as it propagates [99]. Therefore, it is important to estimate the arrival time for pressure-time history prediction. The dimensionless scaled arrival time is derived here and shown in Equation (3-11) and (3-12). The specific arrival times (i.e., t_a) can be determined and compared with the CFD simulation data. As shown in Figure 3-6, the equation predicted arrival times agree well with the CFD simulation results.

$$\tau_a = \frac{t_a c_o}{r} \quad (3-11)$$

$$\frac{t_a c_o}{r} = -0.38 \times \log\left(R + \frac{r}{\sqrt[3]{V}} + 11.33\right)^{-3.36} \times (1 - lr)^{0.15} \times \left(\frac{W}{L}\right)^{-0.11} \times \left(\frac{H}{L}\right)^{0.07} \times \left(\frac{P_i}{P_o}\right)^{0.20} + 0.99 \quad (3-12)$$

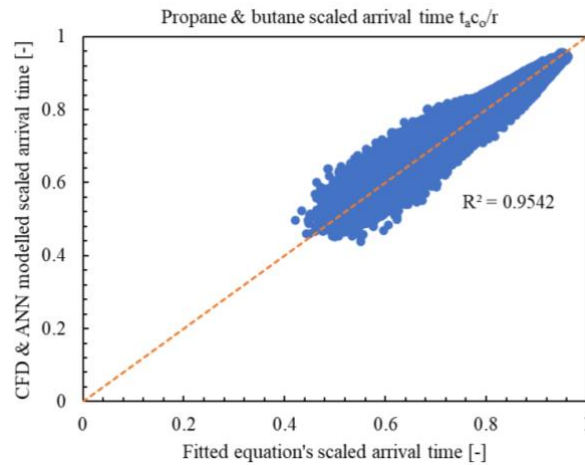


Figure 3-6. Comparison between CFD simulation data and equation predicted scaled arrival time.

3.3.4 Peak pressure rise time

The peak pressure rise time indicates the exact time when either the positive or the negative overpressures reach the peak values. By using the duration mentioned above, arrival time, and peak pressure rise time, the exact form/profile of the pressure wave can be determined. Therefore, to obtain the detailed pressure-time profile as the input for structural response analysis, it is essential to accurately determine the peak pressure rise time. The equations to predict the positive and negative peak pressure rise times are derived and shown in Equations (3-13) and (3-14). The peak pressure rise time can be well predicted compared with the CFD modelling data, as shown in Figure 3-7.

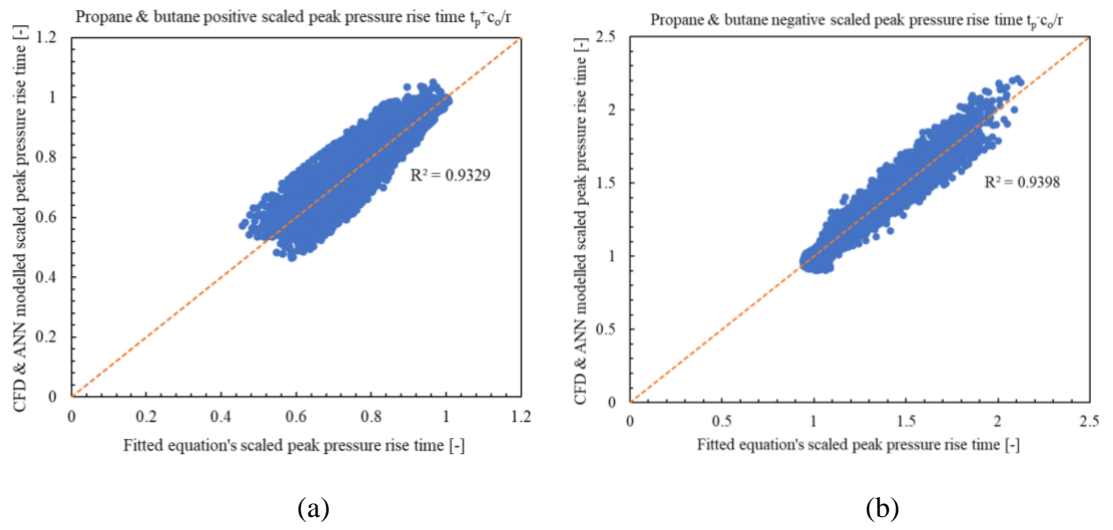


Figure 3-7. Comparison between CFD simulation data and equation predicted scaled peak pressure rise time: (a) positive; (b) negative.

$$\begin{aligned} \frac{t_p^+ c_o}{r} = & -1.66 \times \left(3.82R + \frac{r + 23.40}{\sqrt[3]{V}} + 4.84 \right)^{-0.80} \times (1 \\ & - 0.79lr)^{0.36} \times \left(\frac{L \times H}{W^2} \right)^{0.08} \times \left(\frac{P_i}{P_o} \right)^{0.28} + 1.03 \end{aligned} \quad (3-13)$$

$$\begin{aligned} \frac{t_p^- c_o}{r} = & 0.70 \times \left(0.23R + \frac{r - 0.93}{\sqrt[3]{V}} - 0.35 \right)^{-0.75} \times (1 \\ & - 0.99lr)^{0.05} \times \left(\frac{L \times H}{W^2} \right)^{-0.15} \times \left(\frac{P_i}{P_o} \right)^{0.15} + 1 \end{aligned} \quad (3-14)$$

3.3.5 Impulse

Impulse is the integral time function of the overpressure, which is calculated as the area enclosed by pressure and duration [100]. It can be used to assess the resulting stresses in a structure subjected to sudden and impulsive loading [96, 101]. Accordingly, the impulse calculation equation can be approximately represented as below [11]:

$$i = \frac{1}{2} P_s t_d \quad (3-15)$$

The dimensionless scaled impulse is derived and shown in Equation (3-16). Compared to CFD modelling data, the predicted impulse agrees well with the CFD modelling results, as shown in Figure 3-8.

$$\frac{i^+ c_o}{r P_o} = 0.19(R + 39.70)^{-0.0001} \times (1 - lr)^{0.64} \times \left(\frac{W}{L}\right)^{-0.24} \times \left(\frac{H}{L}\right)^{0.11} \times \left(\frac{P_i}{P_o}\right)^{0.54} \times \left(\frac{r}{\sqrt[3]{V}}\right)^{-1.89} \quad (3-16)$$

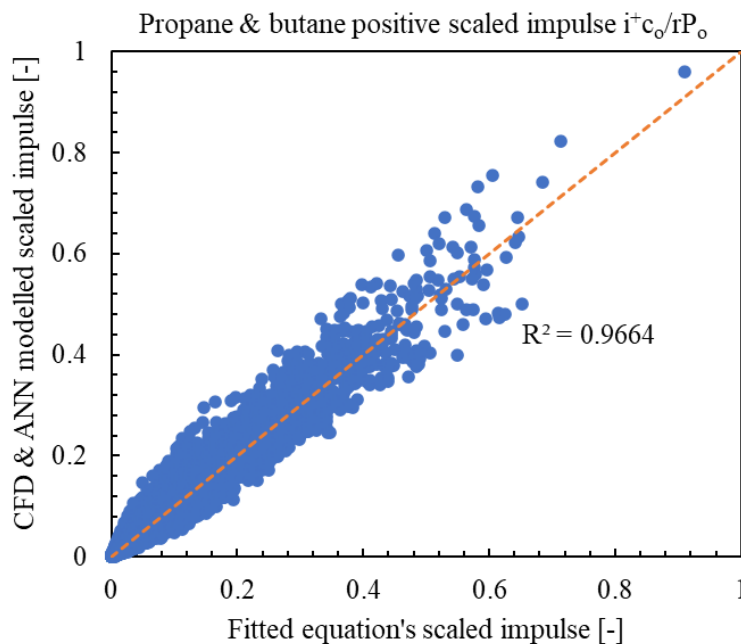


Figure 3-8. Comparison between CFD simulation data and equation predicted scaled impulse.

3.3.6 Pressure prediction equations' fitting test

Having derived the above equations for side-on peak pressure, duration, arrival time, peak pressure rise time and impulse predictions, the fitting goodness test is conducted. Root Mean Square Error (RMSE) is used to check the prediction accuracy compared to the numerical data [83, 102]. The calculated RMSE values are listed in Table 3-2, as shown the best fitted equations give good estimations of the respective BLEVE pressure variables as compared with the numerical data.

The available numerical data can also be used to determine the probabilistic distribution types of the BLEVE pressure variables. Figure 3-9 shows the distribution histograms of each normalized parameters and the corresponding specific Probabilistic Distribution Function (PDF). As shown, most scaled parameters (i.e., $\Delta\bar{P}_s^+$, τ_d^+ , τ_d^- , \bar{t}^+ and τ_p^-) conform to the generalized extreme value (GEV) distribution, τ_a and τ_p^+ obey the extreme value (EV) distribution, and $\Delta\bar{P}_s^-$ follows the lognormal distribution. The fitting values between the scaled BLEVE parameters and their corresponding specific distribution are less than 0.015, indicating a good fitting degree. The corresponding PDF parameters are also given in Table 3-2. Table 3-2 also gives the 95% Confidence Interval (CI) of each fitted parameter [103]. These PDFs can be used to model BLEVE pressure distributions if a probabilistic analysis is needed.

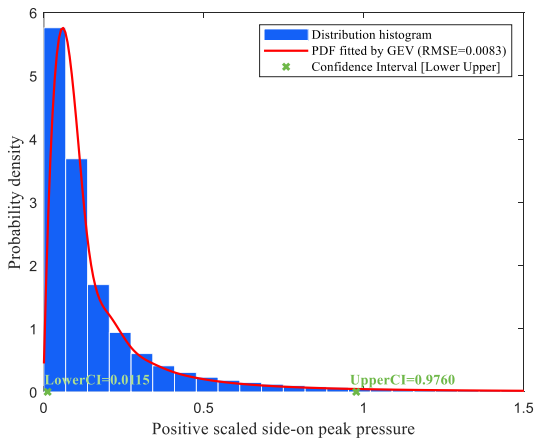
Table 3-2. Fitting distribution, mean and standard deviation for critical parameters.

	$\Delta\bar{P}_s^+$	$\Delta\bar{P}_s^-$	τ_d^+	τ_d^-	τ_a	τ_p^+	τ_p^-	\bar{t}^+
<i>DIST</i>	GEV (Type II)	LOG	GEV (Type II)	GEV (Type II)	EV	EV	GEV (Type II)	GEV (Type II)
<i>K</i>	0.7363	N/A	0.1562	0.3971	N/A	N/A	0.3456	1.0806
<i>σ</i>	0.0612	0.7522	0.0594	0.1185	0.0643	0.0595	0.0588	0.0041
<i>μ</i>	0.0632	-2.6513	0.1330	0.1861	0.8407	0.8974	1.0275	0.0033
<i>CI_{lower}</i>	0.0115	0.0156	0.0636	0.0658	0.5998	0.6751	0.9653	0.0004
<i>CI_{upper}</i>	0.9760	0.3045	0.4205	1.0916	0.9209	0.9732	1.4680	0.1338
RMSE	0.0083	0.0054	0.0087	0.0068	0.0142	0.0075	0.0081	0.0086

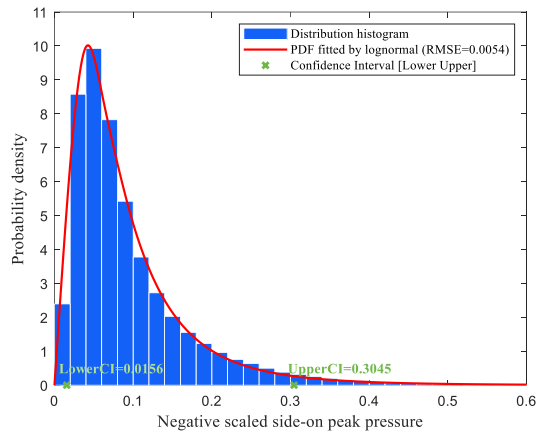
Note: GEV function: $f(x|k, \mu, \sigma) = \frac{1}{\sigma} \left(1 + k \frac{(x-\mu)}{\sigma} \right)^{-\frac{k+1}{k}} e^{-\left(1 + k \frac{(x-\mu)}{\sigma} \right)^{\frac{1}{k}}}$

$$\text{LOG function: } f(x|\mu, \sigma) = \frac{1}{x\sigma\sqrt{2\pi}} e^{-\frac{(\ln x - \mu)^2}{2\sigma^2}}$$

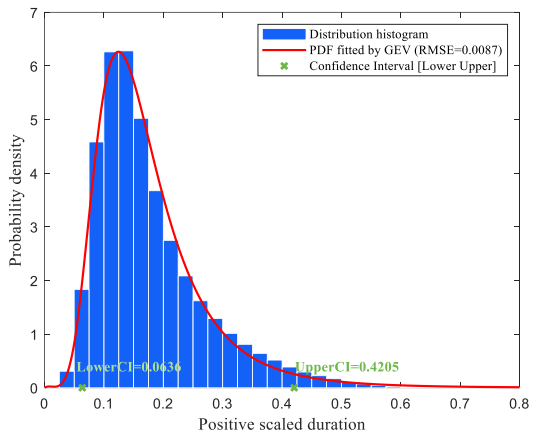
$$\text{EV function: } f(x|\mu, \sigma) = \frac{1}{\sigma} e^{\left(\frac{x-\mu}{\sigma}\right)} e^{-e^{\left(\frac{x-\mu}{\sigma}\right)}}$$



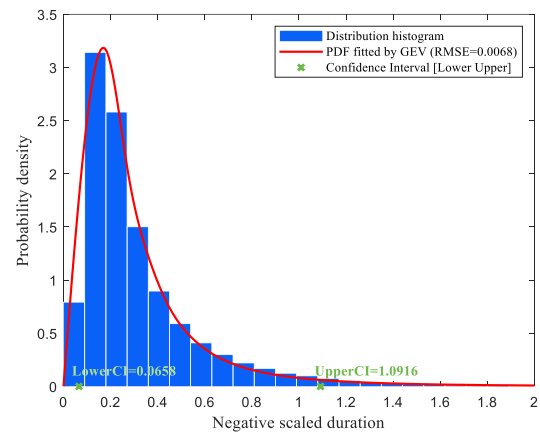
(a)



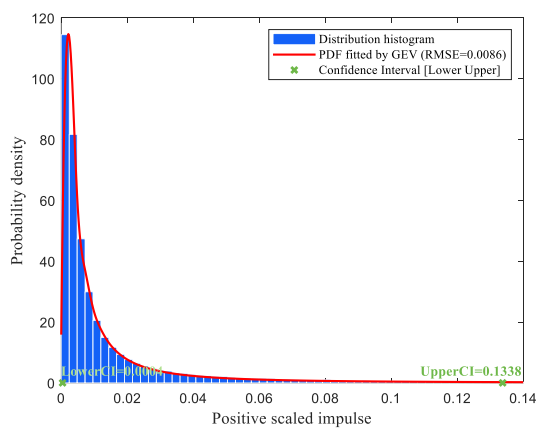
(b)



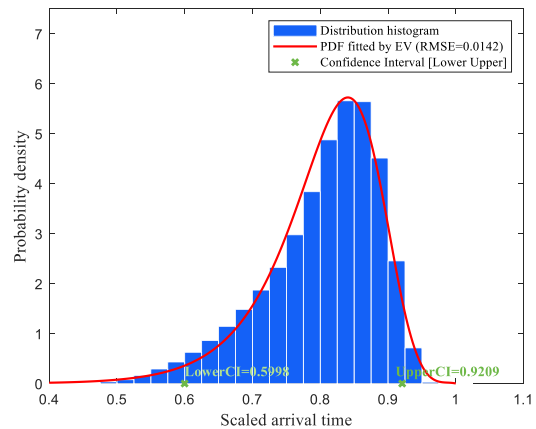
(c)



(d)



(e)



(f)

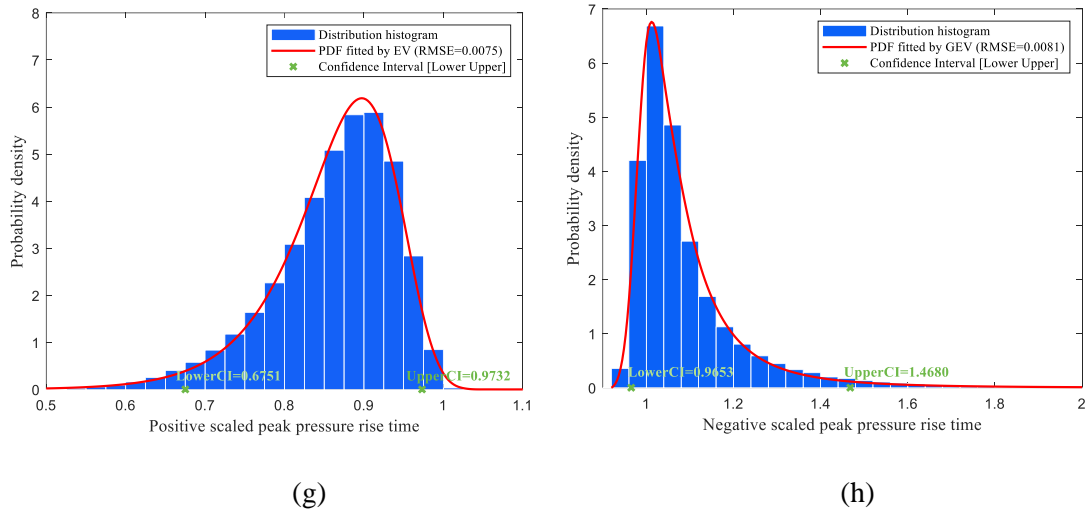
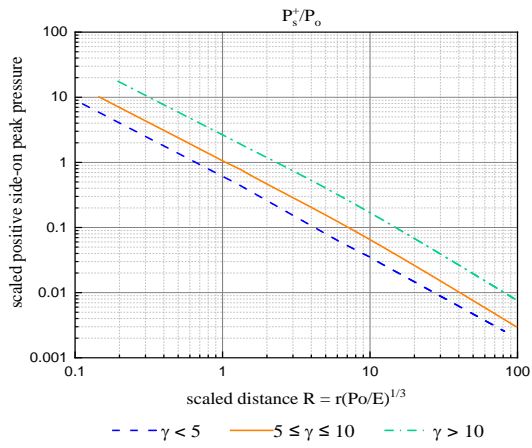


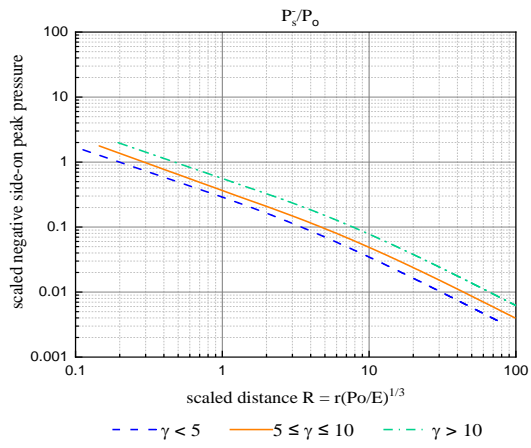
Figure 3-9. Histogram of pressure prediction model fitting test: (a) positive scaled side-on peak pressure; (b) negative scaled side-on peak pressure; (c) positive scaled duration; (d) negative scaled duration; (e) positive scaled impulse; (f) scaled arrival time; (g) positive scaled peak pressure rise time; (h) negative scaled peak pressure rise time.

3.4 BLEVE pressure prediction charts

To facilitate easy applications by engineers in practice, this section presents prediction charts, offering a more user-friendly and straightforward way for estimating the BLEVE pressure-time profile compared to prediction equations. In the BLEVE pressure prediction charts, the values of side-on peak pressure, duration, arrival time, peak pressure rise time and impulse (i.e., P_s^+ , P_s^- , t_d^+ , t_d^- , t_a , t_p^+ , t_p^- and i^+) in the y-axis are obtained from the pressure prediction equations derived above. In comparison, the values in the x-axis are the scaled distances (R), which can be determined using the BLEVE energy (E) and distance from BLEVE to target location (r). The BLEVE energy calculation is strongly dependent on γ , as seen in Equation (3-1), which affects the determination of R in the x-axis coordinator of the chart. Therefore, corresponding to the three γ ranges (i.e., $\gamma < 5$, $5 \leq \gamma \leq 10$ and $\gamma > 10$), for each pressure prediction chart from Figure 3-10 to Figure 3-13, three separate curves are plotted. In each γ range, the plotted curve is the average data of the upper and lower limit values.

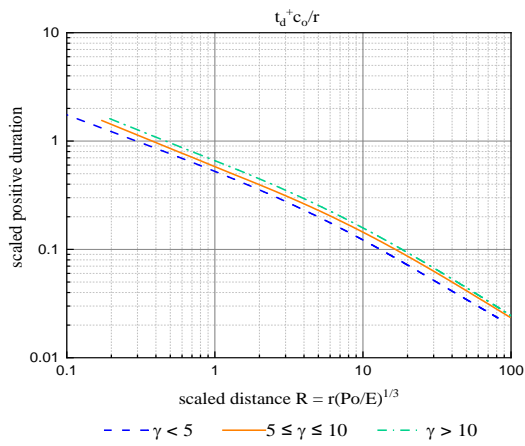


(a)

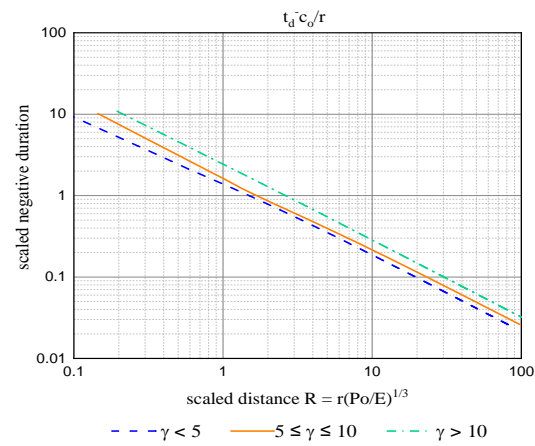


(b)

Figure 3-10. Scaled side-on peak pressure: (a) positive pressure; (b) negative pressure.

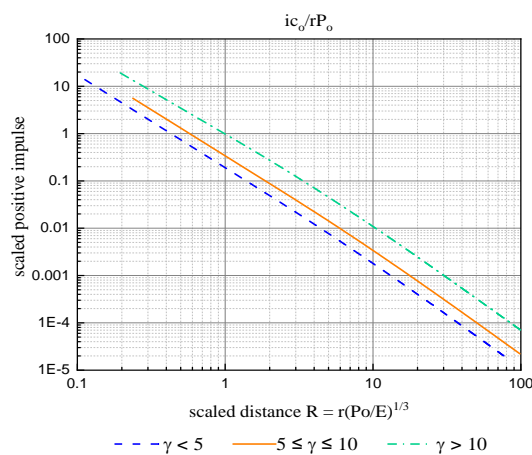


(a)

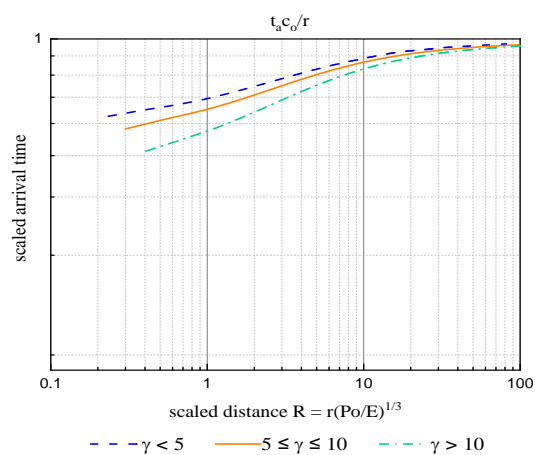


(b)

Figure 3-11. Scaled duration: (a) positive pressure duration; (b) negative pressure duration.



(a)



(b)

Figure 3-12. (a) Scaled impulse; (b) Scaled arrival time.

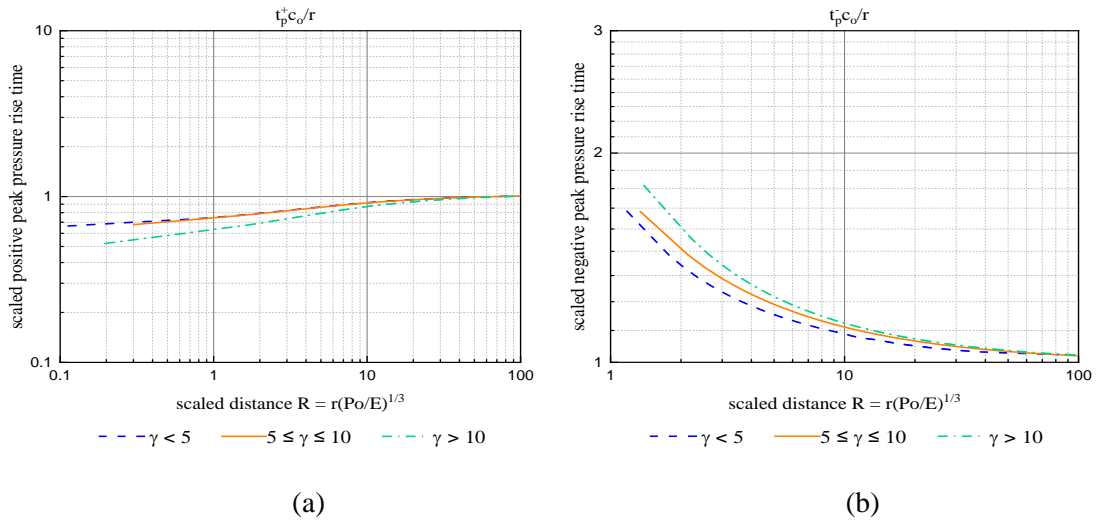


Figure 3-13. Scaled peak pressure rise time: (a) positive; (b) negative.

Having depicted the chart for each pressure parameter, all parameters' curves are summarized into the same chart based on the γ range, as shown in Figure 3-14, Figure 3-15 and Figure 3-16. Meanwhile, to allow engineers to read the charts easily, the time-related data (i.e., scaled arrival time and scaled peak pressure rise time) are plotted into a separate chart since these data are on a significantly smaller scale.

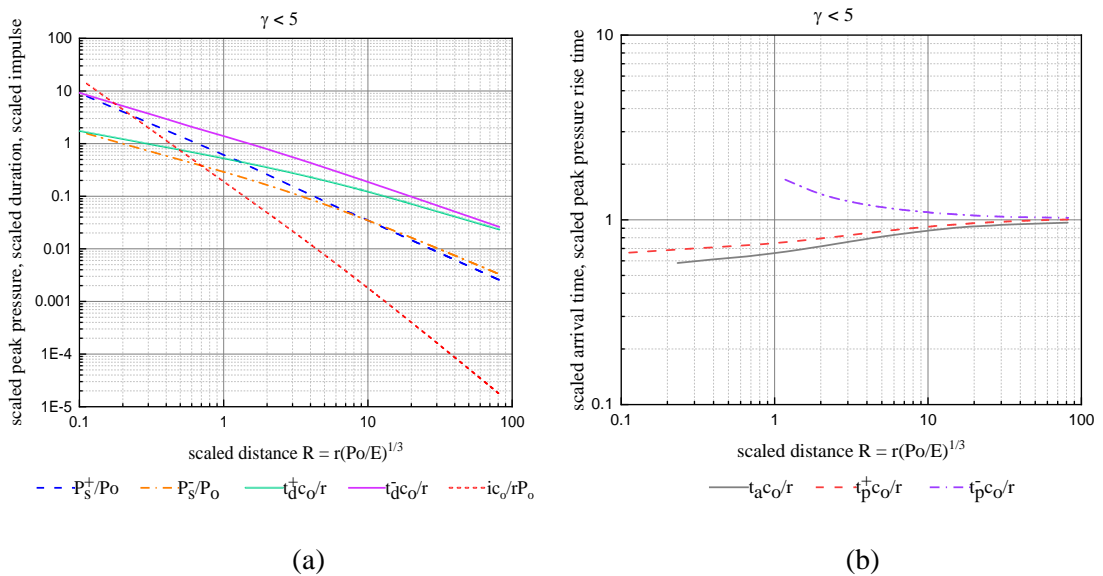
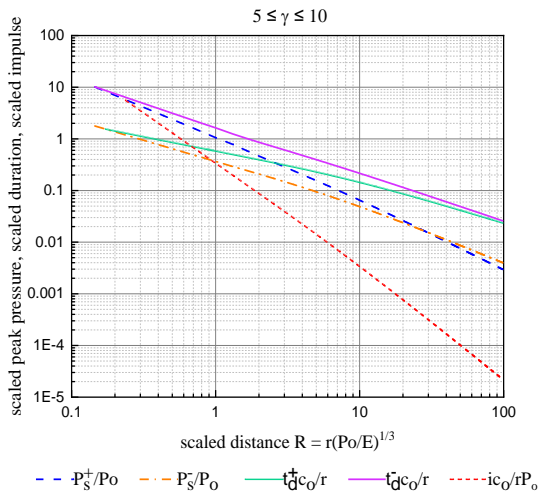
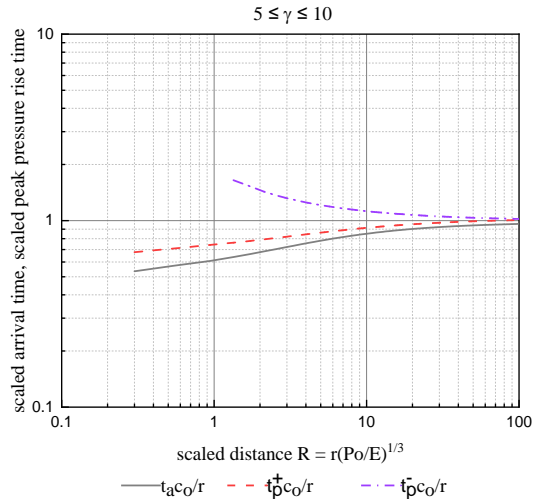


Figure 3-14. $\gamma < 5$: (a) scaled peak pressure, duration & impulse; (b) scaled arrival time & peak pressure rise time.

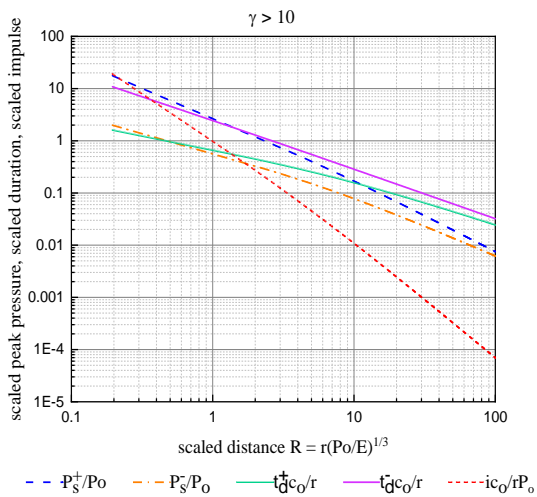


(a)

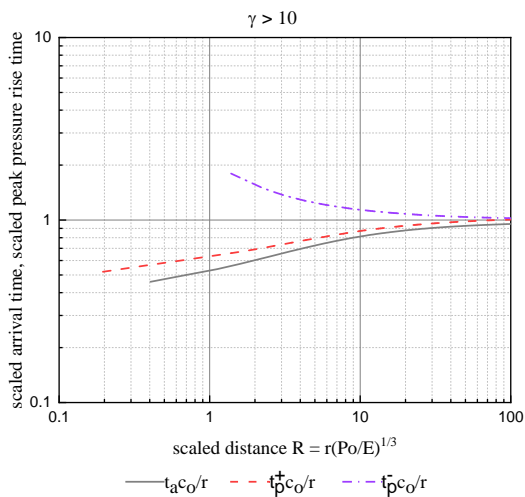


(b)

Figure 3-15. $5 \leq \gamma \leq 10$: (a) scaled peak pressure, duration & impulse; (b) scaled arrival time & peak pressure rise time.



(a)



(b)

Figure 3-16. $\gamma > 10$: (a) scaled peak pressure, duration & impulse; (b) scaled arrival time & peak pressure rise time.

3.5 Evaluation of the pressure prediction equations and charts

3.5.1 Comparison of predicted data with experimental data

Six sets of BLEVE experiments [28, 48, 49, 51], which were carried out in open space with r larger than 5 m, were selected for the comparison and verification of the accuracy of the developed empirical formulae and charts in predicting the BLEVE pressures. The side-on peak pressure, duration, arrival time, peak pressure rise time and impulse data (i.e., P_s^+ , P_s^- , t_d^+ , t_d^- , t_a , t_p^+ , t_p^- and i^+) obtained in tests were extracted from the literature. The input data of tank length (L), tank width (W), tank height (H), liquid ratio (lr), and initial failure pressure (P_i) in the experiments are given in the respective papers, which were directly used to calculate P_s^+ , P_s^- , t_d^+ , t_d^- , t_a , t_p^+ , t_p^- and i^+ based on the empirical formulae and charts. Since the prediction equations and charts are derived based on FLACS simulation data, the performance ranking of the proposed equations is evaluated according to the FLACS guideline [70], where the performance ranking is divided into three categories, namely ‘excellent’ (i.e., within 25% deviations), ‘acceptable’ (i.e., prediction errors between 25% and 50%) and ‘not perform well’ (i.e., errors larger than 50%), respectively.

Table 3-3 lists the data obtained from the available experimental tests in the literature. Table 3-4 and Table 3-5 list the predicted results from the proposed empirical formulae and the charts, respectively. The corresponding errors with respect to the experimental data are also given in the tables. It is seen that the prediction errors with respect to the side-on peak pressures, arrival time, and peak pressure rise time (i.e., P_s^+ , P_s^- , t_a , t_p^+ and t_p^-) are mainly less than 25%. Figure 3-17 to Figure 3-21 compare the predicted and experimental data of P_s^+ , P_s^- , t_a , t_p^+ and t_p^- . As shown the deviations of the most predicted results from the experimental data are within 25%, which can be concluded that the performance is in general ‘Excellent’. Considering many uncertainties and complexity of BLEVE events, these comparison results indicate the proposed empirical formulae and charts yield good predictions of the above BLEVE pressure parameters in open space.

However, as shown in Figure 3-22 to Figure 3-24, the performances of the proposed methods in predicting the positive and negative duration (i.e., t_d^+ and t_d^-), and the impulse (i.e., i^+), are not as good with most prediction deviations from the experimental data in the 25% to 50% range, and only a relatively few prediction results

are within 25% deviation. This is because the FLACS simulation underpredicts the BLEVE pressure duration [23], shown in Table 3-6, owing to the inherent issue of the flux-corrected transport (FCT) scheme [104] used in the FLACS-BLAST module. Since the empirical formulae and charts in this study were developed based on the FLACS simulation results [23] and the ANN model prediction results and the ANN model was also trained with mainly the FLACS simulation results [24], the predicted duration of the BLEVE pressure-time history has a relatively larger error. Since the impulse is estimated as the area of side-on peak pressure and duration, the predicted impulse therefore also has a relatively larger error. Nonetheless, the performances in predicting t_d^+ , t_d^- and i^+ of the proposed empirical formulae and charts can still be categorized as ‘Acceptable’ since the deviations of majority of the predicted results from the experimental data are within the 50% range. Since the number of BLEVE experiments that provide the pressure-time profiles are limited in literature, it is not reliable to derive an unbiased adjustment parameter based on the current small size of experimental database to improve the prediction accuracy of t_d^+ , t_d^- and i^+ .

It is also worth noting that the small-scale BLEVE tank (i.e., 0.026 m³) used in the experiment by Stawczyk [51] is included in the comparison, while the BLEVE data used in developing the pressure prediction model ranges from 0.288 m³ to 78.4 m³. Similarly, the large-scale experiment conducted by Johnson and Pritchard [49] with a monitoring distance of 150 m is also considered in the evaluation, whereas the data used to develop the empirical formulae and charts are in the range of 5 m to 50 m. These off-range experimental data were used to evaluate the performance of the proposed empirical formulae and charts in predicting the BLEVE pressures because limited available experiments provided pressure-time profiles. By including them, this could augment the above estimated performance errors. As shown in Table 3-4 and Table 3-5, the averaged errors for P_s^+ , P_s^- , t_a , t_p^+ and t_p^- are within 30%, which means the proposed formulae and charts are capable of predicting P_s^+ , P_s^- , t_a , t_p^+ and t_p^- for both small and large scale BLEVEs, even when the BLEVE volume and explosion target distance are beyond the training data range.

Table 3-3. Experimental data.

		Experiment								
	r [m]	P_s^+ [kPa]	P_s^- [kPa]	t_a [s]	t_d^+ [s]	t_d^- [s]	i^+ [Pas]	t_p^+ [s]	t_p^- [s]	
Birk 2007	20	8.77	-6.87	0.0620	0.0190	0.0290	83.32	0.0706	0.0987	
	30	5.94	-4.21	0.0877	0.0206	0.0290	61.32	0.0955	0.1245	
	40	4.07	-2.84	0.1178	0.0178	0.0296	36.16	0.1224	0.1539	
Stawczyk	10	13.75	-11.05	0.0260	0.0145	0.0115	99.80	0.0344	0.0478	
Johnson 1990	150	0.43	-0.44	0.4680	0.0641	0.0550	13.82	0.4965	0.5584	
Melhem test 06	15	27.58	-14.31	0.0263	0.0121	0.0329	166.66	0.0272	0.0565	

Table 3-4. Equation predicted data and the corresponding errors with experimental results.

BLEVE Prediction Equations										
	r [m]	R	P_s^+ [kPa]	P_s^- [kPa]	t_a [s]	t_d^+ [s]	t_d^- [s]	i^+ [Pas]	t_p^+ [s]	t_p^- [s]
Birk 2007	20	4.30	8.13	-6.00	0.0488	0.0084	0.0111	34.00	0.0526	0.0652
	30	6.45	4.63	-3.99	0.0765	0.0095	0.0113	22.09	0.0811	0.0952
	40	8.60	3.10	-2.95	0.1046	0.0104	0.0115	16.10	0.1100	0.1250
Stawczyk	10	4.95	6.73	-4.94	0.0247	0.0042	0.0058	13.98	0.0272	0.0328
Johnson 1990	150	59.18	0.31	-0.52	0.4208	0.0119	0.0107	1.87	0.4424	0.4518
Melhem test 06	15	3.47	23.96	-10.85	0.0328	0.0087	0.0158	104.22	0.0356	0.0511
AVERAGE ERROR			24.16%	19.80%	14.17%	55.34%	60.95%	64.77%	18.96%	22.70%

Table 3-5. Chart predicted data and the corresponding errors with experimental results.

BLEVE Prediction Charts										
	r [m]	R	P_s^+ [kPa]	P_s^- [kPa]	t_a [s]	t_d^+ [s]	t_d^- [s]	i^+ [Pas]	t_p^+ [s]	t_p^- [s]
Birk 2007	20	4.30	9.72	-8.13	0.0467	0.0130	0.0236	62.65	0.0502	0.0702
	30	6.45	5.80	-5.45	0.0737	0.0147	0.0246	40.18	0.0782	0.1005

Table 3-5 (Continued)

Birk 2007	40	8.60	4.16	-4.06	0.1012	0.0160	0.0252	29.22	0.1067	0.1308
Stawczyk	10	4.95	8.12	-7.10	0.0238	0.0060	0.0105	23.66	0.0254	0.0345
Johnson 1990	150	59.18	0.38	-0.48	0.4224	0.0133	0.0155	1.58	0.4403	0.4543
Melhem test 06	15	3.47	12.80	-9.96	0.0341	0.0111	0.0214	72.10	0.0369	0.0541
AVERAGE ERROR			20.29%	27.52%	17.06%	35.99%	27.34%	50.01%	22.17%	18.97%

Table 3-6. Pressure-time parameters at 20m of both the experimental and FLACS data [23].

Birk 2007 r=20m									
	P_s^+ [kPa]	P_s^- [kPa]	t_a [s]	t_d^+ [s]	t_d^- [s]	i^+ [Pas]	t_p^+ [s]	t_p^- [s]	
Experiment	8.77	-6.87	0.0620	0.0190	0.0290	83.32	0.0706	0.0987	
FLACS	8.95	-5.05	0.0671	0.0086	0.0120	38.64	0.0691	0.0844	
ERROR	2.02%	26.46%	8.24%	54.54%	58.76%	53.62%	2.11%	14.53%	

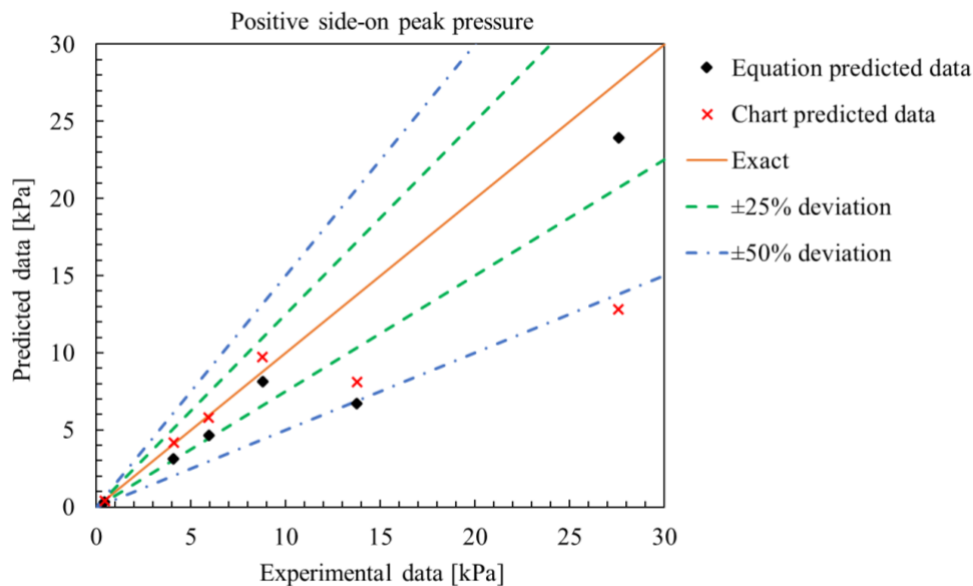


Figure 3-17. Comparison between experimental data and predicted positive side-on peak pressure (by pressure prediction equation & chart).

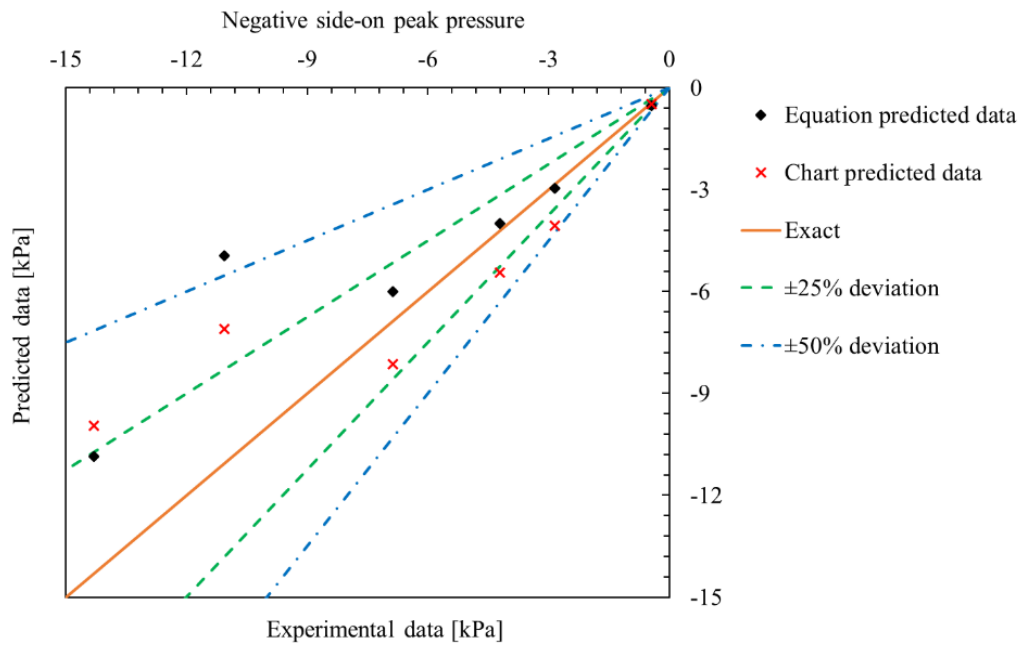


Figure 3-18. Comparison between experimental data and predicted negative side-on peak pressure (by pressure prediction equation & chart).

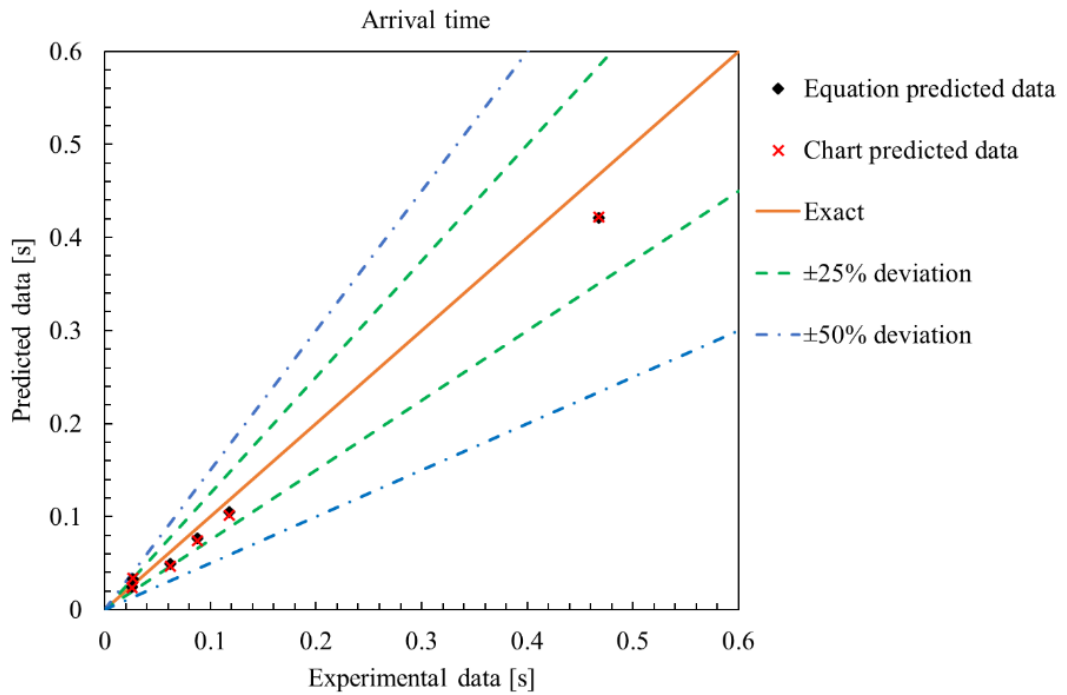


Figure 3-19. Comparison between experimental data and predicted arrival time (by pressure prediction equation & chart).

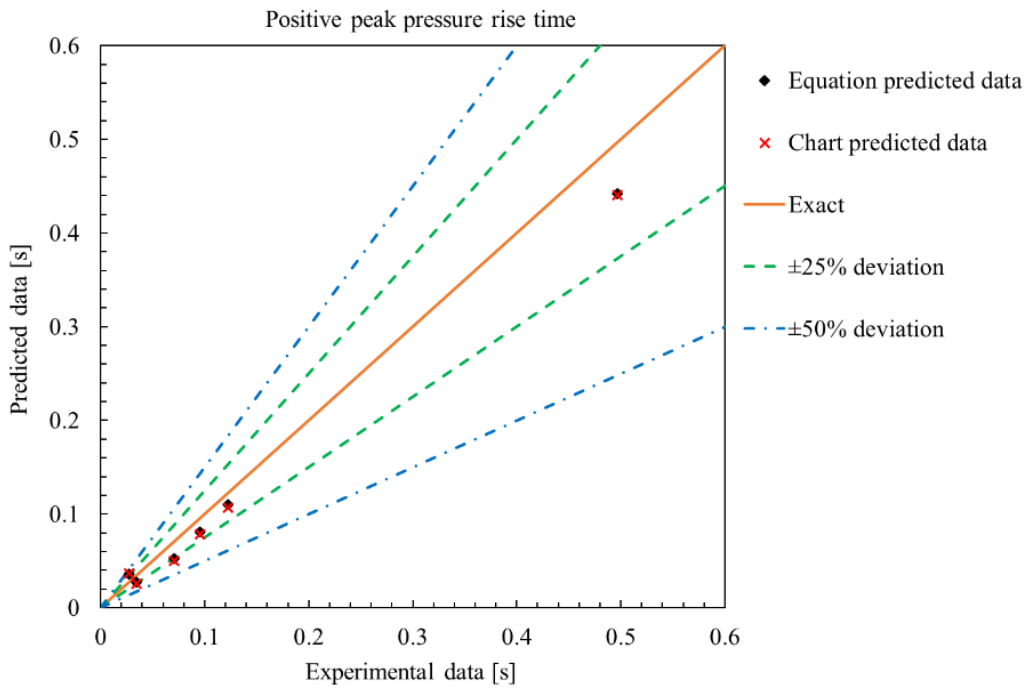


Figure 3-20. Comparison between experimental data and predicted positive peak pressure rise time (by pressure prediction equation & chart).

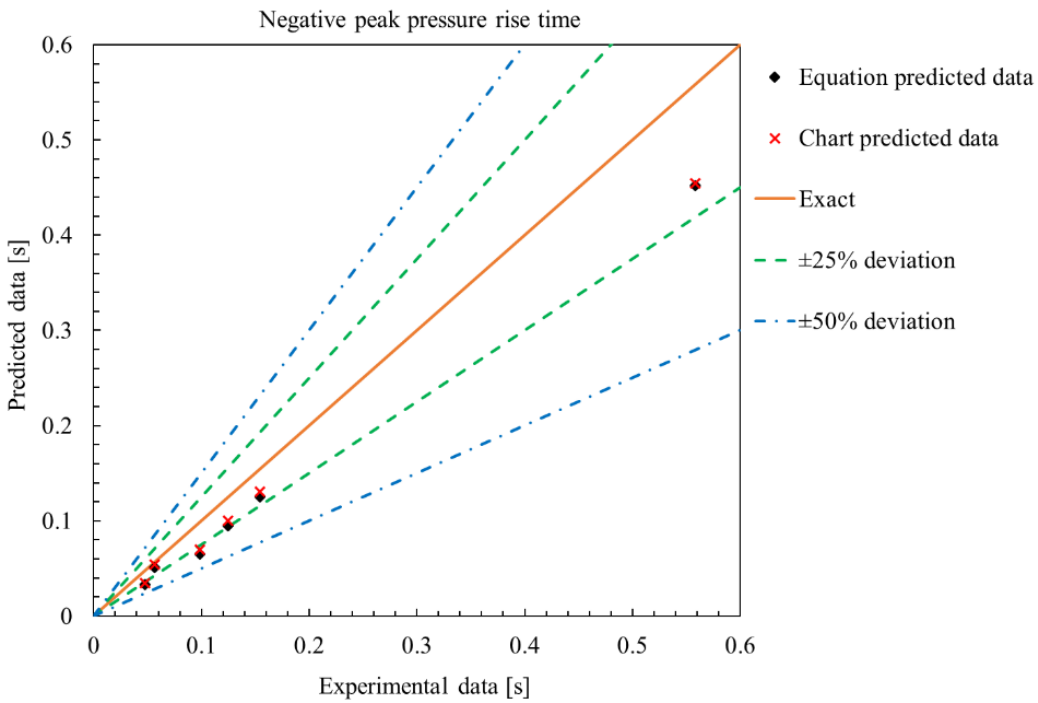


Figure 3-21. Comparison between experimental data and predicted negative peak pressure rise time (by pressure prediction equation & chart).

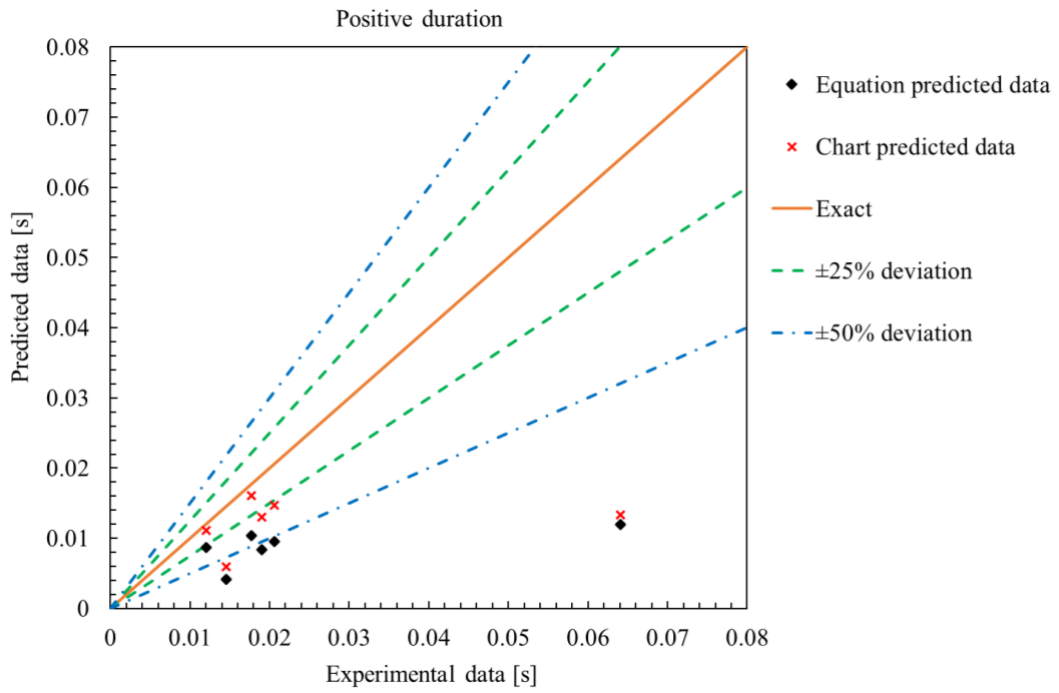


Figure 3-22. Comparison between experimental data and predicted positive duration (by pressure prediction equation & chart).

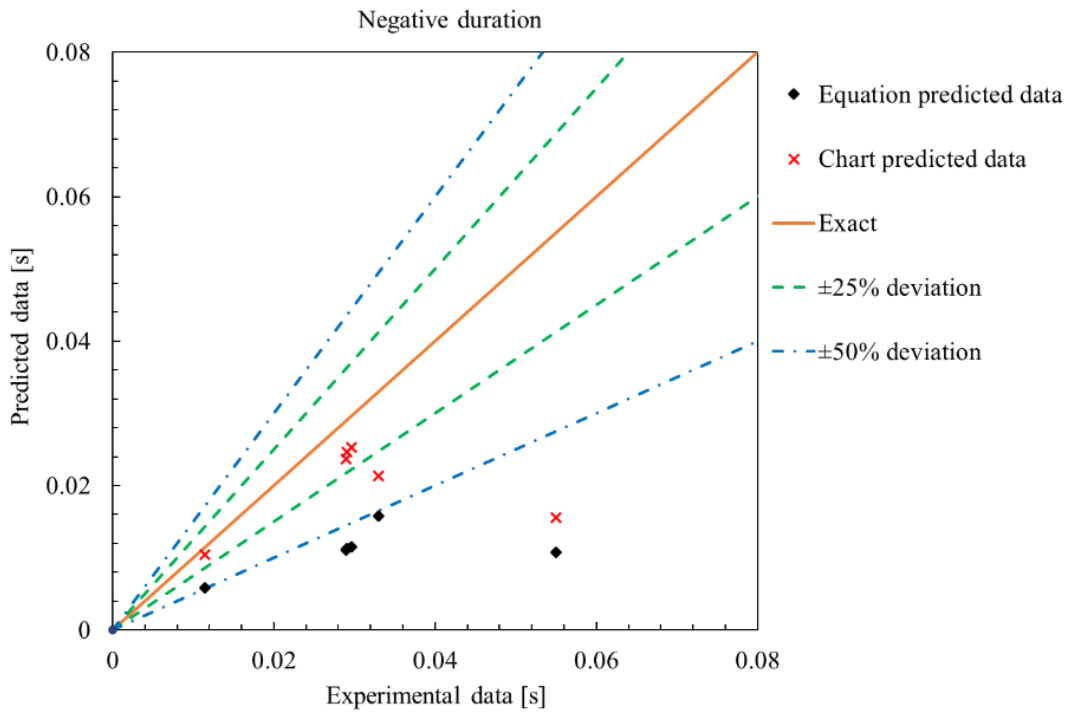


Figure 3-23. Comparison between experimental data and predicted negative duration (by pressure prediction equation & chart).

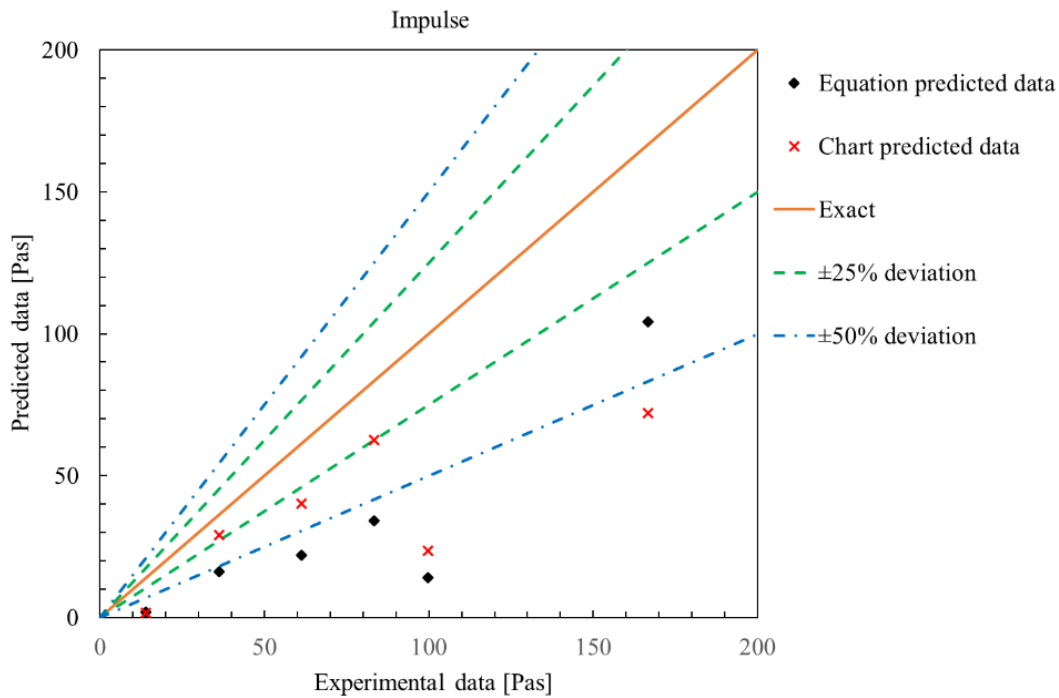


Figure 3-24. Comparison between experimental data and predicted impulse (by pressure prediction equation & chart).

3.5.2 Comparison of the new prediction methods with the empirical methods

The prediction accuracy of the proposed equations and charts is further assessed by comparing the prediction results with those obtained from other empirical methods commonly used in research and practice.

Without loss of generality, test No. 02-1 of Birk et al. [28] (as seen in Table 3-3) is chosen as the reference. In this experiment, the BLEVE vessel was a 2 m³ tank (i.e., $D = 0.953$ m and $L = 2.7$ m) filled with 51% liquefied propane. The failure pressure was 1800 kPa, the liquid failure temperature was 330 K, and the vapour failure temperature was 334 K. The pressure data at 20 m stand-off distance was recorded during the test, as shown in the first row of Table 3-3.

The cylinder tank used in the Birk et al. experiment had the length L of 2.7 m. Therefore, the equivalent rectangular tank's width and height can be approximately estimated as:

$$W = H = \sqrt{\frac{V}{L}} = 0.86 \text{ m}$$

As the failure temperature is 330 K (i.e., above the superheat limit temperature) and the failure pressure is 1800 kPa, the BLEVE energy is calculated as 10.1 MJ by Equation (3-1), (3-3) and (3-4). Subsequently, using the BLEVE pressure prediction equations from (3-5) to (3-16), P_s^+ , P_s^- , t_d^+ , t_d^- , t_a , t_p^+ , t_p^- and i^+ are determined and summarized in Table 3-4. Similarly, using the BLEVE pressure prediction charts, the results of critical parameters can be read from the respective curves, and the corresponding outputs are given in Table 3-5. The results are then compared with those predicted using another two empirical methods.

3.5.2.1 Prugh's TNT equivalence method

One of the most widely-used empirical methods for BLEVE overpressure prediction is the TNT equivalence method proposed by Prugh [63]. Prugh's TNT equivalence method is a more advanced pressure prediction model compared to the original TNT equivalence method. The main difference between them is that the phase changing liquid flashing and vapour expansion of a BLEVE are considered in Prugh's TNT equivalence method. In contrast, only the initial mass of a BLEVE content is considered in the original TNT equivalence method. For instance, based on the content's rupture temperature, a vaporization fraction factor f can be used to determine the final phase of liquid flashing volume and the total explosion expansion volume for blast wave generation in Prugh's TNT equivalence method. Therefore, the equivalent TNT mass can be converted more precisely. The same case study (i.e., test No. 02-1 of Birk et al. [28]) is predicted using Prugh's TNT equivalence method. The pressure can be predicted following Equations (3-17) to (3-20). Using the calculated scaled distance R of $14.09 \text{ m/kg}^{1/3}$, the side-on peak pressure, duration, arrival time and impulse can be obtained from the TNT equivalence curves. The specific results are given in Table 3-7.

$$f = 1 - e^{-2.63 \left(1 - \left(\frac{T_c - T_i}{T_c - T_b} \right)^{0.38} \right) \left(\frac{C_{prop}}{L_{prop}} \right) (T_c - T_b)} \quad (3-17)$$

where the average specific heat for liquified propane at boiling point is $C = 2430$ J/kg/K and the average latent heat of vaporization at boiling point is $L = 427000$ J/kg.

$$V^* = V + W_L \left[\frac{f}{\rho_{vap}} - \frac{1}{\rho_{liq}} \right] \quad (3-18)$$

$$W_{TNT} = \frac{2.4 \times 10^{-4} \times P_i \times V^*}{\gamma - 1} \times \left[1 - (101/P_i)^{(\gamma-1)/\gamma} \right] \quad (3-19)$$

$$R = \frac{r}{(W_{TNT})^{1/3}} \quad (3-20)$$

where W_L [kg] is the liquid weight inside the vessel; γ is the specific heat ratio; ρ_{liq} [$kg\ m^{-3}$] and ρ_{vap} [$kg\ m^{-3}$] are the liquid density and vapour density at explosion state.

3.5.2.2 Hemmatian's empirical method

Based on the TNT equivalence method and previous comparative studies [10, 56-59], another more up-to-date empirical method to predict BLEVE overpressure was proposed by Hemmatian et al. [69, 2017b]. Equation (3-21) to Equation (3-24) illustrate the prediction process of this method. In this empirical method, the Real-gas-behaviour and Adiabatic Irreversible Expansion (RAIE) assumption is made to calculate the BLEVE energy, which is 12.78 MJ. An updated energy conversion ratio (i.e., $\beta = 0.4$) is provided to determine the equivalent TNT mass. In this case study, an equivalent mass of 1.09 kg TNT is obtained, and its corresponding scaled distance at 20 m is $19.42\ m/kg^{1/3}$. Eventually, using the prediction charts for TNT blast, the side-on peak pressure, duration, arrival time and impulse can be obtained and shown in Table 3-9.

$$e = 43.97 - 213.9lr - 0.152T_i + 1.349 \times lr \times T_i - 0.0004361 \times T_i^2 - 0.002045 \times lr \times T_i^2 + 1.55 \times 10^{-6} T_i^3 \quad (3-21)$$

$$E = e \times V \quad (3-22)$$

$$W_{TNT} = \frac{\beta \times E \times 10^3}{4680} \quad (3-23)$$

$$R = \frac{r}{(W_{TNT})^{1/3}} \quad (3-24)$$

where e [MJ/m^3] is the mechanical energy released per cubic meter; lr is the liquid ratio.

Figure 3-25 compares the predicted pressure-time histories by the four methods and the recorded time history from the experiment. It should be noted that Prugh's method and Hemmatian's empirical method cannot predict the pressure rise time, and the pressure is therefore assumed to rise to the peak instantly. As shown, both Prugh's TNT equivalence method and the proposed empirical equations and charts can predict the BLEVE side-on peak pressure accurately. However, the proposed models yield better predictions of the pressure-time history compared to the recorded time history using Prugh's TNT equivalence method.

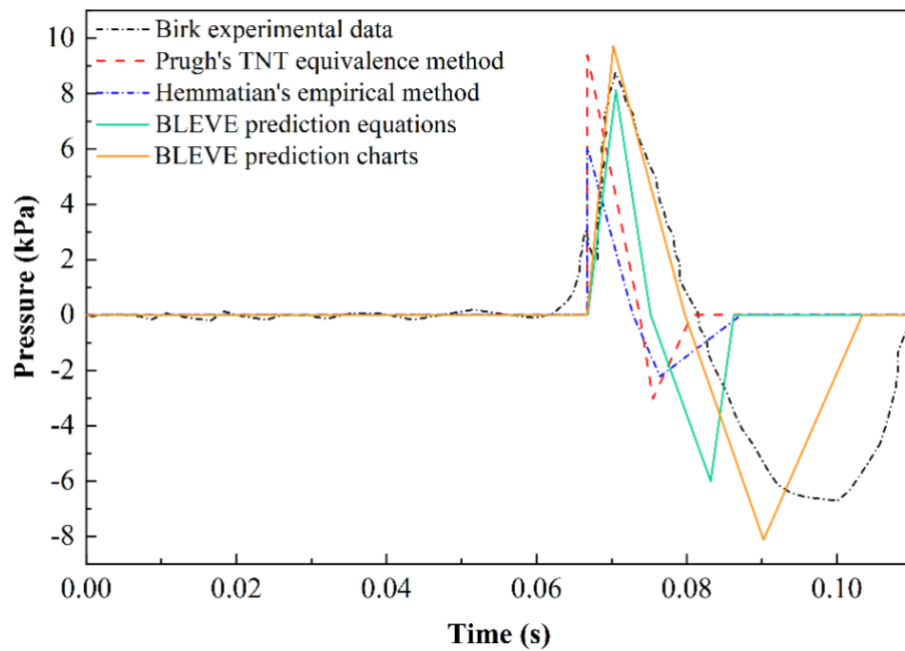


Figure 3-25. Comparison of experimental data with those predicted by the Prugh's TNT equivalence method, Hemmatian's empirical method and the proposed equations and charts in this study.

3.5.2.3 Comparison of all the available experimental data

The above comparison is conducted using one experimental example. To further verify the proposed methods, by repeating the same calculation procedure presented above, another five sets of experiments were used to evaluate the prediction accuracies of these methods. The corresponding results are summarized in Table 3-7 to Table 3-10. The best performance model, i.e., the one with the smallest error compared to experimental data, is highlighted in red.

Table 3-7. Pressure parameters predicted by Prugh's TNT equivalence method and the corresponding errors with respect to the available experimental data.

		Prugh's TNT equivalence method								
	r [m]	R	P_s^+ [kPa]	P_s^- [kPa]	t_a [s]	t_d^+ [s]	t_d^- [s]	i^+ [Pas]	t_p^+ [s]	t_p^- [s]
Birk 2007	20	14.09	9.39	-3.03	0.0433	0.0070	0.0070	29.80	N/A	N/A
	30	21.14	4.95	-1.92	0.0766	0.0081	0.0184	17.03	N/A	N/A
	40	28.19	3.03	-1.72	0.0851	0.0087	0.0184	14.19	N/A	N/A
Stawczyk	10	16.36	7.98	-2.83	0.0220	0.0032	0.0079	11.61	N/A	N/A
Johnson 1990	150	67.64	0.51	-0.66	0.4080	0.0171	0.0288	8.65	N/A	N/A
Melhem test 06	15	12.15	10.10	-3.03	0.0370	0.0062	0.0161	30.87	N/A	N/A
AVERAGE ERROR			28.65%	58.79%	23.23%	62.65%	46.63%	67.41%	N/A	N/A

Table 3-8. Error between the experimental results and those predicted by Prugh's TNT equivalence method, BLEVE equations & charts.

Parameters	Average Error	P_s^+ [kPa]	P_s^- [kPa]	t_a [s]	t_d^+ [s]	t_d^- [s]	i^+ [Pas]	t_p^+ [s]	t_p^- [s]
	BLEVE prediction equations	24.16%	19.80%	14.17%	55.34%	60.95%	64.77%	18.96%	22.70%
BLEVE prediction charts	20.29%	27.52%	17.06%	35.99%	27.34%	50.01%	22.17%	18.97%	
Prugh's TNT equivalence method	28.65%	58.79%	23.23%	62.65%	46.63%	67.41%	N/A	N/A	

Table 3-9. Pressure parameters predicted by Hemmatian's empirical model and the corresponding errors with respect to the available experimental data.

		Hemmatian's empirical model								
	r [m]	R	P_s^+ [kPa]	P_s^- [kPa]	t_a [s]	t_d^+ [s]	t_d^- [s]	i^+ [Pas]	t_p^+ [s]	t_p^- [s]
Birk 2007	20	19.42	6.06	-2.22	0.0505	0.0059	0.0144	17.51	N/A	N/A
	30	29.13	3.64	-1.72	0.0793	0.0063	0.0144	10.30	N/A	N/A
	40	38.84	2.83	-1.21	0.1030	0.0072	0.0153	8.24	N/A	N/A
Stawczyk	10	34.25	2.93	-14.14	0.0263	0.0020	0.0041	2.63	N/A	N/A
Johnson 1990	150	94.96	0.71	-0.51	0.4107	0.0139	0.0237	4.90	N/A	N/A
Melhem test 06	15	16.57	8.08	-2.83	0.0435	0.0047	0.0122	17.66	N/A	N/A
AVERAGE ERROR			52.28%	51.24%	19.87%	70.63%	55.49%	81.79%	N/A	N/A

Table 3-10. Error between the experimental results and those predicted by Hemmatian's empirical model, BLEVE equations & charts.

Parameters	Average Error	P_s^+ [kPa]	P_s^- [kPa]	t_a [s]	t_d^+ [s]	t_d^- [s]	i^+ [Pas]	t_p^+ [s]	t_p^- [s]
BLEVE prediction equations		24.16%	19.80%	14.17%	55.34%	60.95%	64.77%	18.96%	22.70%
BLEVE prediction charts		20.29%	27.52%	17.06%	35.99%	27.34%	50.01%	22.17%	18.97%
Hemmatian's empirical model		52.28%	51.24%	19.87%	70.63%	55.49%	81.79%	N/A	N/A

As mentioned above, neither Prugh's TNT equivalence method nor Hemmatian's empirical method is able to predict the peak pressure rise time (i.e., t_p^+ and t_p^-). They assume the shock wave increases instantaneously to the peak value. However, this assumption significantly overestimates the loading rate, which would affect the prediction accuracy of the strain rate of the structural responses.

In comparison of all outputs (i.e., P_s^+ , P_s^- , t_d^+ , t_d^- , t_a , t_p^+ , t_p^- and i^+) in Table 3-8, it is seen that Prugh's TNT equivalence method can predict the positive side-on peak pressure, arrival time and negative duration with acceptable accuracies. However, other prediction results have errors greater than 50%. Meanwhile, Hemmatian's empirical method would lead to an average error of over 50% for most pressure wave parameters, as shown in Table 3-10. BLEVE mechanical energy is the main reason contributing to the differences among Prugh's TNT equivalence method, Hemmatian's empirical method and the BLEVE pressure prediction methods proposed here. The

amount of mechanical energy contributing to the overpressure is difficult to obtain with both Prugh's TNT equivalence method and Hemmatian's empirical method since the mechanical energy used to break the vessels and eject the fragments of the vessel is uncertain [69, 2017b]. Therefore, the generated external overpressures may be inaccurate because of the uncertain energy conversion.

3.6 Summary

In this section, using a verified FLACS CFD and ANN model, 90000 sets of BLEVE pressure waves in open space were generated. Altogether 7 BLEVE variables, namely width, height and length of the tank, liquid ratio, tank failure pressure, failure temperature and target location, were considered, which were used to determine 8 parameters, i.e., positive and negative side-on peak pressure, positive and negative duration, arrival time, positive and negative peak pressure rise time and impulse, for defining the BLEVE pressure wave time history and impulse. Empirical formulae and the corresponding charts of these 8 pressure wave parameters as functions of 7 BLEVE variables were established for efficient predictions of BLEVE pressure-time histories in open space. Compared with the recorded data in BLEVE tests available in the literature, the proposed empirical formulae and charts yielded good predictions of the pressure-time history. Since an empirical model of peak pressure rise time is proposed, the developed empirical formulae and charts can depict the BLEVE pressure-time history more accurately than other empirical methods.

Chapter 4 Prediction of BLEVE loading on rigid structures

4.1 Introduction

In the previous chapter, BLEVE in open space has been investigated. However, for designing structures against BLEVE event, BLEVE load acting on structures, instead of the pressure in open space, should be used in the structural response analysis. Therefore, further study is required to accurately predict BLEVE loads on structures. In this study, 1300 sets of BLEVE cases consisting of 650 wave propagation in open space and 650 pressure wave-structure interaction cases are numerically modelled. The open space BLEVE pressure and reflected pressure waves from the rigid structure are simulated, and the corresponding impulses are calculated. The reflection coefficient chart is developed to predict the reflected BLEVE overpressure on the rigid structure. The diffraction and clearing effects on the reflected waves are analysed with respect to the dimensions of the structure. An empirical formula for predicting the reflected impulse is also proposed. The results obtained in this study can be used together with the open space BLEVE pressure predictions presented in Chapter 3 to predict the BLEVE loads on structures.

The related work in this chapter has been published in Process Safety and Environmental Protection.

Wang, Y., Hao, H., Chen, W., Li, J. & Wang, Z. 2023. Prediction of BLEVE loading on a rigid structure. Process Safety and Environmental Protection, 175, 1-16.

4.2 Numerical modelling

To predict BLEVE loading on a rigid structure, the numerical modelling needs to be employed since the empirical method cannot provide accurate prediction as mentioned above. FLACS is selected in this study as it can simulate the BLEVE generation, wave

propagation, and interaction with structures to obtain the reflected overpressure on the structure.

4.2.1 Validation of CFD models

FLACS is a commonly used CFD commercial software to predict BLEVE. For condensed explosives modelling and blast wave propagation, FLACS-Blast module is employed to compute via Euler equations, flux-corrected transport (FCT) scheme and a second-order flux correction [105]. Large-scale experiments are used to calibrate the numerical model, including BAM's tests in Germany [50], Johnson and Pritchard's experiments [49] and Betteridge and Phillips' experiments [53] from the literature. The experimental details are shown in Table 4-1, including the pressurized liquid, failure pressure (P_i), failure status, liquid ratio, BLEVE tank volume (V) and the distance between the BLEVE and target (r). Numerical simulations of BLEVEs for both "non-superheated" and "superheated" cases are validated. In terms of non-superheated BLEVE, only vapour expansion provides the energy to generate the first blast wave. If the internal liquid of BLEVE is in the superheated status, liquid flashing energy and vapour expansion energy should be considered together for blast wave generation. However, it is unable to model two high-pressure regions (i.e., vapour and liquid phase) in FLACS since it can define only one high-pressure region [23]. To accurately simulate BLEVEs under "superheated" status in FLACS, the liquid correction method [23] is applied to calculate the final failure pressure of BLEVE. This method introduces a pseudo-source in the FLACS modelling to simulate the second high-pressure region (i.e., liquid phase). Figure 4-1 (a) presents the pseudo-source and high-pressure regions of BAM tests, which are fully confined by the panels. When the stable pressure is equal to 20% of tank failure pressure (i.e., 5 bar), the corresponding initial pressure of pseudo-source (i.e., 10 bar) is the BLEVE rupture pressure contributed by flashing liquid [23], as shown in Figure 4-1(b). Therefore, the total failure pressure of BAM tests is 35 bar in FLACS simulations. The monitoring points are arranged at the same location as the experimental setup to compare the experimental data and numerical results, as shown in Figure 4-2. In numerical simulations, "PLANE_WAVE" boundary conditions are applied to eliminate the reflection. A uniform grid of 0.2 meters is used in the core domain, as this grid size can achieve the

balance between accuracy and efficiency [23, 24]. Grid size outside the core domain is gradually stretched by a factor of 1.1 to speed up the simulations.

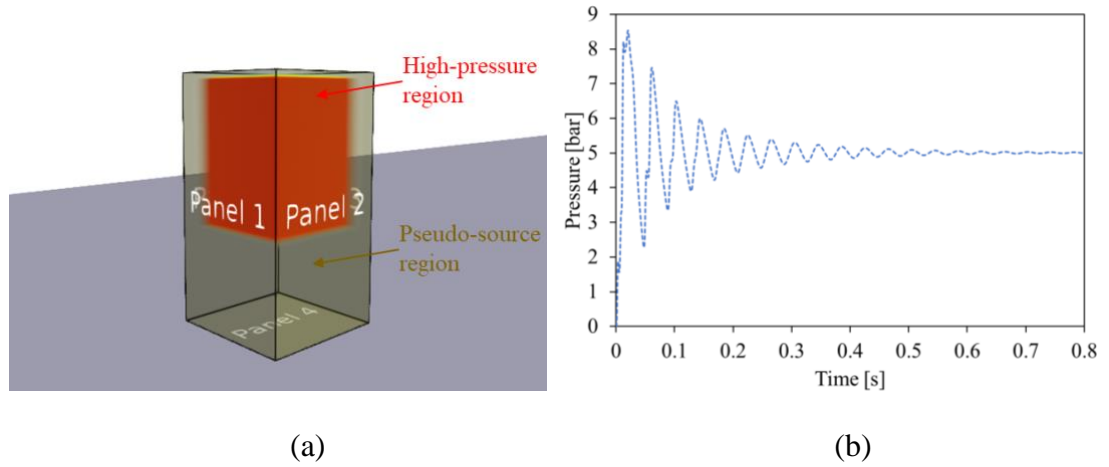


Figure 4-1. Pseudo-source simulation: (a) Modelling in FLACS; (b) Pressure time history of monitor point inside the pseudo-source.

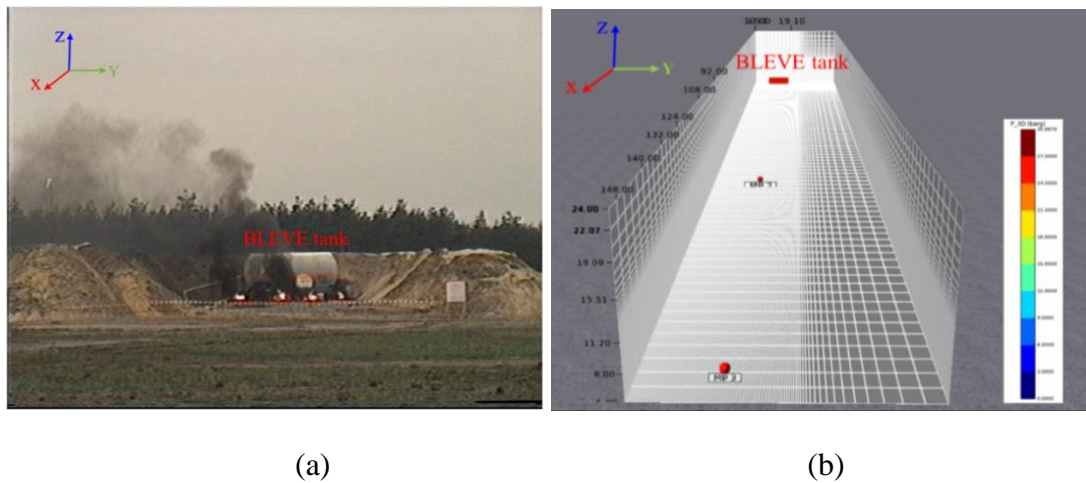


Figure 4-2. Large-scale BLEVE experiments: (a) BAM's test [50]; (b) 3D model in FLACS.

Table 4-1. Details of large-scale BLEVE experiments [49, 50, 53].

Experiments	Fluid	P_i [bar]	Status	Liquid ratio [%]	V [m ³]	r [m]
BAM [50]	Propane	25	Superheated	22	45.36	100/150

Table 4-1 (Continued)

Experiments	Fluid	P_i [bar]	Status	Liquid ratio [%]	V [m ³]	r [m]
	Propane	15	Non-superheated	80	5.659	150
	Butane	14.6	Non-superheated	75	5.659	25
Johnson and	Butane	15.1	Non-superheated	76	5.659	25/50
Pritchard [49]	Butane	15.1	Non-superheated	40	10.796	25/50
	Butane	15.2	Non-superheated	38/76	5.659	25/50
Betteridge and Phillips [53]	LNG	13.01	Non-superheated	37	5.055	40/70/100

Note: failure pressure (P_i), BLEVE tank volume (V), and distance between the BLEVE and target (r).

The accuracy of using FLACS in predicting the BLEVE pressure-time profile is illustrated in Figure 4-3. BAM’s experiment and one of Johnson’s experiments ($P_i = 15$ bar) are used for verifications of BLEVE pressure predictions in “superheated” and “non-superheated” conditions, respectively. As shown, the peak overpressure can be well predicted by FLACS. FLACS overestimates the peak overpressure of BAM by less than 30%. It is worth mentioning that there are multiple oscillating pressure spikes in simulations because the grid cells are stretched to balance the computational accuracy and efficiency due to the large-scale BLEVEs [23].

Multiple performance metrics are used to qualitatively evaluate the performance of FLACS simulations, and each metric has its strength and weakness. Five performance metrics include the geometric mean bias (MG), geometric variance (VG), prediction fraction within a factor of two observations (FAC2), fractional bias (FB) and normalized mean square error (NMSE) [105]. The bias between the results of FLACS simulations (X_p) and experimental data (X_o) can be determined by these metrics, which are defined by Equations (4-1) to (4-5). As specified in the FLACS-CFD user’s manual [105], at least 50% of predicted data should be within the range of FAC2 (i.e., $FAC2 > 50\%$), and the bias (FB & MG) requires $-0.67 < FB < 0.67$ or $0.5 < MG < 2.0$, and random scatter (NMSE & VG) should have a value of $NMSE < 1.5$ or $VG < 4$. The five-performance metrics of these data are given in Table 4-2, indicating all numerical results are within the acceptable range.

Additionally, the scatter and parabola plots are shown in Figure 4-4, indicating the number of predicted data falling into the “Excellent” region. The scatter plot depicts the excellent deviation range and FAC2 region, indicating the majority of the numerical results have a deviation of less than 30% from the experimental data, and 100% of the predicted results fall into the range of FAC2. Meanwhile, the parabola plot further presents the predictive performance of numerical simulations through systemic overprediction or underprediction (i.e., MG) and scatter of the numerical results (i.e., VG). As shown, most numerical results fall into the “Excellent” region, and all the data are within the “Acceptable” region. Thus, FLACS can accurately predict the peak overpressure resulting from large-scale BLEVEs.

$$MG = \exp \left[\ln \left(\frac{X_p}{X_o} \right) \right] \quad (4-1)$$

$$VG = \exp \left[\ln \left(\frac{X_p}{X_o} \right)^2 \right] \quad (4-2)$$

$$FAC2 = \text{the fraction of data where } 0.5 \leq \frac{X_p}{X_o} \leq 2.0 \quad (4-3)$$

$$FB = \frac{\bar{X}_p - \bar{X}_o}{0.5(\bar{X}_p + \bar{X}_o)} \quad (4-4)$$

$$NMSE = \frac{\overline{(X_p - X_o)^2}}{\bar{X}_p \bar{X}_o} \quad (4-5)$$

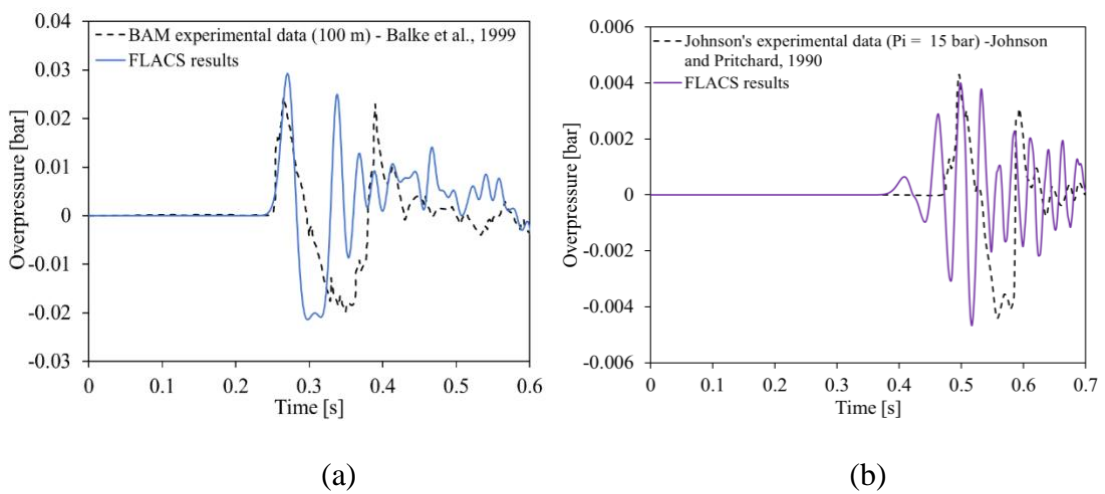


Figure 4-3. Pressure time history (numerical results vs experimental data): (a) BAM’s experiment [50]; (b) Johnson’s experiment [49].

Table 4-2. Performance metrics of numerical results for large-scale BLEVE experiments.

Performance metrics	MG	VG	FAC2	FB	NMSE
Value	0.61 – 1.44	1.00 – 1.29	100 %	0.11	0.03

Note: Geometric mean bias (MG), geometric variance (VG), prediction fraction within a factor of two observations (FAC2), fractional bias (FB) and normalized mean square error (NMSE)

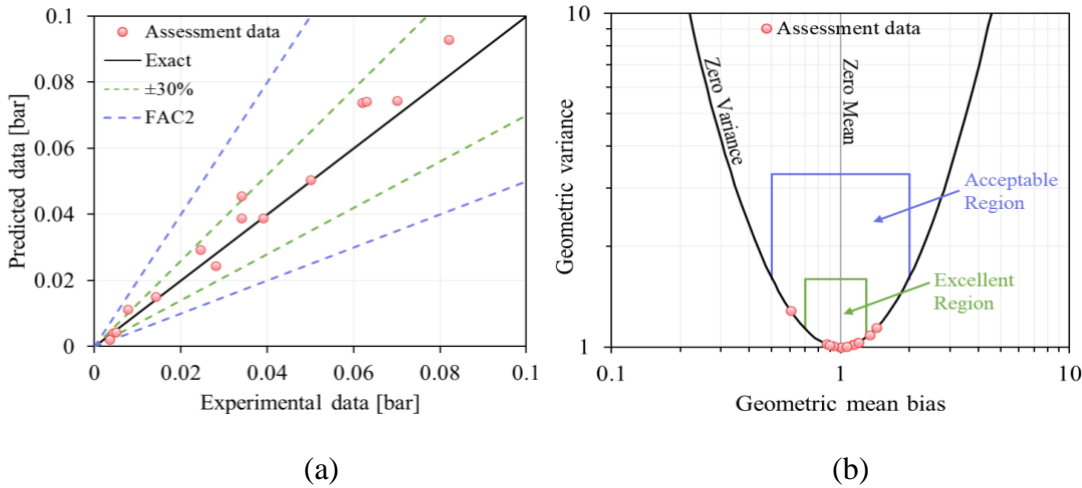


Figure 4-4. Comparison of numerical results and experimental data in (a) scatter plot and (b) parabola plot.

This study focuses on the BLEVE wave reflected on a rigid structure. Hence, the accuracy of blast wave interaction with a structure should be validated. Since no available BLEVE experiment was conducted in obstructed environments, the reflected and diffracted BLEVE waves cannot be directly compared with experimental data. However, the accuracy of FLACS in predicting the interaction of blast waves with structures has been demonstrated in previous studies. For instance, Li and Hao [77] measured the overpressure of vented gas explosions between two tanks in a tank group. The interaction of blast waves and the cylindrical obstacle was simulated to predict the reflected overpressure on the front and rear surfaces of the tank. Numerical simulations achieved reasonable accuracy in predicting overpressure between structure walls as compared to the experimental data, indicating FLACS can model the reflected blast waves well. Liu et al. [106] performed full-scale gas explosion experiments in an urban regulator station (i.e., vented confined space), and pressure sensors were located outside the door and windows. In addition, the numerical simulation was conducted using FLACS, and the predicted peak overpressure agrees well with the experimental

results, proving that FLACS can well capture the wave diffraction. Therefore, the characteristic of blast wave and structure interaction can be well simulated in FLACS. The grid sensitivity analysis of BLEVE loads on a rigid structure using different grid sizes (i.e., 0.4 m, 0.2 m and 0.1 m) is shown in Figure 4-5. A grid size of 0.2 m is the optimal one for achieving a balance of accuracy and computational efficiency. Meanwhile, this grid size is consistent with the authors' previous study (i.e., BLEVE in open space), enabling the same grid setup to be applied in the simulation of BLEVE wave propagation in open space and interaction with a rigid structure.

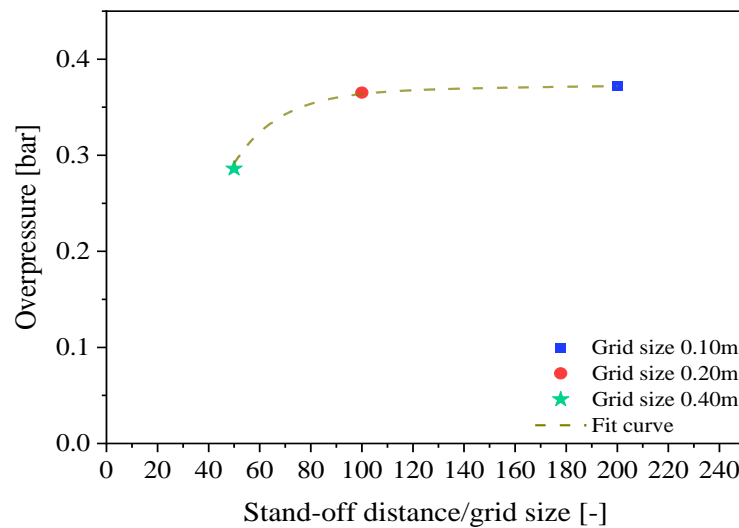


Figure 4-5. Grid sensitivity study of BLEVE loads on a rigid structure.

4.2.2 CFD simulation

After demonstrating the accuracy of FLACS in predicting BLEVE pressures in free air and the pressure wave interaction with structures, the pressure waves from BLEVEs of different conditions in free air and their interactions with a rigid structure of different dimensions are simulated. BLEVE is a complex physical explosion, and many critical parameters affect the BLEVE overpressure and wave propagation, including tank failure pressure, failure temperature, liquid ratio, tank dimensions (i.e., length, width and height) and stand-off distance [92]. In this study, 1300 BLEVE cases are simulated, and the simulations are carried out by randomly and uniformly sampling the respective BLEVE parameters. The BLEVE parameters are defined within the practical ranges, as shown in Table 4-3. BLEVE simulations in open space are carried out first, following the same settings as Li et al. [24]. This study focuses on LPG-

induced BLEVEs. Hence, butane and propane are selected as pressurised liquids. BLEVE tank failure conditions are essential to determine the internal liquid status and the BLEVE energy. To consider “non-superheated” and “superheated” BLEVEs, the failure pressure is defined from minimum experimental pressure (i.e., 5 bar) to critical pressure of the pressurised liquid, and the failure temperature is defined up to its critical temperature. The simulations simplify the BLEVE tank as rectangular to minimise the mass residual issue, since FLACS uses the block control volume as the grid meshing [105]. Based on the European manufacturing standard of LPG tanks, the volume of BLEVE is sampled from 10 m³ to 90 m³ [107]. When the propagating BLEVE pressure wave arrives at a rigid rectangular structure, the interaction of the pressure wave with the structure causes wave reflection and diffraction depending on the wave amplitude, velocity and duration, as well as the structural dimension, geometry and stiffness. As stated above in this study, the structure is assumed as rectangular and rigid, only the dimension is changed. The smallest structural size is 3 m in width, 3 m in height and 0.4 m in thickness, while the largest dimension is 18 m in width, 18 m in height and 3 m in thickness. Usually the maximum reflected overpressure occurs when the blast wave incident angle is perpendicular to the surface of the structure and the minimum when the blast wave incident angle is parallel to the surface of a structure, but this is not necessarily true for shock waves owing to Mach effect and is also incident pressure wave amplitude dependent as indicated in UFC-3-340-02 [18]. In this study, the angle of incidence (α) between the BLEVE centre and structure centre is varied from 0° to 90° to investigate the incident angle effect on BLEVE pressure wave reflection. To prevent the smearing of the BLEVE waves, a uniform grid of 0.2 m is applied in the region containing BLEVE sources and the rigid structure.

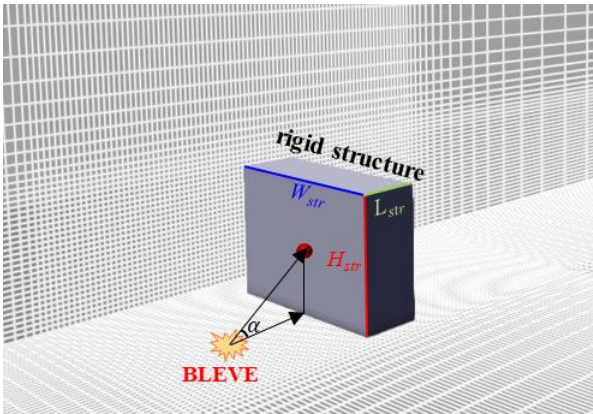


Figure 4-6. Schematic diagram of numerical model.

Table 4-3. Variables of BLEVE simulation [24].

Variable	Butane	Propane
Tank failure pressure, P_l (bar)	5 – 37	5 – 42
Liquid temperature, T_l (°C)	1 – 152	1 – 96
Vapour temperature, T_v (°C)	1 – 304	1 – 192
Liquid status at failure	Non-superheated or superheated	
Liquid fill level, LFL (%)	10 – 90	
Tank width, W_{tank} (m)	0.2 – 3	
Tank length, L_{tank} (m)	0.2 – 10	
Tank height, H_{tank} (m)	0.2 – 3	
Structure width, W_{str} (m)	3 – 18	
Structure thickness, L_{str} (m)	0.4 – 3	
Structure height, H_{str} (m)	3 – 18	
Distance between structure centre and BLEVE centre (m)	0 – 20	
BLEVE height above ground, H_{BLEVE} (m)	0 – 2	
Angle of incidence, α (degree)	0 – 90	

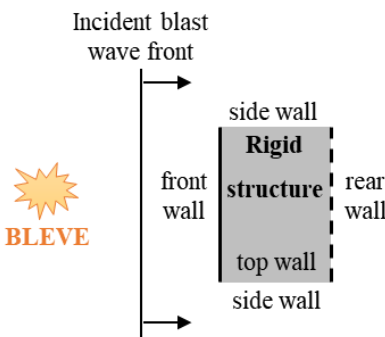
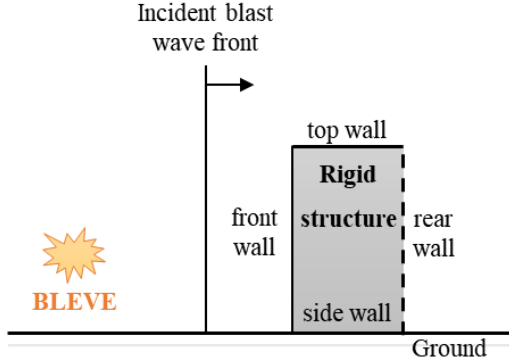
4.3 Blast wave-structure interaction

With the validated CFD models, the interaction between blast waves and a rigid structure is investigated. The interaction is complicated when blast waves act on a finite-size structure due to wave reflection and diffraction. Figure 4-7 shows a schematic diagram of the BLEVE wave interaction with a rigid rectangular structure on the front and rear surfaces from the side and top views. When BLEVE occurs, blast waves propagate outward from the explosion centre, as shown in Figure 4-7 (a). A reflected wave is formed immediately when the incident wave reaches the target surface. Although a portion of the incident wave is reflected from the target surface,

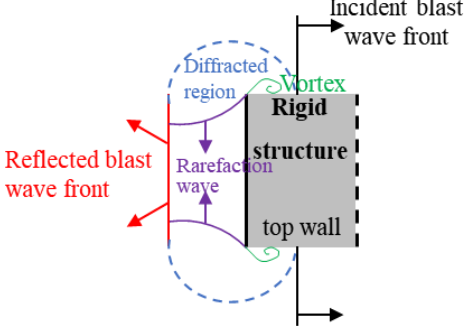
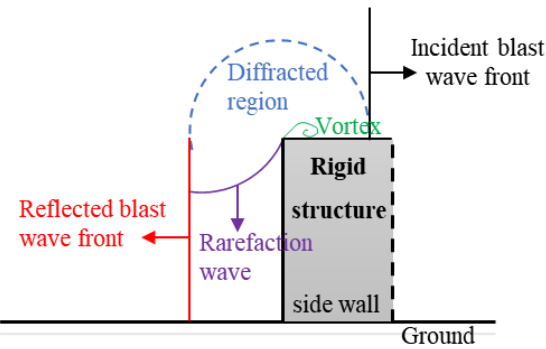
the remaining unblocked incident waves travel along the surface edge, causing a diffraction phenomenon around the free edge. Diffraction generates rarefaction waves, resulting in the pressure imbalance between low-pressure rarefaction waves and high-pressure reflected waves. As the pressure eventually reaches equilibrium, air begins to flow from the high-pressure region to the low-pressure region (i.e., propagates from boundaries to centre) [108-110]. Figure 4-7 (b) illustrates the pressure flow on the structure's top and two side walls during the blast wave propagation. Subsequently, diffracted waves travel along the free edges to the rear surface. BLEVE waves envelop the structure after the diffracted wavefront reaches the rear surface of the structure and forms a pair of vortexes around the free edge, as shown in Figure 4-7 (c). After the diffraction process completes, the blast waves bypass the structure and continue to travel as shown in Figure 4-7 (d) [111, 112]. In fact, the reflected wave can deform a non-rigid structure, affecting the reflected peak overpressure and impulse [113]. However, a rigid structure is assumed in this study, and thus there is no structural deformation. The reflection and diffraction of BLEVE waves on rigid structures with different dimensions are discussed in the following sections.

Side view

Top view



(a)



(b)

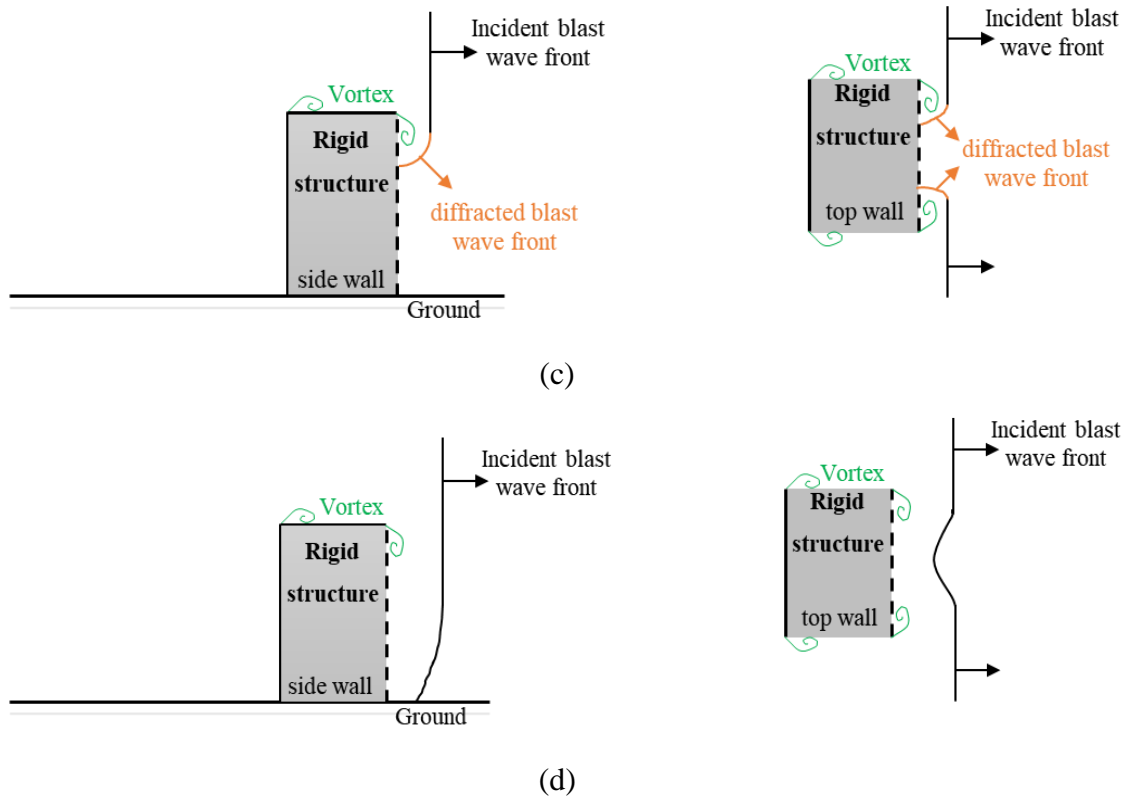


Figure 4-7. Schematic top view and side view of BLEVE wave interaction with a rigid structure [111, 112]: (a) Incident waves at the front surface; (b) Reflected and diffracted waves at the front surface; (c) Diffracted waves at the rear surface; (d) Diffraction complete at the rear surface.

4.4 Reflected overpressure of BLEVE pressure wave

The phenomenon of BLEVE wave-structure interaction is presented in Section 4.3. Since the reflected overpressure is the blast load on the structure, this section presents the BLEVE reflected overpressure and the reflection coefficient chart at the centre point of the front wall.

4.4.1 Reflected overpressure profile

An explosion is defined as a sudden growth in volume and release of energy during a short period, resulting in pressure wave propagation [114]. The typical pressure-time profiles of high explosion and BLEVE are shown in Figure 4-8. Seven essential parameters to determine the pressure-time profile include arrival time (t_a), positive and negative peak pressure (P_s^+ & P_s^-), positive and negative peak pressure rise time (t_p^+ & t_p^-) and positive and negative duration (t_d^+ & t_d^-). BLEVEs generate a much lower pressure rise rate than high explosive detonations, indicating a less significant

loading rate on structure. Meanwhile, BLEVE pressure wave has a longer positive duration than that of high explosive detonations. For example, the positive pressure duration of a typical TNT explosion is usually in an order of a few milliseconds, e.g., about 5.98 ms for a 1-tonne TNT explosion at a stand-off distance of 13.1 m [115]. On the contrary, a BLEVE pressure wave has a relatively long duration. For instance, the duration generated by BLEVE from a 2 m³ tank with a 51% liquid ratio is approximately 25 ms at stand-off distance 20 m [28]. Longer duration usually leads to higher impulse. Therefore, proper modelling of the BLEVE pressure waves is essential for accurately defining the BLEVE loads on structures.

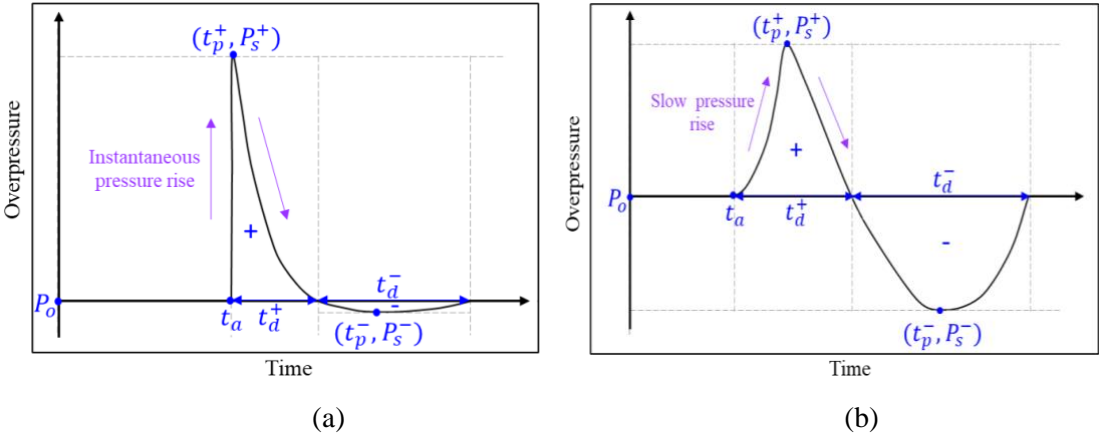


Figure 4-8. Typical overpressure-time profiles: (a) TNT explosion; (b) BLEVE.

Note: ambient pressure (P_0), positive peak overpressure (P_s^+), negative peak overpressure (P_s^-), arrival time (t_a), positive duration (t_d^+), negative duration (t_d^-), positive peak pressure rise time (t_p^+) and negative peak pressure rise time (t_p^-).

When a BLEVE occurs in front of a rigid structure, the propagating pressure wave interacts with the structure and generates blast load on the structure. Due to the interaction between the BLEVE waves and the structure, a portion of the blast waves is reflected from the front surface. The superposition of the reflected overpressure and incident overpressure intensifies the blast overpressure. As compared with BLEVE overpressure in open space, both positive and negative peak overpressures of BLEVE on a rigid structure are amplified while other essential parameters (t_a , t_d^+ , t_d^- , t_p^+ & t_p^-) are less affected, as shown in Figure 4-9. The reflected overpressure in the CFD model is shown in Figure 4-10 when the BLEVE wave propagates to a rigid structure. The relationship between reflected overpressure and incident overpressure (i.e., reflection coefficient) is affected by explosive conditions (e.g., type and weight), stand-off

distance, location between charge and structure, structure configuration (e.g., geometry and dimension), the interaction of blast wave with structure and ground, etc. [96]. High explosive detonation is a chemical explosion and the incident overpressure is mainly determined by the stand-off distance and charge weight. However, BLEVE is a physical explosion, more factors affect the explosion incident overpressure due to the co-existence of vapour and liquid in the BLEVE tank. Hence, the explosion conditions of BLEVE are more complicated since the tank failure pressure, failure temperature, liquid ratio, and tank dimensions (i.e., width, length and height) all affect BLEVE pressures. Therefore, the effects of different factors on the BLEVE should be considered. That is, explosion scenarios with different initial conditions need to be investigated along with different incidence angles between the explosive and structure besides the equivalent explosion energy, structure configuration and stand-off distance.

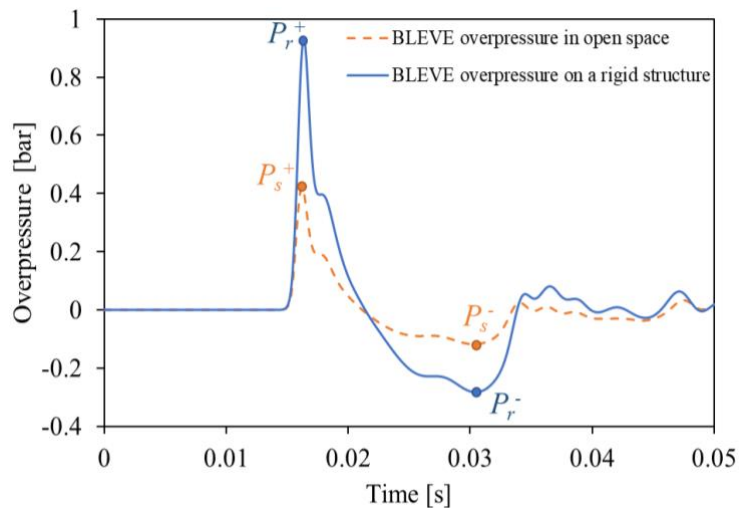


Figure 4-9. BLEVE pressure-time profile (P_s : incident peak overpressure & P_r : reflected peak overpressure).

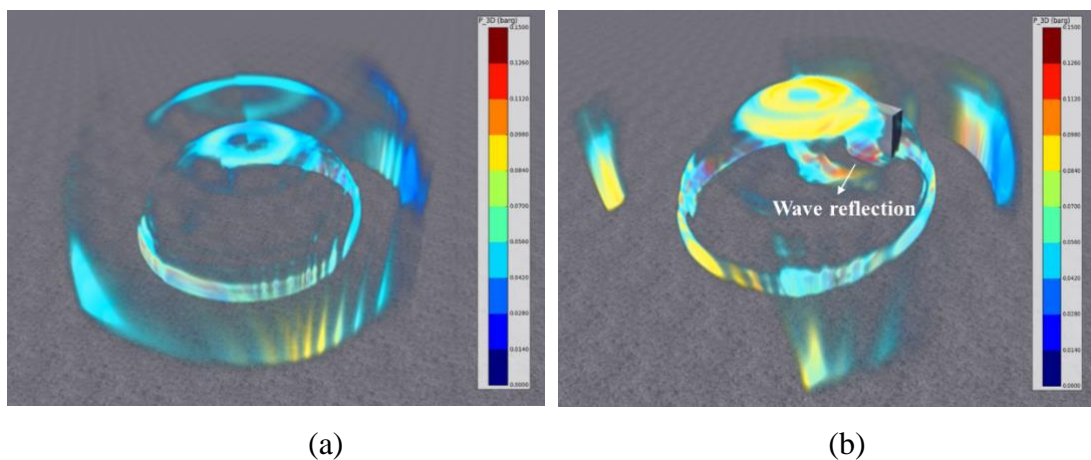


Figure 4-10. BLEVE pressure wave propagation: (a) in open space; (b) interaction with a rigid structure.

4.4.2 Reflection coefficient (C_r) for positive overpressure (P_r^+)

As mentioned above, the reflected peak overpressure may be several times higher than the incident peak overpressure [96]. The reflected peak overpressure can vary widely based on the incident peak overpressure, and the relative angle from the BLEVE centre to the structure centre. Incident peak overpressure is mainly affected by the stand-off distance between BLEVE and structure as well as the BLEVE initial conditions, such as BLEVE failure conditions (i.e., failure pressure and temperature), liquid ratio, and tank dimensions (i.e., width, length and height). Angle of incidence (α) is another essential parameter that has a significant effect on reflection. When the propagation direction of the blast wave is perpendicular to the surface (i.e., $\alpha = 0^\circ$), the highest reflected overpressure is generated when Mach stem is not formed. When the direction of the reflected pressure wave is parallel to the surface (i.e., $\alpha = 90^\circ$), the reflected pressure is equal to the incident pressure. The ratio of the peak reflected overpressure (P_r^+) to the incident peak overpressure (P_s^+) is defined as the reflection coefficient as expressed in Equation (4-6).

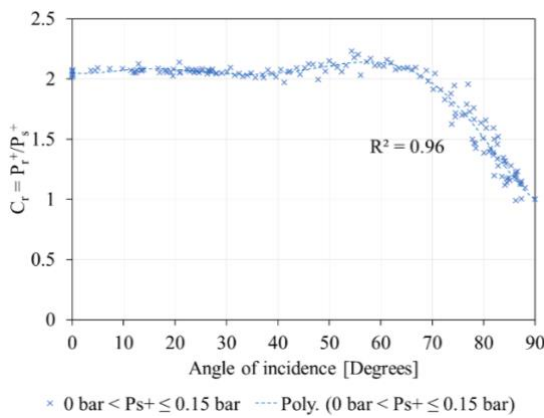
$$C_r = \frac{P_r^+}{P_s^+} \quad (4-6)$$

A total of 1300 sets of BLEVE cases (i.e., 650 in open space and 650 pressure wave and rigid structure interaction cases) are used to derive the BLEVE reflection coefficients. Figure 4-11 shows the BLEVE reflection coefficient charts based on different ranges of incident overpressure, including $0 \text{ bar} < P_s^+ \leq 0.15 \text{ bar}$, $0.15 \text{ bar} < P_s^+ \leq 0.25 \text{ bar}$, $0.25 \text{ bar} < P_s^+ \leq 0.4 \text{ bar}$, $0.4 \text{ bar} < P_s^+ \leq 0.5 \text{ bar}$ and $0.5 \text{ bar} < P_s^+ \leq 1 \text{ bar}$, respectively. The R-square values are over 0.94 for all reflection coefficient charts of BLEVE, indicating good fitting results.

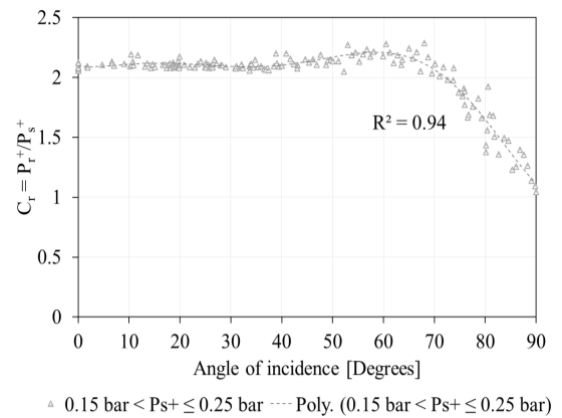
As shown in Figure 4-11, the reflection coefficient decreases in general as the angle of incidence increases from 0 to 90 degrees. However, the reflection coefficient of BLEVE has a very slight increase in the range of the angle of incidence from 50° to 70° . Figure 4-12 compares the reflection coefficient of TNT explosions and BLEVEs. Compared to the BLEVE reflection coefficient chart, the reflection coefficient from a TNT explosion increases rapidly when reaching the critical angle of incidence. The sudden increase in reflected overpressure is due to the incident blast wave heating the air as it passes through. The reflected waves have a faster propagation speed and eventually catch up with the incident blast waves [116]. At the critical angle of

incidence, the reflected wave catches up and merges with the incident wave to form a Mach stem, which is the transition point from regular to Mach-reflected shock waves [117, 118]. The Mach stem can greatly intensify the overpressure [119].

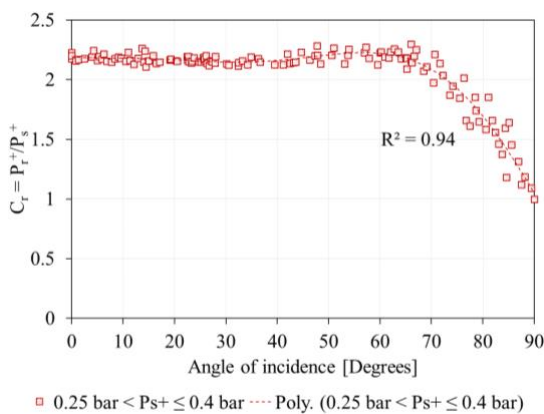
Mach number is the ratio of local flow velocity to the ambient sound speed, which determines whether Mach reflection occurs or not. Given the same incident overpressure and angle, the difference in the reflection coefficient of TNT explosions and BLEVEs is due to the Mach number. When the Mach number is higher than 1.46, a strong shock wave and Mach reflection (MR) occur, which can be addressed by von Neumann's three-shock theory [120, 121]. When the Mach number is lower than 1.46, the weak blast wave and von Neumann reflection (vNR) occur, which can be explained by von Neumann paradox [121-123]. Since BLEVE has a Mach number between 0.035 and 0.76, the weak blast wave and von Neumann reflection occur. It is worth mentioning that the incident peak overpressure is up to 345 bar in the TNT reflection coefficient chart in UFC-3-340-02, while the BLEVE reflection coefficient chart covers the incident peak overpressure up to 1 bar, which is the typical range of BLEVE pressure.



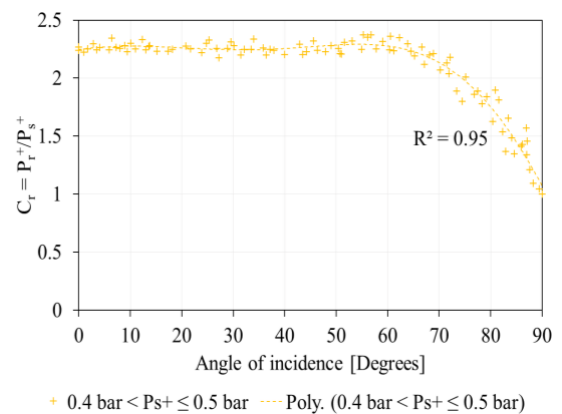
(a)



(b)



(c)



(d)

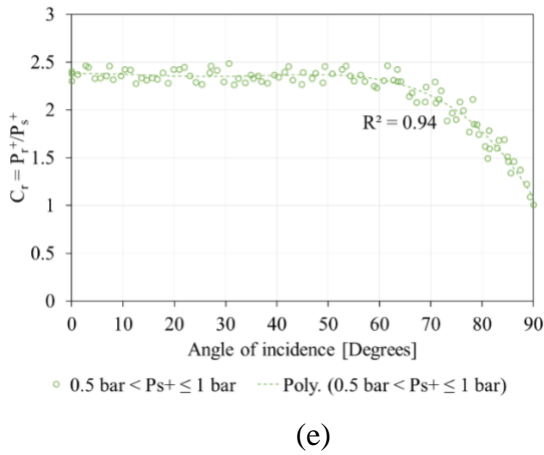


Figure 4-11. BLEVE reflection coefficient for positive overpressure (C_r) charts: (a) $0 \text{ bar} < P_s^+ \leq 0.15 \text{ bar}$; (b) $0.15 \text{ bar} < P_s^+ \leq 0.25 \text{ bar}$; (c) $0.25 \text{ bar} < P_s^+ \leq 0.4 \text{ bar}$; (d) $0.4 \text{ bar} < P_s^+ \leq 0.5 \text{ bar}$; (e) $0.5 \text{ bar} < P_s^+ \leq 1 \text{ bar}$.

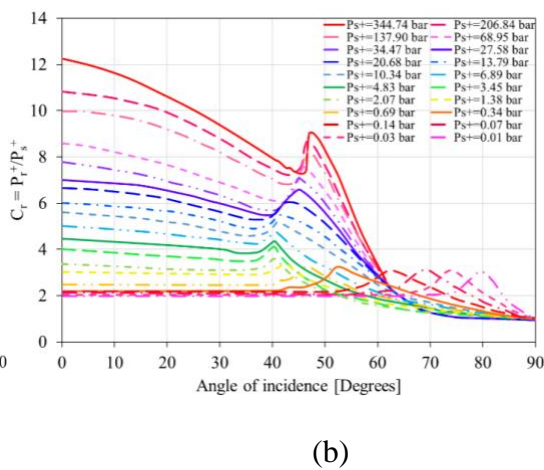
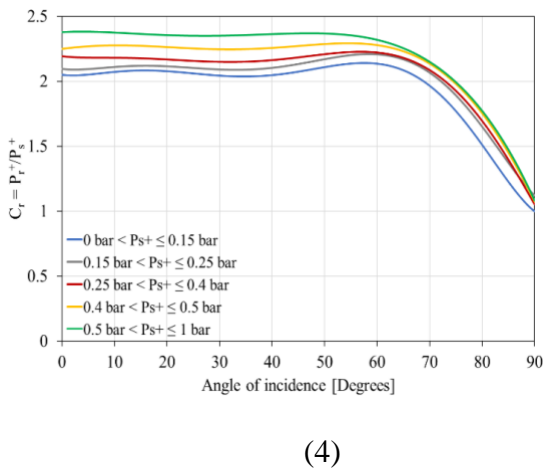


Figure 4-12. Comparison of reflection coefficient for positive overpressure (C_r) charts: (a) BLEVEs (incident overpressure $\leq 1 \text{ bar}$); (b) TNT explosions [18].

4.4.3 Reflected negative overpressure (P_r^-)

It is well known that negative overpressure can generate suction force and the magnitude of negative pressure from high explosive explosion is much smaller than the positive overpressure [96]. Based on the 1300 sets of BLEVE data, it is found that the negative and positive reflected peak overpressures show a strong linear relationship, as given in Equation (4-7). The R-square value is around 0.9, as shown in Figure 4-13.

$$P_r^- = -0.26P_r^+ - 0.059 \text{ (bar)} \quad (4-7)$$

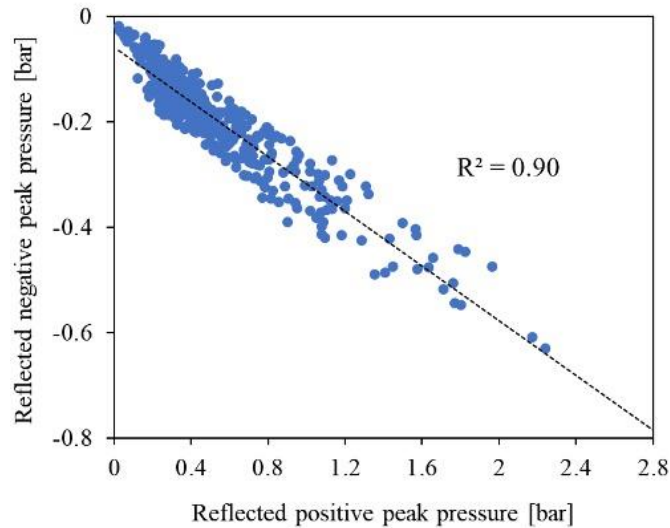


Figure 4-13. Correlation between reflected negative peak pressure (P_r^-) and reflected positive peak pressure (P_r^+).

4.4.4 Peak pressure rise time (t_p)

In addition to the reflected peak overpressures, the pressure rise rate is another essential parameter to determine the BLEVE pressure-time profile, which greatly affects the structural response. To obtain the pressure rise rate, the time to reach the peak positive and negative overpressures is defined as the peak pressure rise time (t_p^+ & t_p^-). It is well known that TNT explosion exhibits an almost instantaneous pressure rise, and the BLEVE pressure rises to the peak at a slower rate, resulting in very different structural responses because of different loading rates. BLEVE pressure rise rate can be calculated as the ratio of peak overpressure to rising time (i.e., $t_p^+ - t_a$). As shown in Figure 4-14, the peak pressure rise times ($t_{p,r}$) of reflected BLEVE overpressure are very similar to the incident ones ($t_{p,i}$). Although the reflected and incident overpressure profiles have almost the same peak pressure rise time, the reflected peak pressure rise rate is greater than the incident peak pressure rise rate due to the higher values of the reflected peak overpressure.

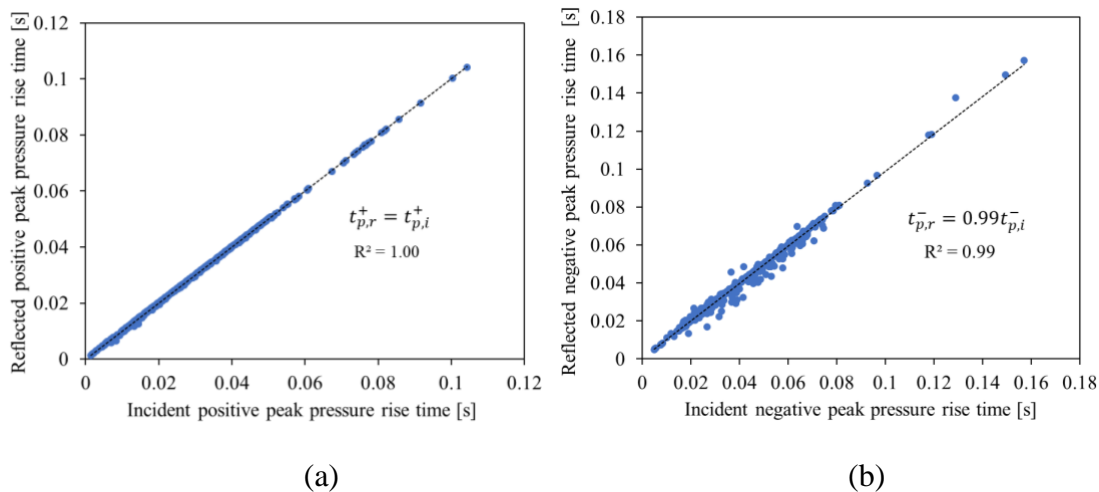


Figure 4-14. Correlation between reflected peak pressure rise time ($t_{p,r}$) and incident peak pressure rise time ($t_{p,i}$): (a) Positive; (b) Negative.

4.5 BLEVE pressure relief

BLEVE reflection has been investigated in Section 4.4, and pressure relief, including wave diffraction, clearing time and reflected impulse, is discussed in this section.

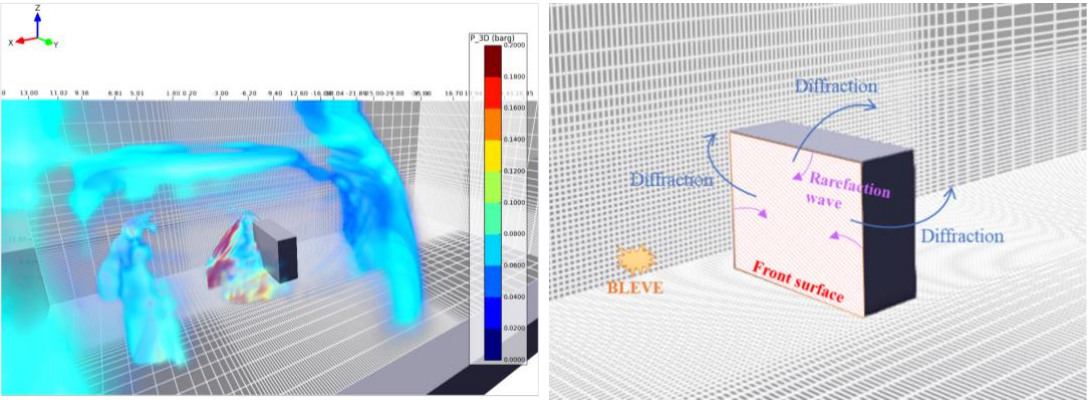
4.5.1 BLEVE wave diffraction

The diffraction of blast waves is essential in the phenomenon of pressure relief. Pressure relief can significantly reduce the overpressure in the positive phase after the peak overpressure, thereby reducing the magnitude of the positive impulse in the reflected pressure-time profile. The dimension of the structure is a critical parameter in determining the amount of relief waves [108]. Figure 4-15 (a) depicts the diffracted blast waves bypassing the free edge on the top and side walls in CFD software. Meanwhile, rarefaction waves are formed in front of the structure. Figure 4-15 (b) provides a schematic diagram showing the diffraction of waves around the structure and the formation of rarefaction waves.

The shortest dimension of a structure is the primary parameter dominating the pressure wave relief. Shi et al. [113] studied the blast wave relief on structural columns, and reported that the column width greatly affected blast wave diffraction. In this study, without losing the generality, the height and the thickness of the rigid structure are

fixed at 5 m and 2 m, respectively; and the width of the structure is varied from 1 m to 10 m to study the effect of structural dimensions on blast wave diffraction and reflected pressure relief, as shown in Figure 4-16. Five monitoring points (MP) on the structure as shown in Figure 4-17 are used to record pressure waves. The BLEVE source is assumed to be a tank with 2.7 m width, 0.86 m height and 0.86 m length. The angle of incidence between the BLEVE source and structure is set as 0 degree. The reflected peak overpressures on the front face of the structure are similar. However, when the structural width is small that pressure diffraction occurs before the wave is fully reflected, the reflected impulse gradually decreases with the reduced width. Figure 4-18 shows the incident and reflected pressure-time profiles from MP1 to MP5, indicating the interaction of the blast wave on the front, top, sides and rear of the structure. Each monitoring point is located at the centre of the respective surface as shown in Figure 4-17. Regarding reflection (i.e., MP1), when the width of the structure is 10 m and 5 m, the reflected pressure and duration are very close, i.e., the structural width and height are large enough for the pressure wave being fully reflected before diffraction. With smaller width of the structure (i.e., $W_{str} = 2.5$ m), the corresponding duration gradually decreases and further reduces the reflected impulse due to the diffraction of the BLEVE waves from the side edges. When the structural width is further reduced (i.e., $W_{str} = 1$ m), more blast waves are diffracted around the side edges of the structure, resulting in a faster release of reflected overpressure. In terms of the monitoring point on the top surface (i.e., MP2), since the blast wave propagates parallel to the free surfaces, there is nearly no reflection. Similarly, for the side surfaces (i.e., MP4 and MP5), the blast loading on the side surfaces is very similar to the BLEVE in open space at the same location. As the structural width increases, the overpressure on the side surfaces of the structure becomes slightly smaller due to the fact that the wave is partially affected by the structure. Since the angle of incidence between BLEVE centre and the structural centre is 0° (i.e., BLEVE tank has the same distance away from both sides of the structure), the overpressures on the MP4 and MP5 are the same. The overpressure on the rear surface (i.e., MP3) is remarkably lower than that of the open space due to the shadowing effects. Meanwhile, the overpressure on the rear surface of structure increases significantly with the decreased structural width. By diffracting from the side edges, more blast waves act on the rear structure with smaller width, and the diffracted waves arrive earlier when the structural width

becomes smaller. Additionally, diffraction generates rarefaction waves. The effect of the pressure flow induced by the rarefaction waves on the clearing time is discussed in Section 4.5.2.



(a) (b)

Figure 4-15. BLEVE wave pressure relief from a rigid structure: (a) CFD model; (b) Schematic diagram.

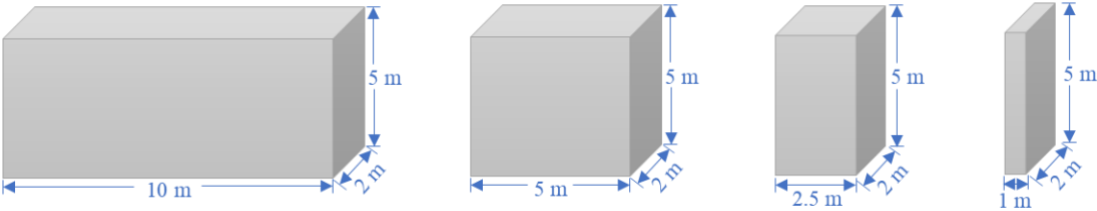


Figure 4-16. Rigid structures with different widths.

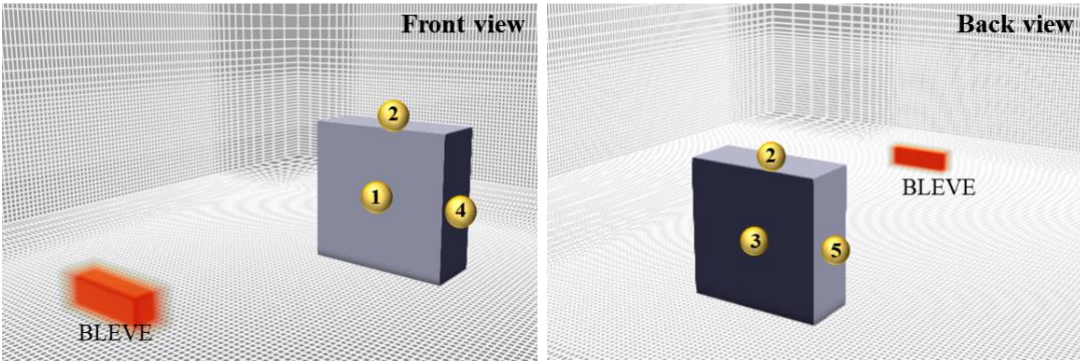


Figure 4-17. Monitoring points at the centre points of different surfaces on a rigid structure.

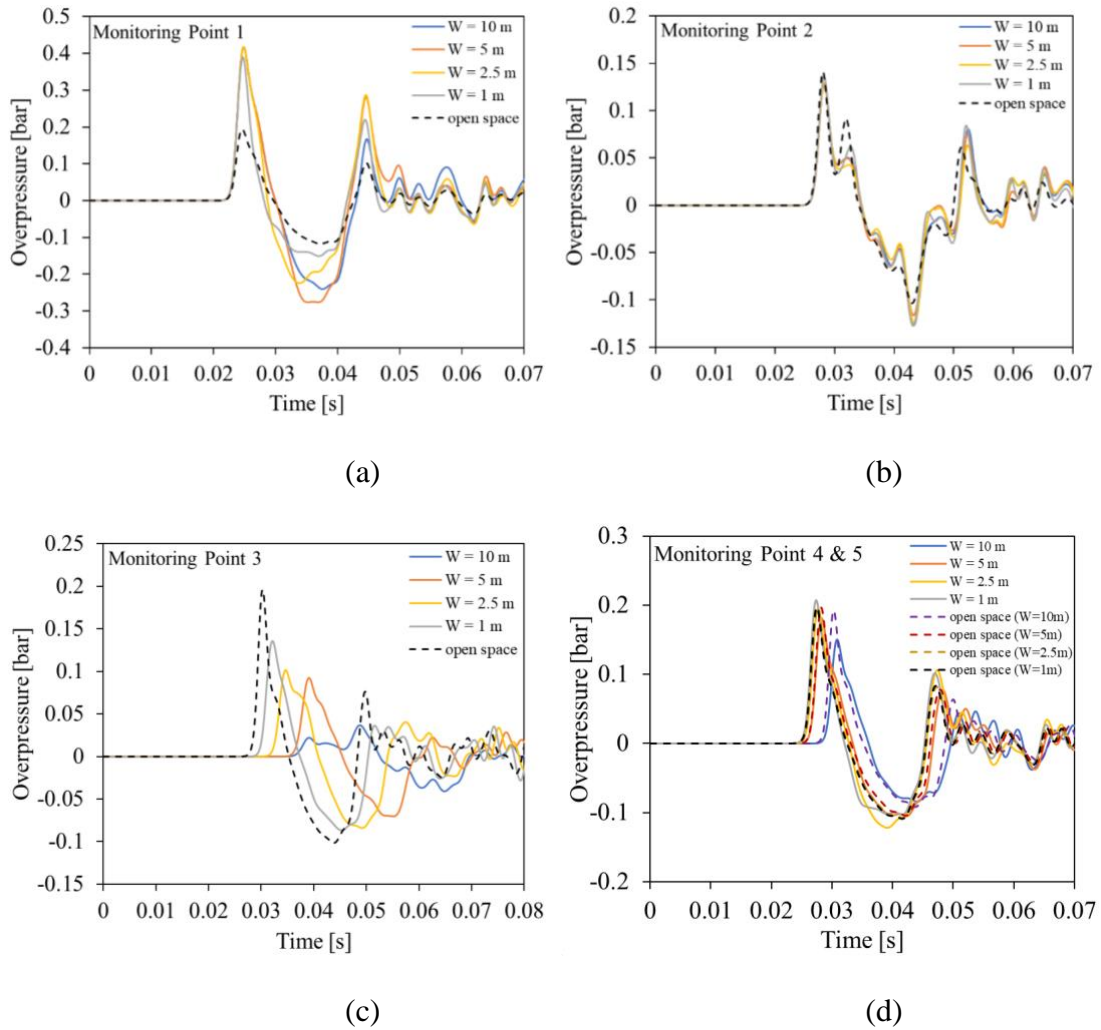


Figure 4-18. Reflected pressure-time histories on a rigid structure surface at monitoring points (MP1-5).

4.5.2 Clearing time (t_c)

Clearing time (t_c) is the time required to release the reflected overpressure from the affected surface, which is determined by the dimension of the structure and the speed of sound in the reflected area (S_r) [18, 124]. The clearing effect usually begins when a blast wave arrives at the free edge of a target surface with finite dimensions [125]. Due to the diffraction phenomenon, the pressure flow is induced by the pressure imbalance between the higher pressure reflected wave and the lower pressure incident wave. Diffraction-generated rarefaction waves propagate along the loading surface, reducing the overpressure acting on the reflected surface and further decreasing the magnitude of the positive impulse [125]. When the relief wave reaches the centre of the front

surface, the reflected overpressure can be fully released. As shown in Figure 4-18 (a), the blast waves in front of the surface are nearly completely reflected when the structure dimensions are large enough. For instance, the blast wave is completely reflected when the width and height of the structure is 10 m and 5 m, respectively. When the width of the structure is reduced to 2.5 m, the blast wave can diffract around the side walls, as well as the top surface, resulting in pressure relief. Figure 4-19 demonstrates the pressure relief in FLACS simulations. When the structural width becomes smaller, pressure waves are diffracted from the free edges of the side walls. The generated rarefaction waves create a pressure flow from high-pressure region (i.e., reflected region) to low-pressure region (i.e., rarefaction waves region), resulting in a reduction in the reflected impulse of the front wall, that is, the reflected overpressure is released.

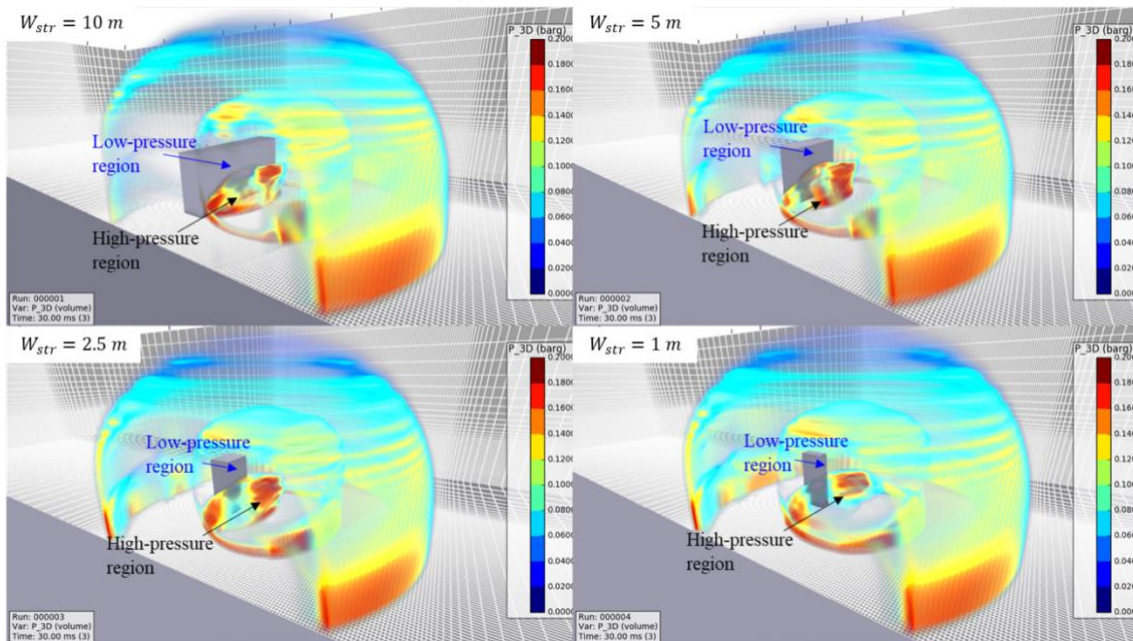


Figure 4-19. Pressure relief in FLACS simulation.

Blast wave clearing is a complex process, and one of the reliable empirical prediction methods is the equation provided in UFC-3-340-02, as given in Equation (4-8). The sound speed in BLEVE reflected region is a function of incident peak overpressure (P_s), as defined by Equation (4-9) and shown in Figure 4-20. The comparison of sound speed associated with TNT explosion and BLEVE is illustrated in Figure 4-21, indicating BLEVE generates higher sound velocity under the same incident peak overpressure. The speed of sound depends on the conditions of the propagating

medium, which is a function of the surrounding pressure and temperature. The sound speed increases with the rising local pressure or temperature [126]. TNT can explode at ambient pressure, while BLEVE occurs at high temperature and high pressure since the fluid in the BLEVE tank needs to be liquefied under high pressure. Due to the higher failure pressure of BLEVEs, the sound speed in BLEVEs is higher than that of TNT explosions at a similar incident peak overpressure. The clearing time is inversely proportional to the sound velocity in the reflected region. Given the same incident overpressure, the sound speed of BLEVE in a reflected zone is higher than that of TNT explosions, indicating a shorter clearing time.

$$t_c = \frac{4S}{(1+R)S_r} \quad (4-8)$$

where clearing distance S [m] = the shortest distance measured between the point of interest, e.g., centre of the front wall to the top or side of the structure, whichever is smaller;

$R = S/G$, where G [m] is the largest distance between the point of interest to the top or side of the structure, whichever is larger; S_r [m/s]= sound speed in the reflected region, can be calculated by

$$S_r = -20.39P_s^2 + 88.05P_s + 348.69 \quad (4-9)$$

where P_s [bar] = incident peak overpressure.

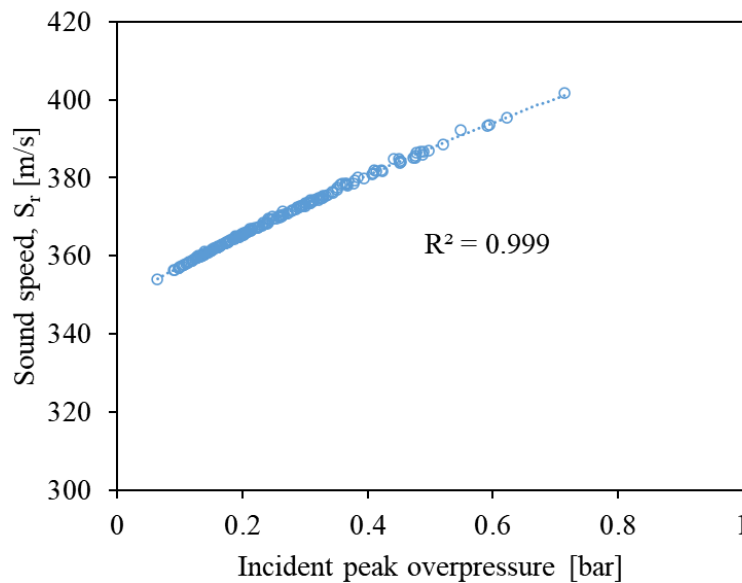


Figure 4-20. Sound speed in the BLEVE reflected region.

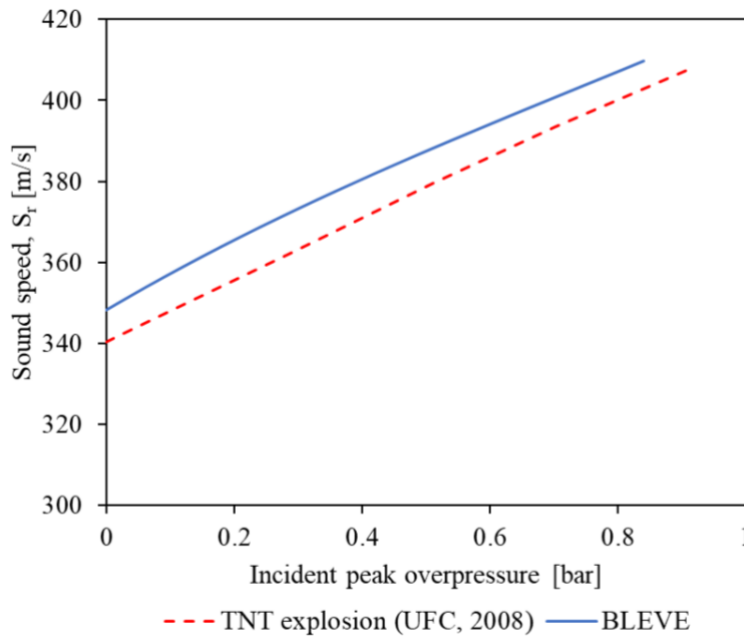


Figure 4-21. Comparison of sound velocity in the reflection regions of TNT explosion (UFC, 2008) and BLEVE.

4.5.3 Reflected impulse (I_r)

In addition to reflected peak overpressure, reflected impulse (I_r) is another essential parameter to characterize the blast load on a structure [110]. By combining the blast overpressure and impulse on a specific structural element, the pressure-impulse diagram can be generated to assess the level of structural damage [127]. Blast impulse is an integral time function of overpressure. Due to the limited structure size, pressure relief phenomenon has a further effect on the reflected impulse, as it can determine how much overpressure is cleared. A portion of incident waves is diffracted along the free edges instead of completely reflected, causing partial blast waves to be cleared and lower reflected impulse. Figure 4-22 shows an ideal model of non-cleared and cleared reflected pressure. The scenario with pressure relief is different from the case of complete reflection, and the cleared pressure decays linearly from the peak reflected overpressure to the stagnant overpressure (i.e., incident overpressure + drag coefficient \times dynamic overpressure) within the clearing time (t_c) [125]. The reflected impulse results are extracted from 650 sets of BLEVE cases by varying BLEVE sources and structural dimensions. As shown in Figure 4-23, the BLEVE reflected impulse (I_r) is

determined by incident impulse (I_i). The R-square value of the linear fitting is around 0.96, and the fitting formula is given as follows:

$$I_r = 2.17I_i - 14.53 (Pa \cdot s) \quad (4-10)$$

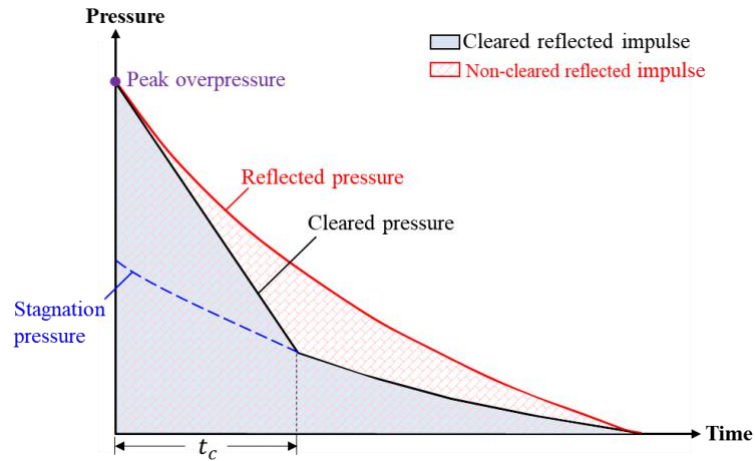


Figure 4-22. Reflected impulse (I_r) [18].

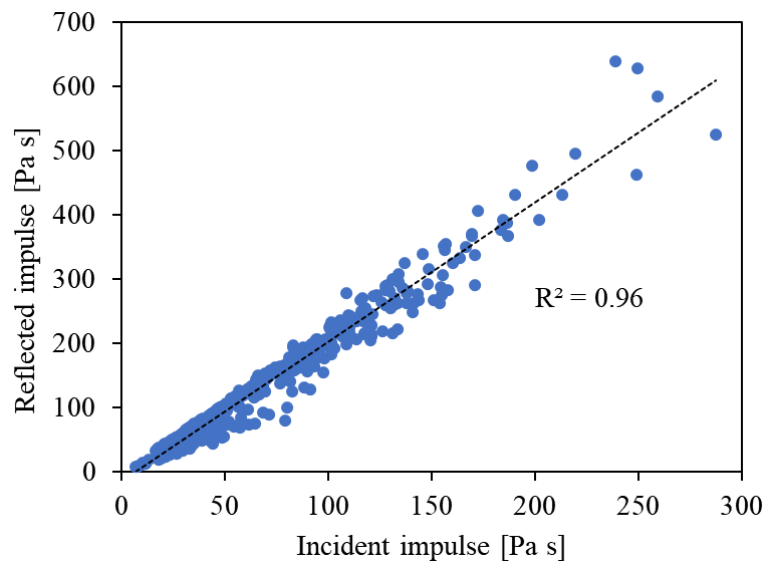


Figure 4-23. Correlation between the reflected impulse (I_r) and incident impulse (I_i) at the centre of the front surface.

4.6 Case study

To predict the BLEVE reflected peak overpressure and impulse on the front surface of a rigid structure, the aforementioned results can be used in combination with the BLEVE overpressure in open space proposed by the authors in a previous study [92]. An example is given in this section to demonstrate the prediction process. The previous study developed empirical models to predict BLEVE peak overpressure and impulse occurring in open space. When a BLEVE wave acts on a structure, the reflected peak overpressure can be obtained using the proposed reflection coefficient charts (i.e., Figure 4-11), and the reflected impulse can be determined by using Equation (4-10) with the incident impulse.

BLEVE test No. 02-1 of Birk et al. [28] was employed as an example in the authors' previous study [92], where the developed empirical model was used to predict the peak overpressure and impulse of BLEVE in open space. The 2 m^3 (V_{tank}) tank has a diameter of 0.953 m and a length (L_{tank}) of 2.7 m. Liquid propane is stored inside, filling to 51% of the tank's volume. BLEVE occurs under failure conditions at a pressure of 18 bar, the liquid temperature of 330 K and the vapour temperature of 334 K, respectively. Assuming that the stand-off distance is 20 m from the BLEVE centre to the rigid structure with the dimensions of 3 m width (W_{str}), 3 m height (H_{str}) and 0.4 m thickness (L_{str}), the reflected peak overpressure and impulse at the centre of a rigid structure are predicted as follows. Figure 4-24 shows the schematic diagram of two cases (i.e., open space and on a rigid structure).

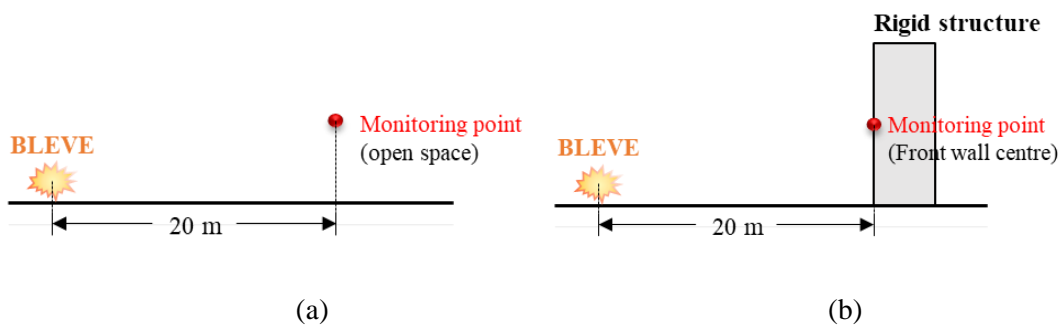


Figure 4-24. Schematic diagram of two cases: (a) open space; (b) at the front centre of rigid structure.

For the case of open space [92], the equivalent rectangular tank's width (W_{tank}) and height (H_{tank}) can be calculated as:

$$W_{\text{tank}} = H_{\text{tank}} = \sqrt{\frac{V_{\text{tank}}}{L_{\text{tank}}}} = \sqrt{\frac{2}{2.7}} = 0.86 \text{ m}$$

The peak overpressure (P_s^+ & P_s^-), durations (t_d^+ & t_d^-), arrival time (t_a), peak pressure rise time (t_p^+ & t_p^-) and impulse (I_i^+) for BLEVE in open space are calculated and listed in Table 4-4.

Table 4-4. Predictions by using the equations in Wang et al. [92].

P_s^+ [bar]	P_s^- [bar]	$t_{d,i}^+$ [s]	$t_{d,i}^-$ [s]	$t_{a,i}$ [s]	$t_{p,i}^+$ [s]	$t_{p,i}^-$ [s]	I_i^+ [Pa · s]
0.0813	-0.0600	0.0084	0.0111	0.0488	0.0526	0.0652	34

The incident angle:

$$\alpha = \arctan\left(\frac{H_{\text{str}}/2 - H_{\text{tank}}/2}{\text{stand-off distance}}\right) = \arctan\left(\frac{3/2 - 0.86/2}{20}\right) = 3.06^\circ$$

Using Figure 4-11 (a), the reflection coefficient:

$$C_r = \frac{P_r^+}{P_s^+} = 2.05$$

The reflected positive peak overpressure:

$$P_r^+ = 2.05 \times 0.0813 = 0.17 \text{ bar}$$

The negative peak overpressure is predicted by Equation (4-7):

$$P_r^- = -0.26 \times 0.17 - 0.059 = -0.10 \text{ bar}$$

Using Equation (4-10), the reflected impulse:

$$I_r = 2.17I_i - 14.53 = 59.25 \text{ Pa} \cdot \text{s}$$

Obtaining the sound velocity in the reflection region from Figure 4-20:

$$S_r = 356 \text{ m/s}$$

Using Equation (4-8), the clearing time:

$$t_c = \frac{4S}{(1+R)S_r} = \frac{4 \times (3/2)}{(1+1.5/3) \times 356} = 0.011 \text{ s}$$

The arrival time:

$$t_{a,r} = t_{a,i} = 0.0488 \text{ s}$$

The reflected overpressure duration and peak pressure rise time are close to the incident ones, expressed as:

$$t_{d,r}^+ = t_{d,i}^+ = 0.0084 \text{ s}$$

$$t_{d,r}^- = t_{d,i}^- = 0.0111 \text{ s}$$

$$t_{p,r}^+ = t_{p,i}^+ = 0.0526 \text{ s}$$

$$t_{p,r}^- = t_{p,i}^- = 0.0652 \text{ s}$$

The above results indicate that clearing time is longer than the positive phase duration, implying the pressure wave is fully reflected. As shown in Figure 4-25, the reflected overpressure at the centre of the front surface is presented and compared with the corresponding incident pressure-time histories, i.e., experimental data [28] and the predicted results using Wang's equation [92].

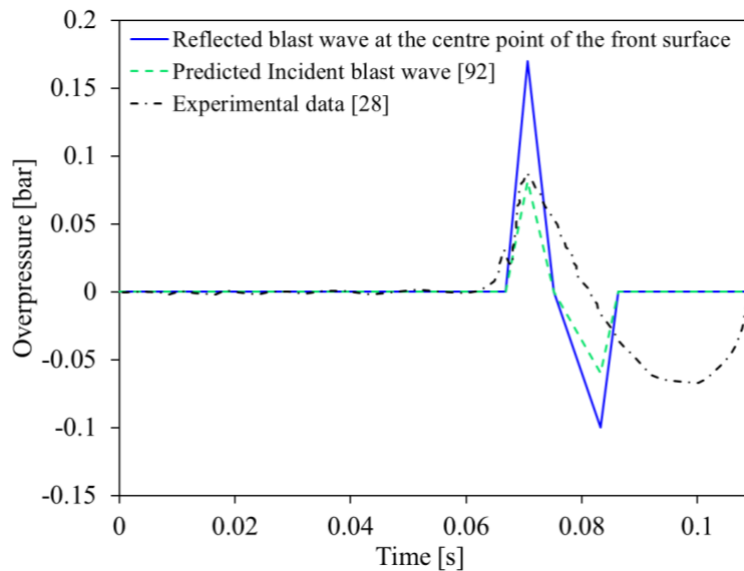


Figure 4-25. Reflected and incident pressure-time histories.

As discussed above, the BLEVE load acting on top and side faces of the structure can be approximated by the free-field pressure waves. It should be noted that the prediction

of BLEVE load on rear surface is more complicated as indicated above and is also less significant. For these reasons, BLEVE load prediction on rear face of structures is not included in this study.

4.7 Summary

In this section, a total of 1300 sets of BLEVE cases consisting of 650 in open space and 650 pressure wave-rigid structure interaction cases are simulated by using FLACS. Reflected overpressure and impulse induced by BLEVE on a rigid rectangular structure are obtained and analysed. The following conclusions can be drawn:

1. Reflection coefficient (C_r) charts for positive overpressure on a rigid structure are developed based on different angles of incidence and the incident peak overpressure in open space.
2. Von Neumann reflection rather than Mach reflection occurs in BLEVE when the angle of incidence reaches the critical incidence angle.
3. The relationship between negative reflected peak overpressure (P_r^-) and positive reflected peak overpressures (P_r^+) is proposed as equation (4-7).
4. Incident and reflected BLEVE pressure-time profiles have very similar peak pressure rise time. However, the reflected BLEVE pressure rise rate is larger than the incident one as the reflected peak overpressure is higher than the incident peak overpressure.
5. The sound speed chart of BLEVE in the reflected region is proposed to calculate the clearing time. BLEVE waves require a shorter clearing time (t_c) than shock waves from TNT explosions at similar incident peak overpressure and structural dimensions.
6. The empirical formula (4-10) is proposed to predict the BLEVE-induced reflected impulse (I_r) on a rigid structure.
7. The results presented in this study together with BLEVE pressure predictions reported in a previous study can be used to estimate BLEVE loads on structures.

Chapter 5 Prediction of BLEVE loading on flexible structures

5.1 Introduction

In Chapter 4, rigid structure assumption, as commonly used in analysing blast wave interaction with structures, was adapted in investigating the BLEVE pressure wave interaction with structures to predict BLEVE loads on structures. However, real structures are not rigid and the duration of BLEVE wave is much longer than that from high explosives and may be in the order of structural natural vibration period. Neglecting structural deformation, therefore, may lead to inaccurate predictions of BLEVE loads acting on the structure because structural deformation during the action of BLEVE wave would change the wave and the structure interaction. In this study, intensive numerical simulations are carried out using a validated computer model to investigate the influences of structural stiffness and BLEVE wave duration on the reflected BLEVE pressure on the structure. Based on the numerical results, prediction charts are proposed as a function of the BLEVE wave duration and structural fundamental vibration period for reliable predictions of BLEVE loads on structures. The findings of this study can be used to predict explosion loads in structural design against BLEVE.

The related work in this chapter has been submitted to a journal for review.

<p><i>Wang, Y., Chen, W., Hao, H., 2024. Prediction of BLEVE loading on structures. Journal of Loss Prevention in the Process Industries, 105325.</i></p>

5.2 Numerical validation and modelling

5.2.1 BLEVE simulation by using FLACS

FLACS is a widely used CFD tool for the safety evaluation of industrial accidents, including vapour cloud explosion, hydrogen safety, detonation of condensed explosives, and blast wave propagation, etc. [105]. Reynolds-averaged Navier-Stokes

(RANS) equations are applied by invoking the ideal gas equation of state and standard $k - \varepsilon$ model for turbulence [72]. To model condensed explosives and blast wave propagation, the Euler equations with FCT scheme and a second-order flux correction are employed [104].

In the modelling, both “non-superheated” and “superheated” BLEVE are considered. This section also focused on the BLEVEs induced by LPG (i.e., butane and propane). The authors [20] have demonstrated that FLACS simulations can predict LPG-induced BLEVE overpressure in open space with the error less than 25% by comparing with experimental data [15, 28, 49]. The 0.2 m grid size in three directions (i.e., x-, y- and z-directions) is selected to balance the prediction accuracy and efficiency.

Previous studies [7, 92, 128] have verified that the FLACS can also well predict BLEVE loads on the rigid structure. The FLACS models of BLEVE in open space and BLEVE loads acting on a rigid structure are shown in Figure 5-1. This study primarily addresses the prediction of the pressure-time profile resulting from a BLEVE on a flexible structure, which is more practical in the real world. However, the structure is set rigid and its material properties cannot be changed in FLACS software. Therefore, in this study, both ANSYS Fluent module and ANSYS Mechanical module in ANSYS Workbench are employed to simulate the BLEVE loads on a flexible structure.

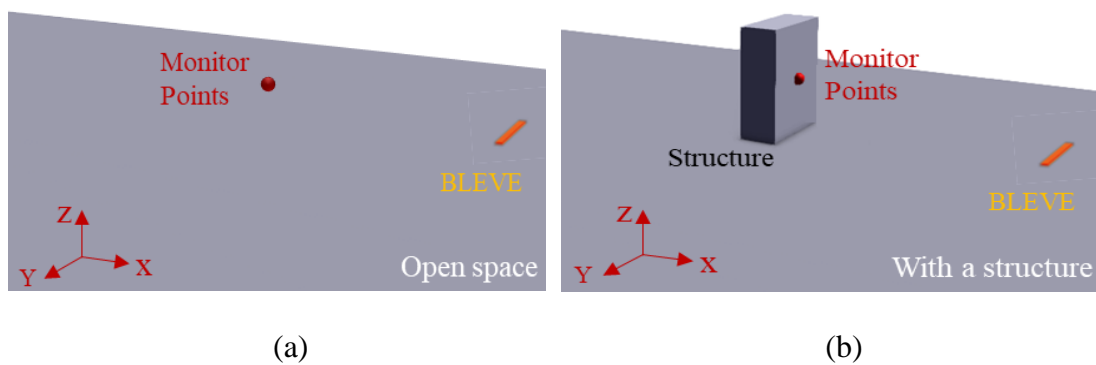


Figure 5-1. FLACS model: (a) BLEVE in open space; (b) BLEVE acts on a structure.

5.2.2 BLEVE wave–structure interaction by using ANSYS Workbench

5.2.2.1 Method selection

To study how the structural deformation affects the wave-structure interaction during the action of BLEVE wave, it is necessary to simulate the blast wave propagation and

its interaction with the structure in CFD software. When investigating the interaction between BLEVE wave and structure, in addition to the condition of BLEVE source, the structural stiffness is another critical parameter to affect the reflected BLEVE waves. ANSYS Workbench can be used for the simulations. It is worth noting that ANSYS Workbench is unable to model the BLEVE. However, the blast pressure-time profile from FLACS can be applied to the boundary of ANSYS Fluent model as input to simulate BLEVE wave propagation and wave-structure interaction. In other words, the initial BLEVE pressure profile can be simulated by FLACS and extracted as an input load applied onto the boundary of ANSYS Fluent model in ANSYS Workbench, and the simulation of the interaction of BLEVE waves with flexible structure can then be performed. To predict the BLEVE wave and structure interaction, a partitioned approach is employed. Namely, two solvers (i.e., ANSYS Fluent and ANSYS Mechanical APDL) are applied to simulate the blast wave propagation and structural response, respectively.

In terms of ANSYS Fluent, it lacks a specific explosive algorithm or subroutine for solving the blast-related problem [129]. Nevertheless, the software is good at solving complex fluid dynamics problems, allowing users to analyse and predict fluid behaviour in various scenarios [130]. When BLEVE waves interact with a structure, the structure response should be further investigated by ANSYS Mechanical [131]. To solve the FSI problems, two approaches, namely one-way coupling and two-way coupling, are considered. For one-way coupling method, the results of the ANSYS Fluent module are used as inputs or boundary conditions to the Static Structural module. Although this method can save computational time, it neglects the effect of structural deformation on the blast wave due to no feedback loop between the two modules. In contrast, two-way coupling approach considers the interaction and feedback between the fields or physics being simulated. The simulation of the blast wave propagation in ANSYS Fluent and the structural analysis in the Transient Structural module can be connected into a loop through System Coupling and iteratively exchange information with each other during the simulation process. The BLEVE waves in the fluid flow simulation affect the structure, and in turn, the deformation of the structure affects the reflected blast waves. This bi-directional exchange of information continues until a converged solution is reached. The two-way coupling scheme considers the influence of the deforming structure on the fluid and

can also guarantee energy conservation at the interface [132, 133]. Therefore, a two-way coupling is adopted in this study to consider the response of the structure to the blast wave reflection.

5.2.2.2 Model validation

In terms of two-way coupling method, ANSYS Fluent module and Transient Structural module are combined by System Coupling. The BLEVE wave propagation is simulated by ANSYS Fluent. The density-based solver and transient solution are employed to solve the governing equation of continuity, momentum and energy in the coupled-implicit formulations. The energy equation model and standard $k - \varepsilon$ model with standard wall functions are applied. The gravitational acceleration in the z -direction is set. The ideal gas model is chosen for the air domain. The initial gauge pressure of 0 Pa as the reference operating pressure, and the blast pressure-time profile is applied as the pressure-inlet boundary condition of the air domain. A User Defined Function (UDF) is employed to import the pressure-time profile. The BLEVE overpressure data in open space obtained from FLACS is compiled as a UDF file. The pressure waves propagate normally to the boundary. Advection Upstream Splitting Method (AUSM) is chosen to provide the exact resolution of contact and shock discontinuities for convective flux calculation [134]. For the spatial discretization schemes, the least squares cell-based method is employed to evaluate the gradient, second order upwind is applied for flow, turbulent kinetic energy and dissipation rate calculation. Default relaxation factors are used in solution control. Subsequently, the structure is modelled with the Transient Structural module. The bottom of the structure is fixed on the ground, and the other surfaces of the structure are set as fluid-solid interfaces. The structure has various stiffness and the material properties are specified. Finally, the FSI problem can be solved by transferring and integrating the results of BLEVE wave pressure and structure simulation through System Coupling.

In the literature, there are no conducted BLEVE experiments in obstructed environments. However, FLACS has demonstrated its capability to accurately predict the BLEVE load acting on a rigid structure [128]. The accuracy of ANSYS Workbench in predicting the BLEVE wave-structure interactions can be compared with the results from FLACS. The flowchart illustrating the simulation process from FLACS to ANSYS, and the finite element model employed for simulating the BLEVE wave-

structure interaction in ANSYS are shown in Figure 5-2. The grid sensitivity study is performed in ANSYS Workbench using the mesh sizes of 0.4m, 0.2m, 0.1m and 0.05m to simulate BLEVE wave interaction with a flexible structure, as depicted in Figure 5-3. The difference in reflected peak overpressure between the 0.05 m and 0.1 m grid sizes is only 4.9%. However, the computational time increases exponentially if the grid size is reduced from 0.1 m to 0.05 m. Therefore, a mesh size of 0.1m is used to achieve the best trade-off between computational accuracy and efficiency. To illustrate the prediction accuracy in ANSYS Fluent, an example is employed. A BLEVE scenario is simulated using FLACS in a 2 m³ pressurized storage tank with a rupture pressure of 18 bar. The reflected pressure at the front centre of a rigid structure situated 20 m away is monitored. At the same time, the pressure-time profile of BLEVE at 10 m in open space is simulated and extracted as input for ANSYS Fluent, and further coupled with ANSYS Mechanical to monitor the reflected overpressure at the front centre of the structure wall. Figure 5-4 shows a close agreement in reflected peak overpressure, with 1.15% difference between the results obtained from ANSYS and FLACS, indicating the two-way coupling in ANSYS Workbench can accurately simulate the BLEVE wave propagation and FSI. Therefore, this approach is employed in the subsequent simulations.

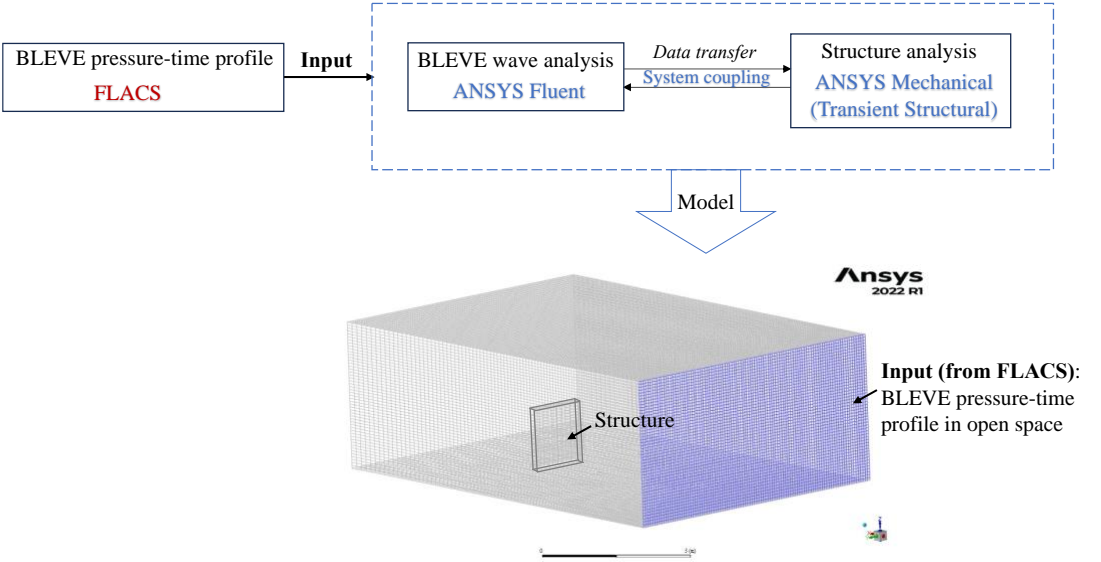


Figure 5-2. Schematic diagram of the whole simulation process and finite element model in ANSYS.

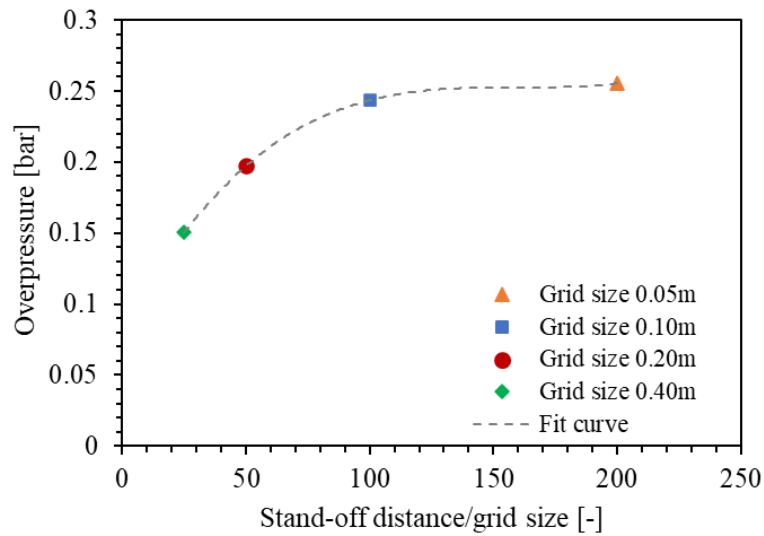


Figure 5-3. Mesh convergence study in ANSYS.

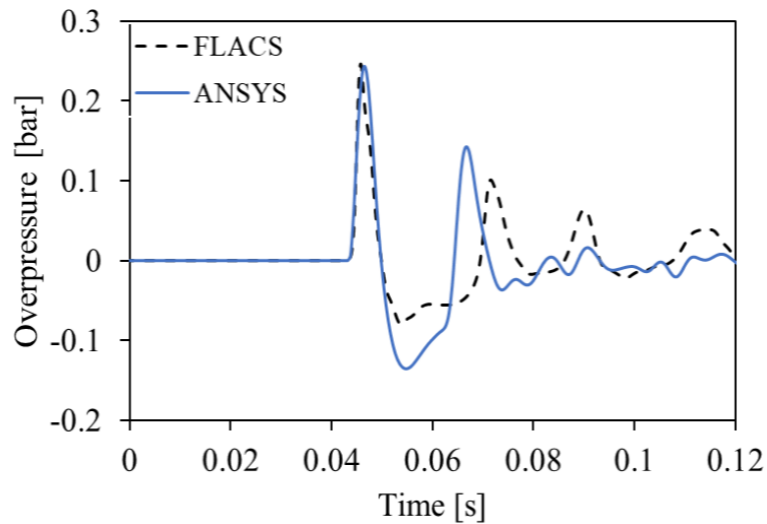


Figure 5-4. Comparing ANSYS and FLACS prediction of BLEVE reflected pressure-time profile.

5.3 Reflected BLEVE positive pressure

Structural stiffness and incident BLEVE wave duration are two critical factors, which have a significant effect on the interaction between blast wave and structure when considering the structural deformation during the action of BLEVE wave. This section conducts an in-depth analysis of their influence on the reflected BLEVE pressure.

5.3.1 Effect of the structural stiffness

A previous study [113] has shown that structural deformation has minimal effect on wave structure interaction for high explosive explosions, even on a very flexible structure. This is due to the fact that TNT explosion typically has an extremely short duration, i.e., in the order of a few milliseconds and thus the structure does not have a prominent deformation during the action of blast wave on the structure. However, the duration of BLEVE pressure wave is much longer than that of high explosive pressure wave. Therefore, the conclusion from [113] may not be applicable to the scenario of BLEVE wave interaction with structures, since the longer duration of BLEVE could provide sufficient time for structure to deform during the action of BLEVE wave, which affects the reflected pressure-time profile. Therefore, the BLEVE loads on a flexible structure should be analysed by considering the effects of structural deformation.

To determine the effect of structural stiffness on BLEVE reflected pressure-time profile, numerical simulations are carried out. A BLEVE is firstly simulated in FLACS considering a 2.5 m³ pressurized tank at a failure pressure of 41 bar. The pressure-time profile at a distance of 3 m away from the BLEVE centre is extracted as an input load applied onto the boundary of ANSYS Fluent model with a structure of dimension 1.5 m in width, 1 m in height and 0.1 m in thickness in the model as shown in Figure 5-2. To study the influences of structural stiffness on the BLEVE wave-structure interaction, several cases with the structural stiffness of rigid, 10⁷ N/m, 10⁶ N/m and 10⁵ N/m are considered in the simulations. The stand-off distance between the BLEVE centre and the front centre of the structure is 3 m. The generated blast loads on structures are compared in Figure 5-5, which depicts the variations in reflected peak overpressure, duration and the pressure rise rate with respect to structures of different stiffnesses. The reflected peak overpressure and pressure rise rate for each case are given in Table 5-1. As shown, a stiffer structure results in a higher reflected peak overpressure. Decreasing the stiffness of the structure leads to a reduction in the peak reflected overpressure. With lower structural stiffness, the structure is susceptible to larger deformation, which reduces the pressure reflection. Moreover, larger structural deformation indicates more BLEVE pressure wave energy is converted to kinetic energy associated with structural response. It should be noted that plastic deformation and structural damage are not considered in the simulation. Therefore, there is no

energy absorption. In reality, energy absorption owing to plastic deformation and structural damage would further reduce the reflected pressure wave if it occurs during the action of the BLEVE wave. Additionally, structural deformation also prolongs the duration of the BLEVE wave and structure interaction, hence resulting in slightly longer duration of reflected pressure wave. This phenomenon is the result of the enhanced energy transfer and coupling between the blast wave and the flexible structure, leading to a prolonged interaction time and thus a longer duration of the reflected blast wave. The corresponding pressure rise rate of the reflected pressure also slows down because of the structural deformation. This significantly reduces the loading rate and hence the structural response strain rate, which may lead to changes in structural response mode and damage mechanism.

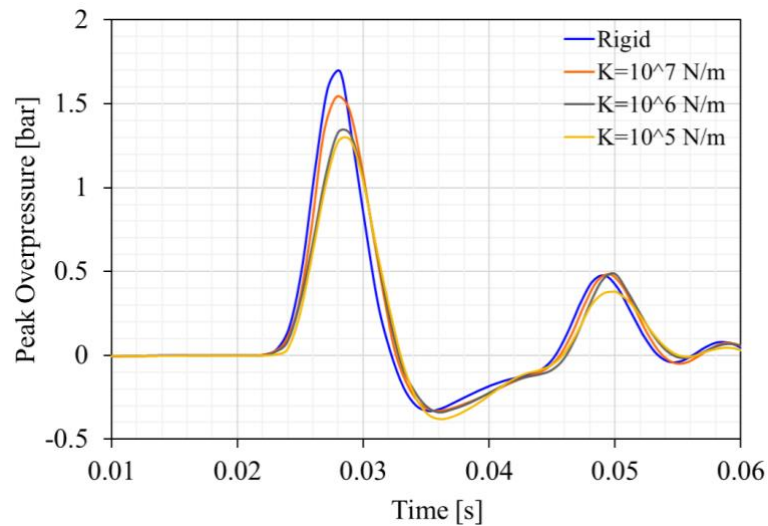


Figure 5-5. Reflected pressure-time profile from structures of different stiffnesses.

Table 5-1. Reflected peak overpressure and pressure rise rate for each case.

Stiffness	Reflected peak overpressure P_r^+ [bar]	Pressure rise rate R_p^+ [bar/s]
Rigid	1.69	272.50
$K = 10^7 N/m$	1.54	263.20
$K = 10^6 N/m$	1.33	221.35
$K = 10^5 N/m$	1.28	213.81

As structural stiffness increases, the structural vibration period (T) decreases. To enhance the applicability of the analysis and facilitate meaningful conclusions about the blast wave-structure interaction in various scenarios and structures, the dimensionless ratio of the positive duration of blast load (t_d) to the structural vibration period (T) is chosen as the parameter to quantify the BLEVE wave-structure interaction. When the positive duration of BLEVE wave is shorter than the structural vibration period (i.e., $t_d/T < 1$), the variation in structural stiffness significantly affects the coupling between the blast wave and structure. Specifically, reducing structural stiffness can amplify the dynamic response [135, 136], which leads to smaller peak reflected pressure, implying significant BLEVE wave-structure interaction effect. On the other hand, if t_d/T is large, corresponding to a small T or a stiff structure, the BLEVE wave-structure interaction effect is less prominent since the structural deformation is small.

In this study, the dimensions of the considered structural model are 1m width, 1m length and 0.1m thickness, with the structural stiffness ranging from 5×10^4 N/m to rigid (infinite). The incident duration (t_d) is chosen as 0.0145 s, which is the typical incident BLEVE duration from the experiment [51]. Figure 5-6 illustrates that the reflected peak overpressure increases with the increased structural stiffness (i.e., reduced T and increased t_d/T since t_d remains unchanged). When the t_d/T is larger than 2.0, the reflected peak overpressure becomes stabilized, further increase in the t_d/T ratio has insignificant effect on the reflected peak pressure, implying the structural deformation has minimum effect on the BLEVE wave-structure interaction because the deformation of a stiff structure is small. When the $t_d/T < 1$, the coupling between the blast wave and the structure has considerable influence. This is because a reduced stiffness leads to higher flexibility, making the structure more susceptible to deformation under the blast wave, and the BLEVE wave-structure interaction pronouncedly affects the reflected pressure wave. Besides the relief of wave reflection owing to structural deformation, the increased flexibility enables more energy transfer between the blast wave and the structure, resulting in more obvious coupling. At the same time, the increased coupling allows the structure to undergo more pronounced dynamic responses, further mitigating the reflected peak overpressure. On the other hand, a stiff structure corresponds to small structural deformation, especially during the phase of BLEVE wave acting on the structure, energy transfer and coupling

between them are greatly weakened, resulting in a less pronounced effect on the reflected peak overpressure. The present results indicate when T is $0.5 t_d$ or less, the structural deformation can be neglected in modelling the BLEVE wave-structure interaction.

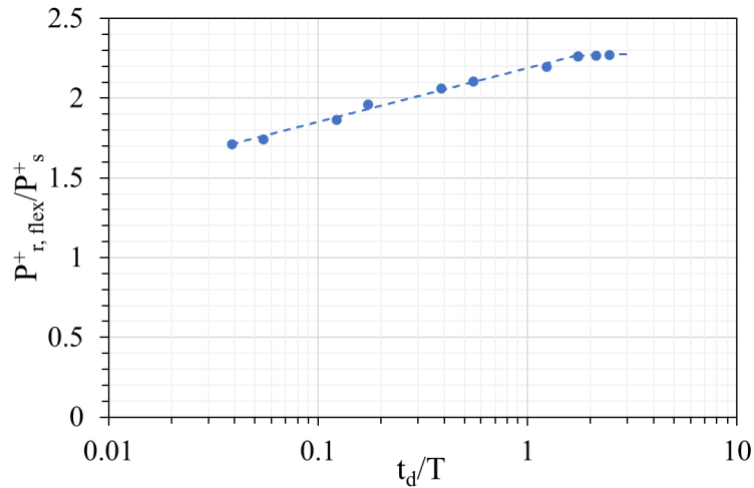


Figure 5-6. The ratio of the positive reflected peak overpressure ($P_{r,flex}^+$) to incident peak overpressure (P_s^+) versus t_d/T

5.3.2 Effect of the incident BLEVE wave duration

Besides the structural stiffness, the duration of the incident BLEVE wave is another key factor affecting the wave-structure interaction and subsequently the reflected pressure-time profile. In this section, the effect of incident blast wave duration on the positive reflected peak overpressure ($P_{r,flex}^+$) is discussed.

The incident duration is chosen to range from 0.01 to 0.08s, which covers the observed positive BLEVE pressure time histories in experimental tests [28, 49-51]. Based on the above model, the reflected peak overpressure under incident blast wave of different durations is compared in Figure 5-7. Since the incident BLEVE wave duration has a significant influence on peak overpressure, the results are categorized into four specific ranges (i.e., 0.01~0.02s; 0.02~0.04s; 0.04~0.06s; 0.06~0.08s) based on the incident BLEVE wave duration. The pressure ratio ($P_{r,flex}^+/P_s^+$) can be determined using the fitted line corresponding to a specific range. As the incident BLEVE wave duration increases, the interaction between the blast wave and structure can become more significant. The blast wave interacts with the structure for an extended period, providing enough time for structure to deform and hence affects the BLEVE wave-

structure interaction. This extended coupling time allows for a more complex energy transfer between the wave and the structure, potentially resulting in a more significant interaction and influencing the dynamic response of the structure, as well as leading to the variation in the reflected pressure-time profile. More energy transfer leads to a gradual decrease in the intensity of the reflected wave, resulting in a modified pressure-time profile. As a result, the peak overpressure is smaller, and the pressure rise rate during the reflection phase may be slower. However, when the incident BLEVE wave duration is long enough, the reflected peak pressure stabilizes at a relatively constant level. On the contrary, a shorter duration of incident BLEVE wave would result in a shorter coupling time between the wave and the structure, and make the BLEVE wave-structure interaction effect less prominent. This limited interaction time may lead to a more sudden and intense reflected pressure-time profile with a higher peak overpressure and a faster pressure rise rate, similar to the pressure wave interacting with a rigid structure.

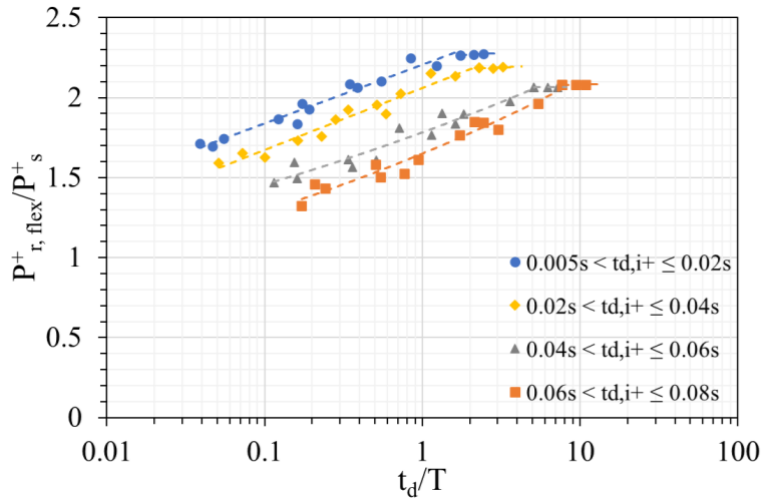


Figure 5-7. The ratio of the positive reflected peak overpressure ($P_{r,flex}^+$) to incident peak overpressure (P_s^+) versus t_d/T for various incident duration ranges.

5.4 Reflected negative peak pressure, duration and peak pressure rise time

Reflected positive pressure has been studied in Section 3. As shown in Figure 5-8, other parameters, such as the reflected negative peak pressure (P_r^-), duration (t_d^+ & t_d^-) and peak pressure rise time (t_p^+ & t_p^-) are essential parameters to determine the

reflected pressure-time profile of BLEVE load on structures, which are discussed in this section.

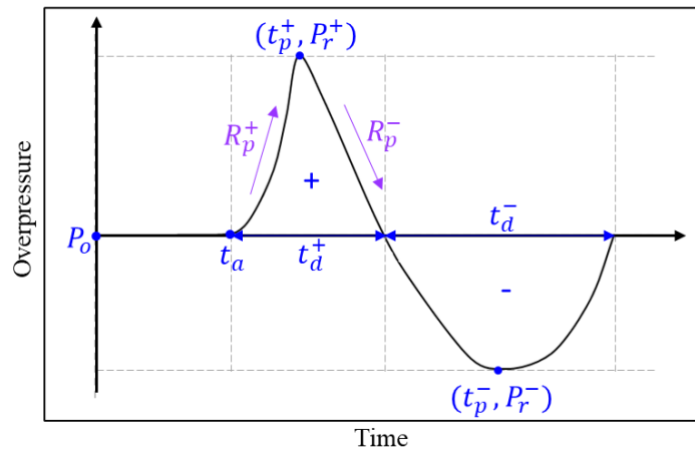


Figure 5-8. Typical BLEVE overpressure-time profile.

5.4.1 Reflected negative peak overpressure

Following the positive pressure phase, the blast wave enters a period where the pressure transitions to a negative phase. It is widely recognized that negative overpressure can create a suction force, the magnitude of the negative pressure arising from gas explosions is considerably smaller when compared to the positive overpressure [96, 137]. The BLEVE negative peak overpressure on a rigid structure has been studied by the authors [128]. The negative reflected peak overpressure (P_r^-) on a rigid structure can be calculated by Equation (5-1) [128]. Figure 5-9 compares BLEVE negative overpressure on the flexible and rigid structure, showing both structural stiffness and blast wave duration have little effect on the reflected negative pressure.

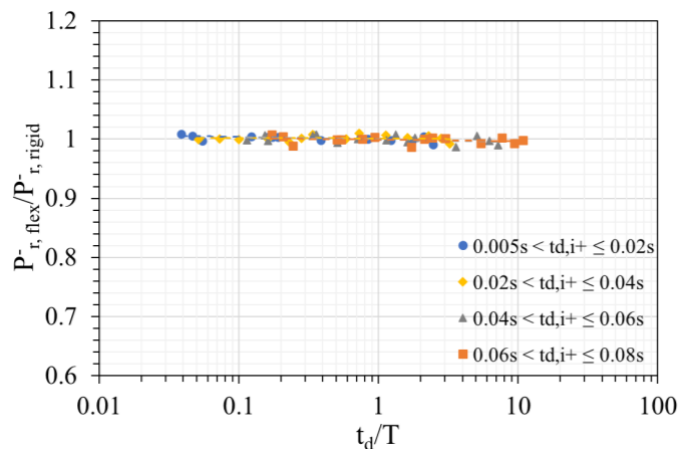


Figure 5-9. The ratio of the negative reflected peak overpressure on flexible structure

($P_{r,flex}^-$) to rigid structure ($P_{r,rigid}^-$) versus t_d/T .

$$P_r^- = -0.26P_r^+ - 0.059 \text{ (bar)} \quad (5-1)$$

5.4.2 Reflected overpressure duration

The overpressure duration is a critical factor in assessing structural response [96, 101]. The duration of the blast wave is determined by measuring the time from the point when the pressure commences increasing or decreasing from zero to the point at which the pressure reverts to atmospheric levels [11]. Figure 5-10 shows the ratio of the positive reflected wave duration ($t_{d,flex}^+$) to the incident positive wave duration ($t_{d,i}^+$) with respect to t_d/T ratio. It can be seen that a more flexible structure and/or BLEVE wave with a longer duration t_d are associated with more pronounced coupling during the wave-structure interaction, which results in a longer positive duration of the reflected pressure-time profile, but has little effect on the negative duration of the overpressure.

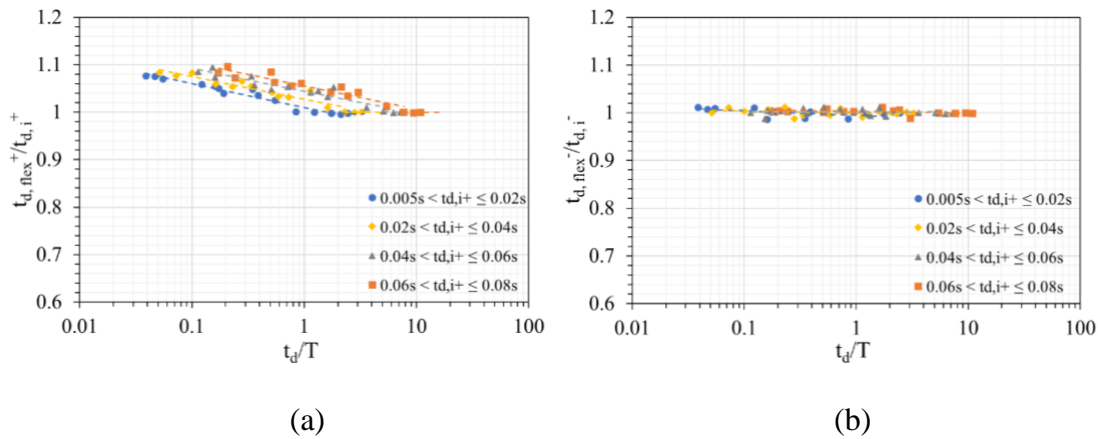


Figure 5-10. The ratio of the reflected duration ($t_{d,flex}$) to incident duration ($t_{d,i}$) versus t_d/T : (a) Positive ($t_{d,flex}^+$); (b) Negative ($t_{d,flex}^-$).

5.4.3 Reflected peak pressure rise time and pressure rise rate

The pressure rise rate is another key factor to be considered in the structural response analysis. When blast wave reaches the peak positive and negative overpressure, the corresponding time is referred as peak pressure rise time (t_p^+ & t_p^-) in pressure-time profile as shown in Figure 5-8. The pressure rise rate (R_p) can be obtained by

calculating the ratio of the peak overpressure to the rising time (i.e., peak pressure rise time t_p^+ – arrival time t_a).

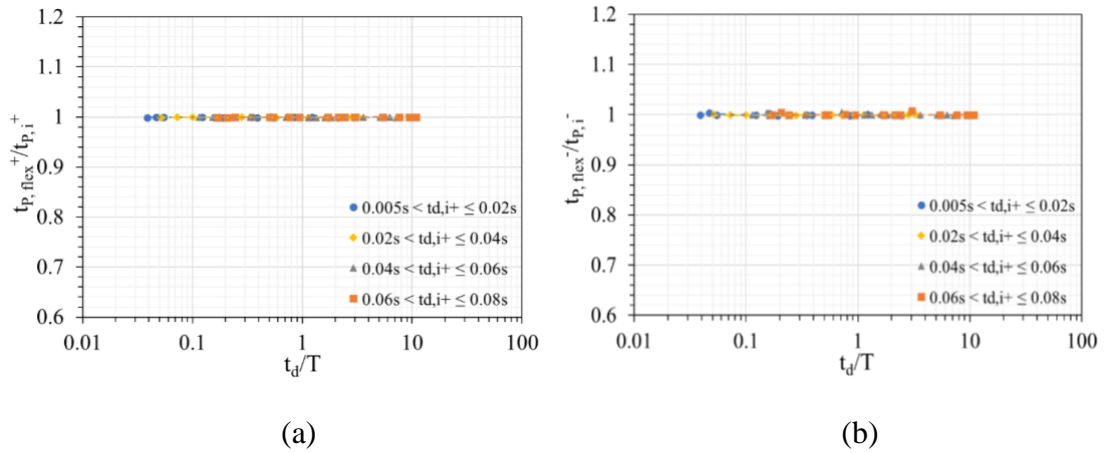


Figure 5-11. The ratio of the reflected peak pressure rise time ($t_{p,flex}$) to incident peak pressure rise time ($t_{p,i}$) versus the ratio of t_d/T : (a) Positive ($t_{p,flex}^+$); (b) Negative ($t_{p,flex}^-$).

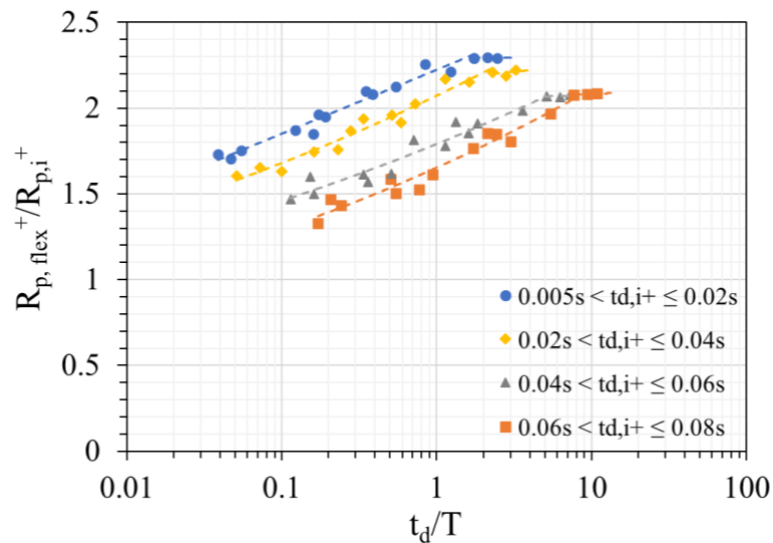


Figure 5-12. The ratio of the reflected pressure rise rate ($R_{p,flex}^+$) to incident pressure rise rate ($R_{p,i}^+$) versus the ratio of t_d/T

To determine the reflected peak pressure rise time owing to the interaction with flexible structures ($t_{p,flex}^+$ & $t_{p,flex}^-$), they are calculated and compared with the incident peak pressure rise time ($t_{p,i}^+$ & $t_{p,i}^-$), as shown in Figure 5-11. The findings indicate that $t_{p,flex}$ and $t_{p,i}$ are very similar, implying that the structural stiffness and incident blast wave duration have minimal influence on the reflected peak pressure

rise time. While various structural stiffness values and incident wave durations do not affect the reflected peak pressure rise time, the flexible structure or longer incident duration leads to a reduced reflected peak overpressure in comparison to the rigid structure or BLEVE wave with shorter durations, thereby contributing to a slower pressure rise rate. The ratio of the reflected pressure rise rate ($R_{p,flex}^+$) to the incident pressure rise rate ($R_{p,i}^+$) is depicted in Figure 5-12.

5.5 Case study

To predict the BLEVE reflected pressure-time profile on a flexible structure, the charts given in Sections 3 and 4 can be used along with the results reported in the previous study, i.e., BLEVE overpressure in open space [92]. In this section, a case study is provided to elucidate the prediction process.

The BLEVE test No. 02-1 by [28] is employed as an example here. The BLEVE tank has a volume of 2 m³. It contains liquified propane with a fill ratio of 51%. BLEVE occurs at pressure up to 18 bar, and the liquid and vapour temperature reach 330 K and 334 K, respectively. Assuming that the dimensions of the cantilever flexible structure are 3 m in width (W_{str}), 3 m in height (H_{str}) and 0.4 m in thickness (L_{str}), along with a density (ρ) of 2400 kg/m³, a Young’s Modulus (E) of 3×10^{10} Pa, and a Poisson’s ratio (ν) of 0.3. The stand-off distance between the BLEVE centre and the front centre of flexible structure is 20 m. The predicted reflected BLEVE wave profile on the flexible structure is given below. The schematic diagrams of BLEVE occurring in open space and BLEVE load on a structure are shown in Figure 5-13.

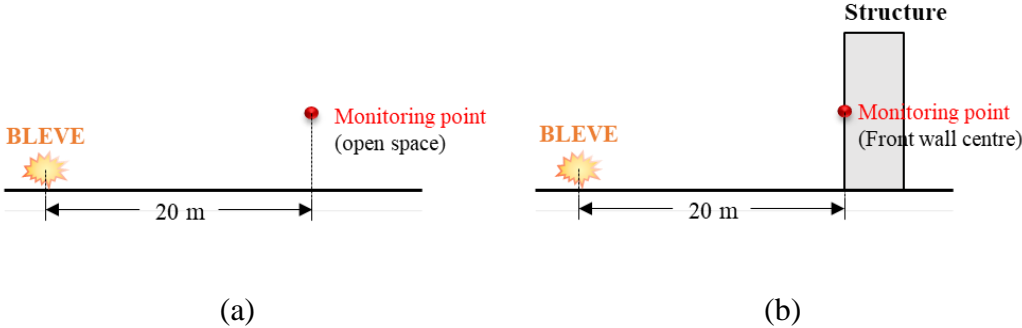


Figure 5-13. Schematic diagram of BLEVE cases: (a) open space; (b) a structure in the area

In the previous study conducted by the authors [92], the peak overpressure (P_s^+ & P_s^-), duration (t_d^+ & t_d^-), arrival time (t_a) and peak pressure rise time (t_p^+ & t_p^-) for BLEVE in open space are calculated and listed in Table 5-2.

Table 5-2. Predicted BLEVE overpressure in open space [92].

	P_s^+ [bar]	P_s^- [bar]	$t_{d,i}^+$ [s]	$t_{d,i}^-$ [s]	$t_{a,i}$ [s]	$t_{p,i}^+$ [s]	$t_{p,i}^-$ [s]
Open space	0.0813	-0.0600	0.0084	0.0111	0.0488	0.0526	0.0652

When analysing the effects of BLEVE loads on a flexible structure, it is necessary to incorporate structural stiffness into the calculations. This inclusion is essential in assessing how structural stiffness affects the characteristics of the reflected pressure wave, therefore enabling the accurate prediction of the reflected pressure-time profile. The structure stiffness in this case study is calculated as follows.

The moment of inertia I :

$$I = \frac{W_{str}L_{str}^3}{12} = 0.016 \text{ m}^4 \quad (5-2)$$

The stiffness of the structure :

$$K = \frac{3EI}{L_{str}^3} = 5.33 \times 10^7 \text{ N/m} \quad (5-3)$$

The structural natural vibration period:

$$T = 2\pi \sqrt{\frac{m}{K}} = 2\pi \sqrt{\frac{3 \times 3 \times 0.4 \times 2400/2}{5.33 \times 10^7}} = 0.057 \text{ s} \quad (5-4)$$

Since the positive phase duration (t_d) of the incident wave is 0.0084s, the ratio of the positive wave duration to the structural natural vibration period is

$$\frac{t_d}{T} = 0.15 \quad (5-5)$$

The ratio of the reflected peak overpressure to incident peak overpressure can be obtained from Figure 5-7 as

$$\frac{P_{r,flex}^+}{P_s^+} = 1.90 \quad (5-6)$$

Thus, the reflected positive peak overpressure:

$$P_{r,flex}^+ = 1.90 \times 0.0813 = 0.155 \text{ bar} \quad (5-7)$$

The reflected negative peak overpressure can be calculated by Equation (5-1):

$$P_{r,flex}^- = -0.26P_{r,flex}^+ - 0.059 = -0.099 \text{ bar} \quad (5-8)$$

Using Figure 5-10(a), the ratio of the duration of the reflected positive pressure to positive phase duration of incident wave is

$$\frac{t_{d,flex}^+}{t_{d,i}^+} = 1.05 \quad (5-9)$$

The reflected positive phase duration is

$$t_{d,flex}^+ = 1.05 \times 0.0084 = 0.0089 \text{ s} \quad (5-10)$$

The reflected negative phase duration ($t_{d,flex}^-$), arrival time ($t_{a,flex}$) and peak pressure rise time ($t_{p,flex}^+$ & $t_{p,flex}^-$) are very similar to the incident ones, which are:

$$t_{d,flex}^- = t_{d,i}^- = 0.0111 \text{ s} \quad (5-11)$$

$$t_{a,flex} = t_{a,i} = 0.0488 \text{ s} \quad (5-12)$$

$$t_{p,flex}^+ = t_{p,i}^+ = 0.0526 \text{ s} \quad (5-13)$$

$$t_{p,flex}^- = t_{p,i}^- = 0.0652 \text{ s} \quad (5-14)$$

Figure 5-14 presents the reflected overpressure on a flexible structure with the above calculated parameters and also compares it with the corresponding reflected pressure-time profiles on a rigid structure and the incident pressure-time profile when BLEVE occurs in open space [92]. The experimental data of recorded pressure-time history in open space [28] is also included for comparison. The peak reflected overpressure on a flexible structure is around 20% less as compared to that on a rigid structure.

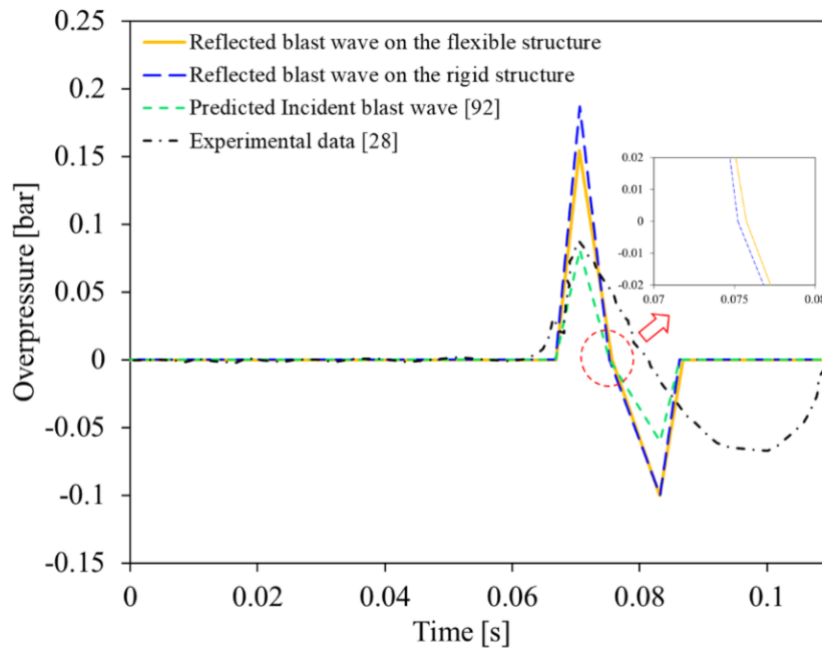


Figure 5-14. Reflected pressure-time profiles (on the rigid and flexible structure) and incident pressure-time profiles (experimental data [28] and predicted results [92]).

5.6 Summary

This section aims to predict the reflected pressure-time profile generated by a BLEVE on a flexible structure for reliable prediction of BLEVE loads on structures. The interaction of BLEVE waves with flexible structures is simulated by using ANSYS Fluent for the blast wave propagation coupled with ANSYS Mechanical for structure analysis. Based on the results obtained, the following conclusions can be drawn.

1. A more flexible structure with larger structural deformation during the action of BLEVE wave on the structure leads to a smaller peak reflected pressure and longer duration, i.e., a BLEVE load of smaller amplitude but longer duration acting on the structure.
2. Under the same structural stiffness, longer duration of the incident BLEVE wave leads to lower reflected peak overpressure. When the ratio of positive BLEVE wave duration to the natural period of the structure is small, the effect of BLEVE wave-structure interaction is prominent. Increasing the t_d/T ratio increases the peak reflected pressure. When t_d/T is larger than 2.0, further increasing the ratio has an insignificant effect on the reflected pressure,

indicating the structural deformation can be neglected in modelling the BLEVE wave-structure interaction.

3. Structural stiffness and incident wave duration have little effect on the reflected negative pressure and reflected peak pressure rise time. However, as the structure becomes more flexible or the incident wave duration of the BLEVE wave increases, the pressure rise rate is slower due to a reduction in the reflected peak overpressure.

Chapter 6 Conclusions and future works

6.1 Main findings

This thesis offers valuable insights into BLEVE pressure prediction and its implications on structural response predictions and BLEVE resistant design. The empirical formulae and charts for predicting BLEVE pressure-time profile, including BLEVE pressure wave in open space and BLEVE loads acting on a structure, are derived, which can provide engineers with practical tools for addressing BLEVE-resistant structural design and optimizing safety measures.

In Chapter 2, existing BLEVE experiments are summarized and divided into near-field and far-field categories based on distance from the BLEVE centre to the target. Additionally, current BLEVE prediction models, including empirical, numerical and ANN methods, are discussed and compared. It found that theoretical-based empirical models are easy to use but often generate inaccurate predictions due to their reliance on TNT equivalent curves. Meanwhile, CFD simulations are more accurate but time-consuming, and ANN models are efficient but require large data to be trained. Therefore, models that yield accurate BLEVE load prediction and are easy to use should be developed for use in analyses and design of structures against BLEVE loads.

In Chapter 3, the empirical models for predicting BLEVE pressure-time profiles in open space are developed. By utilizing simulation results and an ANN model trained using these results, the empirical formulae and charts of eight critical parameters are derived to predict BLEVE pressure simply and quickly. The eight critical parameters are used to define the pressure-time profile, including positive and negative peak pressures, positive and negative pressure rise times, positive and negative durations, arrival time and impulse. These models are a function of seven BLEVE variables, which are width, height and length of the pressurized tank, liquid ratio, failure pressure, failure temperature and target location. Compared with commonly used theoretical-based empirical model, the proposed empirical model can more accurately predict the BLEVE pressure-time profile, including the pressure rise rate, which cannot be predicted by other empirical models.

In Chapter 4, the focus turns to predicting BLEVE loads on structures. A reflection coefficient chart is depicted to predict the reflected BLEVE overpressure on the rigid

structure by considering the angle of incidence between BLEVE centre and structure centre. When the angle of incidence reaches the critical incidence angle, von Neumann reflection occurs in BLEVEs, in contrast to Mach reflection seen in TNT explosions. At the same time, the pressure relief phenomena (i.e., diffraction and clearing effects) are also explored by considering structural dimensions. The sound speed chart of BLEVE in the reflected region is proposed to calculate the clearing time. It is found that BLEVE waves require a shorter clearing time than shock waves from TNT explosions at similar incident peak overpressure and structural dimensions. The proposed empirical models in this study together with BLEVE pressure predictions reported in Chapter 3 can be used to estimate BLEVE loads on structures.

In Chapter 5, considering that structures in the real world are flexible rather than rigid, the effect of structural deformation on BLEVE pressure wave-structure interaction is studied for more accurate BLEVE load prediction. During the action of BLEVE wave, the deformation of structure would significantly affect the wave-structure interaction, as well as ultimately affect the blast loads acting on the structure. This study found that the structural stiffness and incident BLEVE wave duration significantly affect reflected peak overpressure, duration, and pressure rise rate. When the ratio of positive BLEVE wave duration to the natural period of the structure is larger than 2.0, the structural deformation can be neglected in modelling the BLEVE wave-structure interaction. The empirical models are proposed as a function of the BLEVE wave duration and structural fundamental vibration period for reliable predictions of BLEVE loads on structures, allowing for better design of structure against BLEVE to mitigate damage to structures from BLEVE loads.

6.2 Recommendations for future works

- (1) Conducting experiments of BLEVE acting on structures to further verify and refine the reliability of the empirical models developed in this thesis.
- (2) Since the reflected pressure generated by explosions is affected by the shape of the structure, the effects of structural geometry on the BLEVE loads should be further studied.
- (3) To enhance the practicality and realism of BLEVE simulations, future research

should aim at incorporating realistic accident scenarios to simulate real-world BLEVE accidents. Additionally, accessing data from actual BLEVE incidents can assist in refining and validating the empirical models.

- (4) In real-world accidents, it is important to note that a BLEVE event may trigger a Vapor Cloud Explosion and vice versa. Therefore, exploring and considering the consequences of these continuous explosion superpositions is crucial for future research.
- (5) Development of practical safety guidelines and recommendations for engineers in structural design to mitigate structural damage caused by BLEVE loads is needed. The empirical models and charts proposed in this thesis can be used in this endeavor.

References

- [1] Hart, W., *Global LPG: Opportunities and Challenges in an Evolving Market*. 2019.
- [2] NOORLPG. *Applications of LPG | Uses & Importance of Liquid Petroleum Gas - Noor LPG Co. (Pvt) Ltd.* 2021 [cited 2021; Available from: <https://noorlpg.com/application-of-lpg/>].
- [3] Worldometers. *World Natural Gas Statistics* 2021 [cited 2021; Available from: <https://www.worldometers.info/gas/>].
- [4] Badshah, E., et al., *Review of Blast Loading Models, Masonry Response, and Mitigation*. Shock and Vibration, 2017: p. 6708341.
- [5] Overholt, M. *The Importance of Oil and Gas In Today's Economy*. 2016 [cited 2021; Available from: <https://www.tigergeneral.com/the-importance-of-oil-and-gas-in-today-s-economy/>].
- [6] Bariha, N., V.C. Srivastava, and I.M. Mishra, *Theoretical and experimental studies on hazard analysis of LPG/LNG release: a review*. Reviews in Chemical Engineering, 2017. **33**(4): p. 387-432.
- [7] Li, J. and H. Hao, *Numerical simulation of medium to large scale BLEVE and the prediction of BLEVE's blast wave in obstructed environment*. Process Safety and Environmental Protection, 2021. **145**: p. 94-109.
- [8] Donato, V. D., Mezzofiore, G., & Masters, J. 2018. *Three dead in Bologna highway gas tanker explosion*. CNN.
- [9] CSB, *CSB Safety Video: Anatomy of a Disaster*. 2008.
- [10] Abbasi, T. and S. Abbasi, *The boiling liquid expanding vapour explosion (BLEVE): Mechanism, consequence assessment, management*. Journal of Hazardous Materials, 2007. **141**(3): p. 489-519.
- [11] CCPS, *Guidelines for Vapor Cloud Explosion, Pressure Vessel Burst, BLEVE, and Flash Fire Hazards*. 2011, Wiley Online Library. p. 456.
- [12] Eckhoff, R.K., *Boiling liquid expanding vapour explosions (BLEVEs): A brief review*. Journal of Loss Prevention in the Process Industries, 2014. **32**: p. 30-43.

- [13] Salla, J.M., M. Demichela, and J. Casal, *BLEVE: A new approach to the superheat limit temperature*. Journal of Loss Prevention in the Process Industries, 2006. **19**(6): p. 690-700.
- [14] Avedisian, C.T., *The homogeneous nucleation limits of liquids*. Journal of physical and chemical reference data, 1985. **14**(3): p. 695-729.
- [15] Birk, A. and J. VanderSteen, *On the transition from non-BLEVE to BLEVE failure for a 1.8 m 3 propane tank*. Journal of Pressure Vessel Technology, 2006. **128**(4): p. 648–655.
- [16] Van Den Berg, A.C., et al., *BLEVE blast by expansion-controlled evaporation*. Process Safety Progress, 2006. **25**(1): p. 44-51.
- [17] Mitu, M., et al., *Influence of inert gas addition on propagation indices of methane–air deflagrations*. Process Safety and Environmental Protection, 2016. **102**: p. 513-522.
- [18] UFC, *Unified facilities criteria: structures to resist the effects of accidental explosions (UFC 3-340-02)*. US Department of Defense, Washington, DC, 2008.
- [19] Hao, H., et al., *Review of the current practices in blast-resistant analysis and design of concrete structures*. Advances in Structural Engineering, 2016. **19**(8): p. 1193-1223.
- [20] Wang, Y., J. Li, and H. Hao, *A state-of-the-art review of experimental and numerical studies on BLEVE overpressure prediction*. Journal of Loss Prevention in the Process Industries, 2022: p. 104920.
- [21] Hansen, O.R. and M. Kjellander, *CFD modelling of blast waves from BLEVEs*. Chemical Engineering Transactions, 2016. **48**: p. 199-204.
- [22] Hutama, A., *Simulation of BLEVEs in Unconfined and Confined Areas Using FLACS*. 2017, University of Stavanger, Norway.
- [23] Li, J. and H. Hao, *Numerical study of medium to large scale BLEVE for blast wave prediction*. Journal of Loss Prevention in the Process Industries, 2020. **65**: p. 104107.
- [24] Li, J., et al., *Prediction of BLEVE blast loading using CFD and artificial neural network*. Process Safety and Environmental Protection, 2021. **149**: p. 711-723..

- [25] Li, Q., et al., *A comparative study on the most effective machine learning model for blast loading prediction: From GBDT to Transformer*. Engineering Structures, 2023. **276**: p. 115310.
- [26] Li, Q., et al., *Prediction of BLEVE loads on structures using machine learning and CFD*. Process Safety and Environmental Protection, 2023. **171**: p. 914-925.
- [27] Li, Q., et al., *Machine learning prediction of BLEVE loading with graph neural networks*. Reliability Engineering & System Safety, 2024. **241**: p. 109639.
- [28] Birk, A.M., C. Davison, and M. Cunningham, *Blast overpressures from medium scale BLEVE tests*. Journal of Loss Prevention in the Process Industries, 2007. **20**(3): p. 194-206.
- [29] Laboureur, D., et al., *A closer look at BLEVE overpressure*. Process Safety and Environmental Protection, 2015. **95**: p. 159-171.
- [30] Birk, A.M., R. Eyssette, and F. Heymes, *Early moments of BLEVE: From vessel opening to liquid flashing release*. Process Safety and Environmental Protection, 2019. **132**: p. 35-46.
- [31] Birk, A., et al., *Near field blast effects from BLEVE*. Chemical Engineering Transactions, 2016. **48**: p. 283-288.
- [32] Laboureur, D., J.-M. Buchlin, and P. Rambaud. *Small scale experiments on boiling liquid expanding vapor explosions: supercritical BLEVE*. in *Pressure Vessels and Piping Conference*. 2012. American Society of Mechanical Engineers.
- [33] Birk, A.M., et al., *Near-field BLEVE overpressure effects: The shock start model*. Process Safety and Environmental Protection, 2018. **116**: p. 727-736.
- [34] Birk, A., R. Eyssette, and F. Heymes, *Analysis of BLEVE overpressure using spherical shock theory*. Process Safety and Environmental Protection, 2020. **134**: p. 108-120.
- [35] Eyssette, R., F. Heymes, and A.M. Birk, *Ground loading from BLEVE through small scale experiments: Experiments and results*. Process Safety and Environmental Protection, 2021. **148**: p. 1098-1109.
- [36] Tschirschwitz, R., et al., *Mobile gas cylinders in fire: Consequences in case of failure*. Fire Safety Journal, 2017. **91**: p. 989-996.

- [37] Tschirschwitz, R., et al., *Experimental investigation of consequences of LPG vehicle tank failure under fire conditions*. Journal of Loss Prevention in the Process Industries, 2018. **56**: p. 278-288.
- [38] Zhou, Y., et al., *Experimental study of the influence of burst parameters on the initiation of CO₂ BLEVE*. International Journal of Greenhouse Gas Control, 2019. **91**: p. 102817.
- [39] Bjerketvedt, D., et al., *Boiling liquid expanding vapour explosion in CO₂ small scale experiments*. Energy Procedia, 2011. **4**: p. 2285-2292.
- [40] Van der Voort, M., et al., *Blast from explosive evaporation of carbon dioxide: experiment, modeling and physics*. Shock Waves, 2012. **22**(2): p. 129-140.
- [41] Van Der Voort, M.M., et al., *An experimental study on the temperature dependence of CO₂ explosive evaporation*. Journal of Loss Prevention in the Process Industries, 2013. **26**(4): p. 830-838.
- [42] Zhou, Y., et al., *Small Scale Experiments of CO₂ Boiling Liquid Expanding Vapor Explosion in Injection Pipes*. Energy Procedia, 2014. **61**: p. 782-786.
- [43] Li, X., et al., *Experiments on burst pressure and fragment dispersion effects of small-sized pressure vessel BLEVE*. Fuel, 2020. **277**: p. 118145.
- [44] Li, M., et al., *A small-scale experimental study on the initial burst and the heterogeneous evolution process before CO₂ BLEVE*. Journal of Hazardous Materials, 2018. **342**: p. 634-642.
- [45] Chen, S.-N., J.-H. Sun, and G.-Q. Chu, *Small scale experiments on boiling liquid expanding vapor explosions: Vessel over-pressure*. Journal of Loss Prevention in the Process Industries, 2007. **20**(1): p. 45-51.
- [46] Chen, S., J. Sun, and W. Wan, *Boiling liquid expanding vapor explosion: Experimental research in the evolution of the two-phase flow and over-pressure*. Journal of Hazardous Materials, 2008. **156**(1-3): p. 530-537.
- [47] Eyssette, R., *Characterization and Modeling of Near-Field BLEVE Overpressure and Ground Loading Hazards*. 2018, Queen's University (Canada).
- [48] Melhem, G., P. Croce, and H. Abraham, *Data summary of the national fire protection association's BLEVE tests*. Process Safety Progress, 1993. **12**(2): p. 76-82.

- [49] Johnson, D. and M. Pritchard. *Large scale experimental study of boiling liquid expanding vapour explosions (BLEVEs)*. in *Gastech 90, International LNG/LPG Conference & Exhibition*. 1990.
- [50] Balke, C., et al., *Study of the Failure Limits of a Railway Tank Car Filled with Liquefied Petroleum Gas Subjected to an Open Pool Fire Test*. Federal Institute for Materials Research and Testing (BAM), Berlin, Germany. 1999.
- [51] Stawczyk, J., *Experimental evaluation of LPG tank explosion hazards*. Journal of hazardous materials, 2003. **96**(2-3): p. 189-200.
- [52] Giesbrecht, H., et al., *Analysis of explosion hazards on spontaneous release of inflammable gases into the atmosphere*. Ger. Chem. Eng.(Engl. Transl.);(Germany, Federal Republic of), 1981. **4**(5).
- [53] Betteridge, S. and L. Phillips. *Large scale pressurised LNG BLEVE experiments*. in *Institution of Chemical Engineers Symposium*. 2015. **160**: p. 353-364.
- [54] Heymes, F., et al., *An experimental study of water BLEVE*. Process Safety and Environmental Protection, 2020. **141**: p. 49-60.
- [55] Tang, M.J. and Q.A. Baker, *A new set of blast curves from vapor cloud explosion*. Process Safety Progress, 1999. **18**(4): p. 235-240.
- [56] Bubbico, R. and M. Marchini, *Assessment of an explosive LPG release accident: A case study*. Journal of Hazardous Materials, 2008. **155**(3): p. 558-565.
- [57] Crowl, D.A., *Understanding explosions*. Vol. 16. 2010: John Wiley and Sons, New York
- [58] Laboureur, D., et al., *BLEVE overpressure: Multiscale comparison of blast wave modeling*. Process Safety Progress, 2014. **33**(3): p. 274-284.
- [59] Ogle, R.A., J.C. Ramirez, and S.A. Smyth, *Calculating the explosion energy of a boiling liquid expanding vapor explosion using exergy analysis*. Process Safety Progress, 2012. **31**(1): p. 51-54.
- [60] Hemmatian, B., E. Planas, and J. Casal, *Comparative analysis of BLEVE mechanical energy and overpressure modelling*. Process Safety and Environmental Protection, 2017. **106**: p. 138-149.

- [61] Brode, H.L., *Blast Wave from a Spherical Charge*. Physics of Fluids, 1959. **2**(2): p. 217.
- [62] Crowl, D.A., *Using thermodynamic availability to determine the energy of explosion for compressed gases*. Plant/Operations Progress, 1992. **11**(2): p. 47-49.
- [63] Prugh, R.W., *Quantitative evaluation of" BLEVE" hazards*. Journal of Fire Protection Engineering, 1991. **3**(1): p. 9-24.
- [64] Roberts, M.W. *Analysis of boiling liquid expanding vapor explosion (BLEVE) events at DOE sites*. in *Proceedings of EQE International Safety Analysis Workshop*. 2000.
- [65] Smith, J.M. and H.C. Van Ness, *Introduction to chemical engineering thermodynamics, 5th ed*. McGraw-Hill, Inc, New York, 1996.
- [66] Bosch, C. J. H. and Weterings, R. A. P. M. *Methods for the Calculation of Physical Effects: Due to Releases of Hazardous Materials (Liquids and Gases) – 'Yellow Book'*. 2005
- [67] Casal, J. and J.M. Salla, *Using liquid superheating energy for a quick estimation of overpressure in BLEVEs and similar explosions*. Journal of Hazardous Materials, 2006. **137**(3): p. 1321-1327.
- [68] Planas-Cuchi, E., J. Salla, and J. Casal, *Calculating overpressure from BLEVE explosions*. Journal of Loss Prevention in the Process Industries, 2004. **17**(6): p. 431-436.
- [69] Hemmatian, B., J. Casal, and E. Planas, *A new procedure to estimate BLEVE overpressure*. Process Safety and Environmental Protection, 2017. **111**: p. 320-325.
- [70] Gexcon, *FLACS v10. 7 User's Manual*, Norway. 2017.
- [71] Lees, F., *Lees' Loss prevention in the process industries: Hazard identification, assessment and control*. 2012: Butterworth-Heinemann.
- [72] Launder, B.E. and D.B. Spalding, *The numerical computation of turbulent flows*, in *Numerical prediction of flow, heat transfer, turbulence and combustion*. 1983, Elsevier. p. 96-116.

- [73] Ma, G., Y. Huang, and J. Li, *VCE Overpressure Prediction by CFD Modelling*, in *Risk Analysis of Vapour Cloud Explosions for Oil and Gas Facilities*. 2019, Springer. p. 45-79.
- [74] Hansen, O.R., M.T. Kjellander, and J.A. Pappas, *Explosion loading on equipment from CFD simulations*. *Journal of Loss Prevention in the Process Industries*, 2016. **44**: p. 601-613.
- [75] Rui, S., et al., *Experimental and numerical study on the effect of low vent burst pressure on vented methane-air deflagrations*. *Process Safety and Environmental Protection*, 2021. **146**: p. 35-42.
- [76] Wang, Q., et al., *Process of Natural Gas Explosion in Linked Vessels with Three Structures Obtained Using Numerical Simulation*. *Processes*, 2020. **8**(1): p. 52.
- [77] Li, J. and H. Hao, *Numerical and analytical prediction of pressure and impulse from vented gas explosion in large cylindrical tanks*. *Process Safety and Environmental Protection*, 2019. **127**: p. 226-244.
- [78] Li, J., et al., *Calculation of BLEVE energy and overpressures inside a tunnel using analytical and CFD methods*. *Tunnelling and Underground Space Technology*, 2021: p. 104263.
- [79] ANSYS, *ANSYS Fluent Theory Guide*. 2013, ANSYS, Inc.
- [80] Scarponi, G.E., et al., *LPG vessels exposed to fire: Scale effects on pressure build-up*. *Journal of Loss Prevention in the Process Industries*, 2018. **56**: p. 342-358.
- [81] Scarponi, G.E., et al., *An innovative three-dimensional approach for the simulation of pressure vessels exposed to fire*. *Journal of Loss Prevention in the Process Industries*, 2019. **61**: p. 160-173.
- [82] Zhao, Y., et al., *Numerical simulation on BLEVE mechanism of supercritical carbon dioxide*. *Energy Procedia*, 2015. **75**: p. 880-885.
- [83] Peng, Z., J. Li, and H. Hao, *Long-term condition monitoring of cables for in-service cable-stayed bridges using matched vehicle-induced cable tension ratios*. *Smart Structures and Systems*, 2022. **29**(1): p. 167-179.

- [84] Hemmatian, B., et al., *Prediction of BLEVE mechanical energy by implementation of artificial neural network*. Journal of Loss Prevention in the Process Industries, 2019: p. 104021.
- [85] Siddique, N. and H. Adeli, *Computational intelligence: synergies of fuzzy logic, neural networks and evolutionary computing*. 2013: John Wiley & Sons.
- [86] Mijwil, M.M., *Artificial neural networks advantages and disadvantages*. Retrieved from LinkedIn: <https://www.linkedin.com/pulse/artificial-neural-networks-advantages-disadvantages-maad-m-mijwil>, 2018.
- [87] Shi, J., et al., *Vented gas explosion overpressure prediction of obstructed cubic chamber by Bayesian Regularization Artificial Neuron Network – Bauwens model*. Journal of Loss Prevention in the Process Industries, 2018. **56**: p. 209-216.
- [88] Shi, J., et al., *Application of Bayesian Regularization Artificial Neural Network in explosion risk analysis of fixed offshore platform*. Journal of Loss Prevention in the Process Industries, 2019. **57**: p. 131-141.
- [89] Shi, J., et al., *Probabilistic real-time deep-water natural gas hydrate dispersion modeling by using a novel hybrid deep learning approach*. Energy, 2021. **219**: p. 119572.
- [90] Shi, J., et al., *Real-time natural gas release forecasting by using physics-guided deep learning probability model*. Journal of Cleaner Production, 2022. **368**: p. 133201.
- [91] Van Den Berg, A.C., *Blast charts for explosive evaporation of superheated liquids*. Process Safety Progress, 2008. **27**(3): p. 219-224.
- [92] Wang, Y., J. Li, and H. Hao, *Development of efficient methods for prediction of medium to large scale BLEVE pressure in open space*. Process Safety and Environmental Protection, 2022. **161**: p. 421-435.
- [93] Strehlow, R., et al., *The blast wave generated by spherical flames*. Combustion and flame, 1979. **35**: p. 297-310.
- [94] Prugh, R.W., *Quantify BLEVE hazards*. Chem. Eng. Prog., 1991. **87**: p. 66-72.
- [95] Rigby, S.E., et al., *The Negative Phase of the Blast Load*. International Journal of Protective Structures, 2014. **5**(1): p. 1-19.

- [96] Karlos, V. and G. Solomos, *Calculation of blast loads for application to structural components*. Luxembourg: Publications Office of the European Union, 2013.
- [97] Denny, J.W. and S.K. Clubley, *Long-duration blast loading & response of steel column sections at different angles of incidence*. Engineering Structures, 2019. **178**: p. 331-342.
- [98] Costa, M. and G. Doz, *Study of blast wave overpressures using the computational fluid dynamics*. Revista IBRACON de Estruturas e Materiais, 2017. **10**: p. 669-677.
- [99] Rigby, S., *Blast wave time of arrival: A reliable metric to determine pressure and yield of high explosive detonations*. Fire and Blast Information Group Technical Newsletter, 2021(79): p. 18-25.
- [100] Mercx, W., J. Weerheijm, and T.L. Verhagen, *Some considerations on the damage criteria and safety distances for industrial explosions*. HAZARDS XI—New Directions in Process Safety, UMIST, Manchester, 1991.
- [101] Alsharkawi, S.M.a.I., ed. *Structural Engineering and Geomechanics - Blast and impact effects on structures*. Vol. 1. 2020.
- [102] Nguyen, H. and X.-N. Bui, *Predicting blast-induced air overpressure: a robust artificial intelligence system based on artificial neural networks and random forest*. Natural Resources Research, 2019. **28**(3): p. 893-907.
- [103] Modarres, M., M.P. Kaminskiy, and V. Krivtsov, *Reliability engineering and risk analysis: a practical guide*. 2016: CRC press.
- [104] Boris, J.P. and D.L. Book, *Flux-Corrected Transport. I. SHASTA, A Fluid Transport Algorithm That Works*. Journal of Computational Physics, 1997. **135**(2): p. 172-186.
- [105] Gexcon, *FLACS-CFD v22.1r2 User's Manual, Norway*. 2022.
- [106] Liu, Z., et al., *Experimental and Numerical Study on the Gas Explosion in Urban Regulator Station*. Journal of Beijing Institute of Technology, 2020. **29**(2): p. 195-208.
- [107] Kadatec. *LPG Road Tankers & ISO Tank Containers, V9 092017*. 2017.
- [108] Rickman, D.D. and D.W. Murrell, *Development of an improved methodology for predicting airblast pressure relief on a directly loaded wall*. Journal of Pressure Vessel Technology, 2007. **129**(1): p. 195-204.

- [109] Rigby, S.E., A. Tyas, and T. Bennett, *Single-Degree-of-Freedom response of finite targets subjected to blast loading – The influence of clearing*. Engineering Structures, 2012. **45**: p. 396-404.
- [110] Tyas, A., et al., *Prediction of clearing effects in far-field blast loading of finite targets*. Shock Waves, 2011. **21**(2): p. 111-119.
- [111] ASCE, *Design of Blast-Resistant Buildings in Petrochemical Facilities (Second Edition)*. 2010: Task Committee on Blast Resistant Design of the Petrochemical Committee of the Energy Division of the American Society of Civil Engineers.
- [112] Green-Book, T., *Method for the determination of possible damage to people and objects resulting from releases of hazardous materials*. CPR 16E, TNO–The Netherlands Organisation of Applied Scientific Research, 1992.
- [113] Shi, Y., H. Hao, and Z.-X. Li, *Numerical simulation of blast wave interaction with structure columns*. Shock Waves, 2007. **17**(1): p. 113-133.
- [114] Ngo, T., et al., *Blast loading and blast effects on structures—an overview*. Electronic Journal of Structural Engineering, 2007. **7**(S1): p. 76-91.
- [115] Xu, R., et al., *Protective effects of gabion wall against blast waves from large TNT-equivalent explosions*. Engineering Structures, 2021. **249**: p. 113389.
- [116] Janney, S.B., *Blast resistant design of steel structures*. 2007, The University of Tennessee Knoxville
- [117] Johnson-Yurchak, J., *Validation of the Mach Stem Triple Point*. 2020, Lawrence Livermore National Lab.(LLNL), Livermore, CA (United States); California Polytechnic State Univ. (CalPoly), San Luis Obispo, CA (United States).
- [118] Shin, J., et al., *Reflection Coefficients and Reflected Scaled Impulses from Detonations of High Explosives as a Function of Angle of Incidence*. Journal of Structural Engineering, 2017. **143**(7): p. 04017043.
- [119] Rigby, S.E., et al., *Angle of incidence effects on far-field positive and negative phase blast parameters*. International Journal of Protective Structures, 2015. **6**(1): p. 23-42.

- [120] Bulat, P.V., *The History of the Study of Shock Wave's Mach Reflection from the Wedge*. International Electronic Journal of Mathematics Education, 2016. **11**(5): p. 1151-1162.
- [121] Kobayashi, S., T. Adachi, and T. Suzuki, *Examination of the von Neumann paradox for a weak shock wave*. Fluid dynamics research, 1995. **17**(1): p. 13-25.
- [122] Karzova, M.M., et al., *Mach stem formation in reflection and focusing of weak shock acoustic pulses*. The Journal of the Acoustical Society of America, 2015. **137**(6): p. EL436-EL442.
- [123] Kobayashi, S., T. Adachi, and T. Suzuki, *Non-self-similar behavior of the von Neumann reflection*. Physics of Fluids, 2000. **12**(7): p. 1869-1877.
- [124] Lomazzi, L., M. Giglio, and A. Manes. *Analysis of the blast wave–structure interface phenomenon in case of explosive events*. in *IOP Conference Series: Materials Science and Engineering*. 2021. **1038**(1): p. 012083.
- [125] Rigby, S.E., *Blast wave clearing effects on finite-sized targets subjected to explosive loads*. 2014, University of Sheffield.
- [126] Cullis, I., *Blast waves and how they interact with structures*. BMJ Military Health, 2001. **147**(1): p. 16-26.
- [127] Baker, W.E., et al., *Explosion hazards and evaluation*. 1983, New York: Elsevier.
- [128] Wang, Y., et al., *Prediction of BLEVE loading on a rigid structure*. Process Safety and Environmental Protection, 2023. **175**: p. 1-16.
- [129] Sohaimi, A.S.M., et al., *Using Computational Fluid Dynamics (CFD) for Blast Wave Propagation under Structure*. Procedia Computer Science, 2016. **80**: p. 1202-1211.
- [130] Fluent, ANSYS, Inc. 16.0: Canonsburg, Pennsylvania, USA.
- [131] Mechanical_APDL, ANSYS, Inc. 16.0: Canonsburg, Pennsylvania, USA.
- [132] Travanca, J. and H. Hao, *Control of wave-induced vibrations on floating production systems*. Ocean Engineering, 2017. **141**: p. 35-52.

- [133] Benra, F.-K., et al., *A comparison of one-way and two-way coupling methods for numerical analysis of fluid-structure interactions*. Journal of applied mathematics, 2011: p. 853560.
- [134] Liou, M.-S. and C.J. Steffen, *A New Flux Splitting Scheme*. Journal of Computational Physics, 1993. **107**(1): p. 23-39.
- [135] Teich, M. and N. Gebbeken, *Structures subjected to low-level blast loads: Analysis of aerodynamic damping and fluid-structure interaction*. Journal of Structural Engineering, 2012. **138**(5): p. 625-635.
- [136] Xue, Y.L., et al., *A Study on Internal Explosion Testing of the “Rigid-Flexible-Rigid” Three-Layer Sealed Structure*. Shock and Vibration, 2018: p. 1909872.
- [137] Hidallana-Gamage, H.D., D. Thambiratnam, and N. Perera, *Influence of the negative phase and support flexibility on the blast response of laminated glass panels*. Construction and Building Materials, 2017. **154**: p. 462-481.

Appendix I Statement of contribution of co-authors

To whom it may concern,

I, Yang Wang, conducted numerical simulations and analytical investigations, data processing and analysis, and wrote the manuscripts of the papers entitled as follows, which are reviewed and edited by the co-authors. They also provided insights on conceptual design, data processing and data analysis.

- 1. Development of efficient methods for prediction of medium to large scale BLEVE pressure in open space.**
- 2. A state-of-the-art review of experimental and numerical studies on BLEVE overpressure prediction.**
- 3. Prediction of BLEVE loading on a rigid structure.**
- 4. Prediction of BLEVE loading on structures.**

Yang Wang Yang Wang

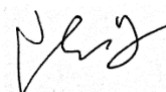
I, as a co-author, endorse that this level of contribution by the candidate indicated above is appropriate.

Prof. Hong Hao



.....

Associate Prof. Wensu Chen



.....

Dr. Jingde Li



.....

Zitong Wang



.....

Appendix II Copyright Clearance

The proof of the rights, granted by publisher for the publications that form the chapters of this thesis are attached below.

Chapter 2

Wang, Y., Li, J., Hao, H., 2022. A state-of-the-art review of experimental and numerical studies on BLEVE overpressure prediction. *Journal of Loss Prevention in the Process Industries*, 104920.



A state-of-the-art review of experimental and numerical studies on BLEVE overpressure prediction
Author: Yang Wang,Jingde Li,Hong Hao
Publication: Journal of Loss Prevention in the Process Industries
Publisher: Elsevier
Date: December 2022
© 2022 Elsevier Ltd. All rights reserved.

Journal Author Rights

Please note that, as the author of this Elsevier article, you retain the right to include it in a thesis or dissertation, provided it is not published commercially. Permission is not required, but please ensure that you reference the journal as the original source. For more information on this and on your other retained rights, please visit: <https://www.elsevier.com/about/our-business/policies/copyright#Author-rights>

BACK CLOSE WINDOW

Chapter 3

Wang, Y., Li, J., Hao, H., 2022. Development of efficient methods for prediction of medium to large scale BLEVE pressure in open space. *Process Safety and Environmental Protection* 161, 421-435.



Development of efficient methods for prediction of medium to large scale BLEVE pressure in open space
Author: Yang Wang,Jingde Li,Hong Hao
Publication: Process Safety and Environmental Protection
Publisher: Elsevier
Date: May 2022
© 2022 Institution of Chemical Engineers. Published by Elsevier Ltd. All rights reserved.

Journal Author Rights

Please note that, as the author of this Elsevier article, you retain the right to include it in a thesis or dissertation, provided it is not published commercially. Permission is not required, but please ensure that you reference the journal as the original source. For more information on this and on your other retained rights, please visit: <https://www.elsevier.com/about/our-business/policies/copyright#Author-rights>

BACK CLOSE WINDOW

Chapter 4

Wang, Y., Hao, H., Chen, W., Li, J. & Wang, Z. 2023. Prediction of BLEVE loading on a rigid structure. *Process Safety and Environmental Protection*, 175, 1-16.



Prediction of BLEVE loading on a rigid structure
Author: Yang Wang,Hong Hao,Wensu Chen,Jingde Li,Zitong Wang
Publication: Process Safety and Environmental Protection
Publisher: Elsevier
Date: July 2023
© 2023 The Author(s). Published by Elsevier Ltd on behalf of Institution of Chemical Engineers.


Journal Author Rights

Please note that, as the author of this Elsevier article, you retain the right to include it in a thesis or dissertation, provided it is not published commercially. Permission is not required, but please ensure that you reference the journal as the original source. For more information on this and on your other retained rights, please visit: <https://www.elsevier.com/about/our-business/policies/copyright#Author-rights>

[BACK](#) [CLOSE WINDOW](#)

Chapter 5

Wang, Y., Chen, W., Hao, H., 2024. Prediction of BLEVE loading on structures. *Journal of Loss Prevention in the Process Industries*, 105325.



Prediction of BLEVE loading on structures
Author: Yang Wang,Wensu Chen,Hong Hao
Publication: Journal of Loss Prevention in the Process Industries
Publisher: Elsevier
Date: August 2024
© 2024 The Authors. Published by Elsevier Ltd.

Creative Commons

This is an open access article distributed under the terms of the [Creative Commons CC-BY](#) license, which permits unrestricted use, distribution, and reproduction in any medium, provided the original work is properly cited.

You are not required to obtain permission to reuse this article.

To request permission for a type of use not listed, please contact [Elsevier Global Rights Department](#).

Are you the author of this Elsevier journal article?